A MULTI-OMIC CHARACTERIZATION OF THE CALVIN-BENSON-BASSHAM CYCLE IN CYANOBACTERIA

by

Nathaphon Yu King Hing

A Dissertation

Submitted to the Faculty of Purdue University

In Partial Fulfillment of the Requirements for the degree of

Doctor of Philosophy

Davidson School of Chemical Engineering

West Lafayette, Indiana

May 2021

THE PURDUE UNIVERSITY GRADUATE SCHOOL
STATEMENT OF COMMITTEE APPROVAL

Dr. John Morgan, Chair

Davidson School of Chemical Engineering

Dr. Chongli Yuan

Davidson School of Chemical Engineering

Dr. Rajamani Gounder

Davidson School of Chemical Engineering

Dr. Mark Hall

Department of Biochemistry

Approved by:

Dr. John Morgan

Dedicated to my parents

ACKNOWLEDGMENTS

I would like to thank my advisor, Dr. John Morgan, for having been always supportive and patient with me all these years. His guidance and encouragement have shaped my research continually. Without his assistance, this work would not have been possible. I am especially grateful for his aid in broadening my horizons and motivating me to pursue my own lines of questioning, and always inspiring me to become a better researcher. I would also like to thank my committee members, Dr. Chongli Yuan, Dr. Mark Hall and Dr. Rajamani Gounder. Dr. Chongli Yuan has been instrumental for having supported me ever since my undergraduate years. Dr. Mark Hall and Dr. Rajamani Gounder have helped me greatly by offering their expertise to my work. To these scientists, I will always appreciate their role as exemplary educators and mentors during my years at Purdue.

I also would like to acknowledge my collaborators, Dr. Feiyan Liang and Dr. Peter Lindblad, and I especially would like to thank Dr. Uma Aryal for his help with our proteomic studies. I would also like to express my gratitude to my fellow lab members, Rohit Jaini, Longyun Guo, Robin Wheeler, Jeremiah Vue, Arnav Deshpande, Meng-Ling Shih, and Melissa Marsing, each of whom have contributed in their own way to my success. I will always be thankful for their help, feedback, and for simply being an integral part of my experience at graduate school. I want to thank my friends, both in and out of graduate school, for their continued emotional support and encouragement.

Finally, I must thank my parents and my siblings for their unconditional support. I cannot recall even a single moment where they did not encourage my love of learning. I dedicate this body of work to my parents, whom I know I could always rely on.

TABLE OF CONTENTS

LIST OF TABLES

LIST OF FIGURES

LIST OF METABOLITE ABBREVIATIONS

3PGA	3-phosphoglycerate
2PG	2-phosphoglycolate
ACA	acetyl coenzyme A
ACO	aconitate
AKG	α-ketoglutarate
AP	acetyl phosphate
CIT	citrate
DHAP	dihydroxyacetone phosphate
E4P	erythrose-4-phosphate
F6P	fructose-6-phosphate
FBP	fructose-1,6-bisphoshate
FUM	fumarate
G6P	glucose-6-phosphate
GA	glycerate
GAP	glyceraldehyde 3-phosphate
GLY	glycine
MAL	malate
OAA	oxaloacetate
PEP	phosphoenol pyruvate
PYR	pyruvate
R5P	ribose-5-phosphate
RU5P	ribulose-5-phosphate
RUBP	ribulose-1,5-bisphosphate
S7P	sedoheptulose-7-phosphate
SBP	sedoheptulose-1,7-bisphosphate
SER	serine
SSA	succinic semialdehyde
SUC	succinate
X5P	xylulose-5-phosphate

LIST OF ENZYME ABBREVIATIONS

CS	citrate synthase
ENO	enolase
FBA	fructose-bisphosphate aldolase
FBP/SBPase	d-fructose 1,6-bisphosphatase/sedoheptulose 1,7-bisphosphatase
FUM	fumarase
G6PDH	glucose-6-phosphate 1-dehydrogenase
G6PI	glucose-6-phosphate isomerase
GAPDH	glyceraldehyde 3-phosphate dehydrogenase
GPM	phosphoglucomutase
MDH	malate dehydrogenase
PDH	pyruvate dehydrogenase complex
PEPC	phosphoenolpyruvate carboxylase
PFK	phosphofructokinase
PGK	phosphoglycerate kinase
PGM	phosphoglycerate mutase
PHGDH	phosphoglycerate dehydrogenase
PKT	phosphoketolase
PRK	phosphoribulokinase
RBCl	ribulose bisphosphate carboxylase large subunit
RBCs	ribulose bisphosphate carboxylase small subunit
RPE	ribulose-phosphate 3-epimerase
RPIa	ribose-5-phosphate isomerase a
SSADH	succinic semialdehyde dehydrogenase
TA	transaldolase
TKT	transketolase
TPI	triose-phosphate isomerase

ABSTRACT

Cyanobacteria are photosynthetic organisms with the potential to sustainably produce carbon-based end products by fixing carbon dioxide from the atmosphere. Optimizing the growth or biochemical production in cyanobacteria is an ongoing challenge in metabolic engineering. Rational design of metabolic pathways requires a deep understanding of regulatory mechanisms. Hence, a deeper understanding of photosynthetic regulation of the influence of the environment on metabolic fluxes provides exciting possibilities for enhancing the photosynthetic Calvin-Benson-Bassham cycle. One approach to study metabolic processes is to use omic-level techniques, such as proteomics and fluxomics, to characterize varying phenotypes that result from different environmental conditions or different genetic perturbations.

This dissertation examines the influence of light intensity on enzymatic abundances and the resulting Calvin-Benson-Bassham cycle fluxes using a combined proteomic and fluxomic approach in the model cyanobacteria *Synechocystis* sp. PCC 6803. The correlation between light intensity and enzymatic abundances is evaluated to determine which reactions are more regulated by enzymatic abundance. Additionally, carbon enrichment data from isotopic labelling experiments strongly suggest metabolite channeling as a flexible and light-dependent regulatory mechanism present in cyanobacteria. We propose and substantiate biological mechanisms that explains the formation of metabolite channels under specific redox conditions.

The same multi-omic approach was used to examine genetically modified cyanobacteria. Specifically, genetically engineered and conditionally growth-enhanced *Synechocystis* strains overexpressing the central Calvin-Benson-Bassham cycle enzymes FBP/SBPase or transketolase were evaluated. We examined the effect of the heterologous expression of each of these enzymes on the Calvin-Benson-Bassham cycle, as well as on adjacent central metabolic pathways. Using

both proteomics and fluxomics, we demonstrate distinct increases in Calvin-Benson-Bassham cycle efficiency as a result of lowered oxidative pentose phosphate pathway activity. This work demonstrates the utility of a multi-omic approach in characterizing the differing phenotypes arising from environmental and genetic changes.

1. INTRODUCTION

1.1 Background

Photosynthesis is a complex and much studied process present in algae, plants and some bacteria. These photosynthetic organisms can incorporate inorganic carbon into many diverse high value products, providing a sustainable alternative to existing bio-industrial processes. Among these organisms, cyanobacteria are of interest for their genetic transformability, quick doubling times and flexible growth conditions. Rapidly growing cyanobacteria can serve as a way to transform atmospheric CO_2 into more useful end products [1]. For example, cyanobacteria have been engineered to produce complex and specific end products like such as astaxanthin [2], ethylene [3], ethanol [4], or omega-3 fatty acids [5].

Additionally, a better understanding of cyanobacterial metabolism raises the possibility of extrapolating any lessons learned to other photoautotrophic organisms which may share many commonalities. On the other hand, the use of photoautotrophs in bio-industrial processes can be difficult due to slower growth rates and lower yields when compared to non-photoautotrophic organisms. Consequently, a systematic approach towards studying photoautotrophic metabolism in model cyanobacteria greatly enhances metabolic engineering efforts to overcome limitations in current photoautotrophs. The increasing accessibility of high-throughput technologies allow for a multi-omics approach towards studying metabolism, a so-called top-down approach that examines entire networks of interactions as opposed to individual biological reactions. The use of fluxomics, which describes the determination of *in vivo* reaction rates, metabolomics, which describes the concentrations of metabolites, and proteomics, which describes the abundances of protein levels, are complementary approaches that can be used to explain different phenotypical outcomes under different conditions or after different genetic manipulations.

In particular, metabolic flux analysis (MFA) is a technique used to estimate the *in vivo* fluxes that determine the physiology of various biological systems [6], which can be used to understand the biological response to various genetic or environmental perturbations. Isotopically non-stationary metabolic flux analysis (INST-MFA) is a particular variant of MFA used to estimate carbon fluxes especially in autotrophic organisms, as the main carbon source, CO_2, is a single carbon substrate. Under a stationary MFA approach, all carbon in the system will tend towards uniform labelling at steady state because nearly all carbon in autotrophic metabolism is derived from the same substrate, CO_2. In comparison, INST-MFA explicitly makes use of the transient, non-stationary behavior after a ^{13}C pulse is introduced to the system to obtain *in vivo* flux estimates. This fluxomic information can be complemented with proteomic information, which reveals the abundances of various enzymes which catalyze the many biological reactions occurring within an organism.

The Calvin-Benson-Bassham cycle, abbreviated hereafter as the Calvin cycle, is the primary metabolic cycle responsible for the fixation of atmospheric CO_2 and generating useful precursors used throughout metabolism. Metabolic engineering of the Calvin cycle is of interest because of its importance in central carbon metabolism. The Calvin cycle generates many precursors that are used in a multitude of downstream biological pathways. However, the characterization of the Calvin cycle remains incomplete in part due to the large number of regulatory mechanisms present in this cycle.

The eponymous Calvin cycle [7] (Figure 1.1) is often divided into three distinct sections: reduction, regeneration, and carbon fixation. During the reduction phase, 3-phosphoglycerate (3PGA) is reduced using ATP to form glycerate-1,3-bisphosphate via phosphoglycerate kinase

(PGK), then further reduced by NADPH to form glyceraldehyde 3-phosphate (GAP) using glyceraldehyde 3-phosphate dehydrogenase (GAPDH).

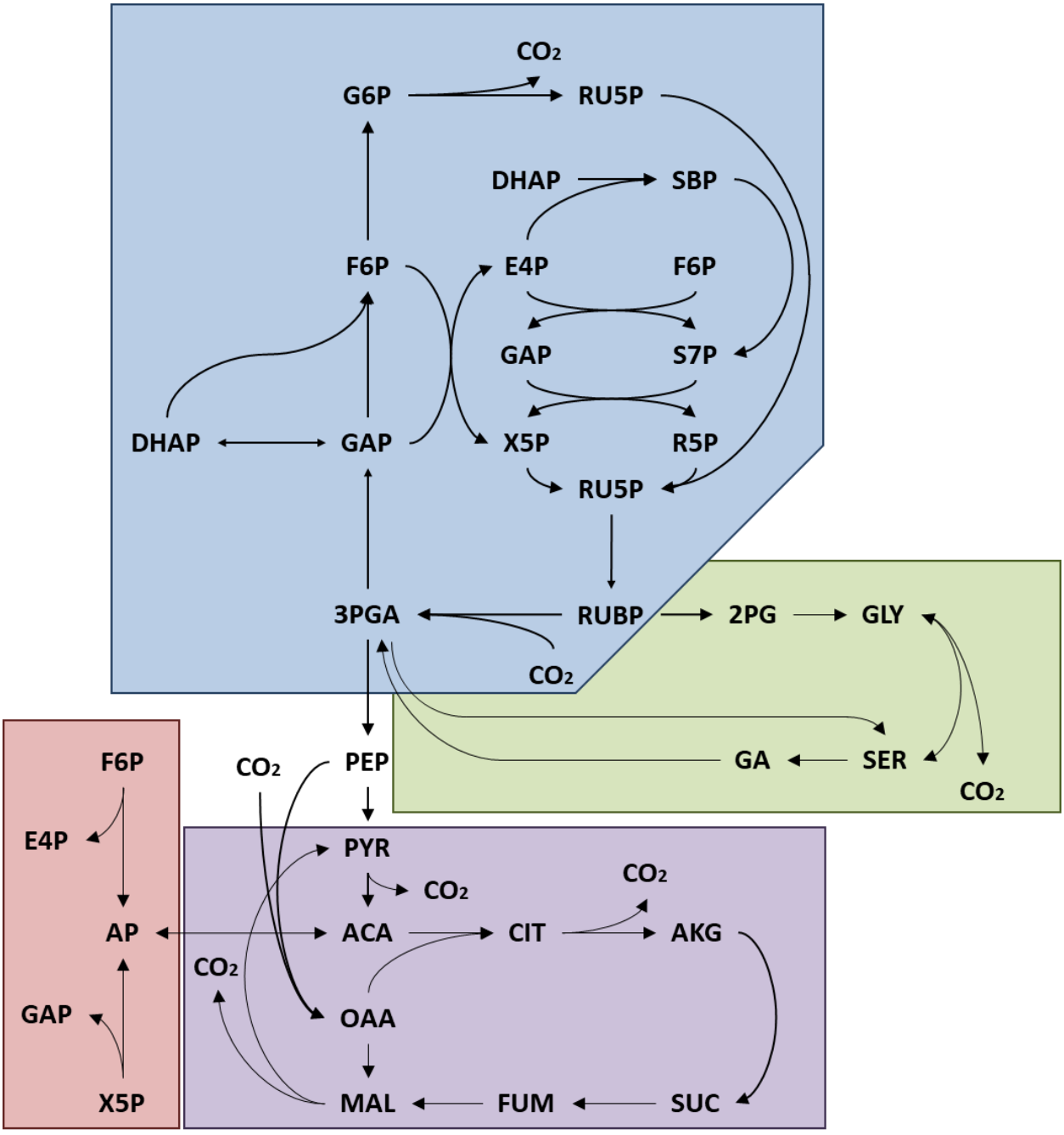

Figure 1.1 A simplified representation of the Calvin cycle and oxidative pentose phosphate pathway (blue), photorespiration (green), phosphoketolase pathway (red) and the tricarboxylic acid cycle (purple)

During the regeneration phase, GAP is reversibly isomerized into dihydroxyacetone phosphate (DHAP) via triose phosphate isomerase (TPI). The enzyme fructose bisphosphate aldolase (FBA) converts GAP and DHAP into fructose-1,6-bisphosphate (FBP), which is subsequently converted into fructose-6-phosphate (F6P). Fructose-6-phosphate undergoes a rearrangement of carbon together with GAP using transketolase (TKT) to form erythrose-4-phosphate (E4P) and xylulose-5-phosphate (X5P). E4P and DHAP can form sedoheptulose-1,7-bisphosphate (SBP). SBP can be dephosphorylated into sedoheptulose-7-phosphate (S7P) using the bifunctional enzyme fructose-1,6-/sedoheptulose-1,7-bisphosphatase (FBP/SBPase). Transaldolase (TA) converts E4P and F6P into GAP and S7P. Transketolase further converts GAP and S7P into five carbon sugars X5P and ribose-5-phosphate (R5P). R5P can be isomerized into ribulose-5-phosphate (RU5P) via ribose-5-phosphate isomerase (RPI). Similarly, X5P can be converted into RU5P via ribulose-phosphate 3-epimerase (RPE). RU5P is then phosphorylated using ATP into ribulose-1,5-bisphosphate (RUBP) via phosphoribulokinase (PRK). Finally, the carbon fixation part of the cycle is accomplished by ribulose-1,5-bisphosphate carboxylase/oxygenase (RuBisCO).

The Calvin cycle, due to its dependency on reducing cofactors ATP and NADPH, is strongly active in the light and largely inactive during the dark. It is notably also connected to other central carbon pathways. F6P can be isomerized into glucose-6-phosphate (G6P) which can be committed to the oxidative pentose phosphate pathway (OPPP) [8]. 3PGA can be converted into phophoenolpyruvate (PEP) which can enter the tricarboxylic acid (TCA) cycle. Additionally, some cyanobacteria possess the phosphoketolase pathway [9], which converts either F6P or X5P into acetyl phosphate, providing an alternative way to enter the TCA cycle. Furthermore, the bifunctional RuBisCO is infamously known for its oxidative side reaction [10]–[12], which is the

first step of the photorespiration pathway. The central position of the Calvin cycle in photosynthetic metabolism makes itself an ideal metabolic engineering target [13].

As befitting of a centrally located metabolic pathway, the Calvin cycle is subject to multiple levels of regulation. Kinetic studies have already revealed allosteric control over the majority of Calvin cycle reactions [14]–[17]. However, modelling the reactions using Michaelis-Menten kinetics together did not always return physiologically realistic steady states [17], implying an incomplete characterization of the cycle. Indeed, it is known that the Calvin cycle, whether in cyanobacteria or in other organisms, is subject to other forms of regulation besides allosteric control, such as light responsive post-translation modifications (PTMs) on Calvin cycle enzymes [18], changing enzyme levels [19], [20], and some level of compartmentalization of enzymes [21]–[24]. These factors are sometimes ignored in prior modelling efforts in favor of simplicity and decreasing computational workload, or because of a lack of available training data. Therefore, the study of the Calvin cycle greatly benefits from a multi-omics approach to unravel an otherwise intractable system by helping to determine which regulatory behaviors are present in the system during different environmental conditions.

1.2 Organization of Dissertation

The intent of this dissertation is to demonstrate how previous attempts at modelling the Calvin cycle can be improved using a multi-omic approach, and how new conclusions might be drawn from multi-omic datasets.

The combined proteomic and fluxomic characterization of the wild-type model cyanobacteria *Synechocystis* sp. PCC 6803 (*Synechocystis*) under light limiting, light saturated, and light inhibiting regimes is discussed in Chapter 2, revealing potential methods of regulation of the carbon fixating cycle. The characterization of metabolically engineered *Synechocystsis* strains

containing growth enhancing overexpression of transketolase and a transgenic fructose-1,6-/sedoheptulose-1,7-bisphosphatase within the Calvin cycle are discussed in Chapter 3. Finally, Chapter 4 provides a summary of the current work, possible avenues of future work, and concluding remarks associated with this research.

2. PROBING LIGHT-DEPENDENT REGULATION OF THE CALVIN CYCLE IN *SYNECHOCYSTIS*

2.1 Introduction

Photoautotrophic organisms like cyanobacteria are of interest for their ability to convert atmospheric CO_2 into biomass or other valuable products [13]. The Calvin cycle is the primary pathway responsible for net CO_2 fixation in oxygenic photosynthetic organisms. In particular, the model cyanobacteria *Synechocystis* sp. PCC 6803 is well studied as a fast-growing cyanobacteria and is a convenient platform for metabolic engineering efforts. The limitations and controlling processes of the Calvin cycle, however, is not completely understood. A better understanding of photosynthetic behavior under different light regimes can greatly expedite metabolic engineering efforts by underlining the regulatory behavior of the Calvin cycle.

One way to investigate the Calvin cycle is to use so-called 'omics' techniques, which include proteomics, metabolomics and fluxomics. The collection and use of large datasets together has the distinct advantage of reducing the chance of missing unexpected interactions that might be missed in a more targeted study. Additionally, these datasets allow for a more cohesive explanation of regulatory behavior because the phenotypical response of any organism can be considered as the sum of many different regulatory processes working together.

Varying enzymatic abundance is one common way in which metabolic processes can be regulated. Therefore, a thorough consideration of the relationship between carbon fluxes and enzymatic abundances changes should result in a deeper understanding of photosynthetic behavior under different light regimes. Here, the use of untargeted proteomics allows us to examine dynamic changes in the proteome as a result of changing light conditions. This is complemented with the use of fluxomics, specifically via the tracking of isotopic labelling in the form of isotopically

nonstationary metabolic flux analysis (INST-MFA), allows for the characterization of *in vivo* fluxes in cyanobacteria or other photosynthetic organisms [25], [26].

2.2 Materials and Methodology

2.2.1 Culturing Conditions

Wild-type *Synechocystis* was cultured in a bioreactor (PBR101, Phenometrics, MI) in 600 mL BG-11 PC media [27] (Tables A.13-A.14) at 30 °C with a magnetic stir bar (300 rpm) while constantly sparging the media with filtered air which provides a source of CO_2. Light was provided continuously at four different conditions (40, 80, 480 and 960 µmol m^{-2} s^{-1}). To estimate the growth rate, the optical density at 730 nm was measured over exponential phase.

2.2.2 Quenching and Extraction of Soluble Metabolites

In order to reasonably obtain estimates of metabolite concentrations, cellular metabolism must first be arrested by quenching cells. Cyanobacterial samples were quenched by injecting 10 mL of culture into 40 mL of pre-chilled (< 20 °C) 60% methanol in 50 mL centrifuge tubes. These centrifuge tubes were kept in either a dry ice and ethanol bath or cold liquid nitrogen and rapidly centrifuged (10 min, 8000 g) to collect cell pellet at -20 °C. The supernatant was disposed of, while the cell pellet was incubated with 500 µL chloroform and methanol (3:7 v/v) under -20 °C for 2 h while occasionally vortexing to extract intracellular metabolites. In two rounds, 500 µL of cold water was added and the samples were centrifuged again, and the upper methanol-water layer was collected. These extracted were pooled together and dried under nitrogen, reconstituted in 60 µL ultra-pure water before being run in LC-MS/MS.

2.2.3 Isotopically Nonstationary Metabolic Flux Analysis

Autotrophic organisms derive carbon almost entirely from the single carbon substrate CO_2, which prevents the use of conventional metabolic flux analysis due to the resulting uniformly labelled ^{13}C patterns during steady state. Isotopically nonstationary metabolic flux analysis (INST-MFA) is a technique to estimate the fluxes throughout a network using an isotopic tracer that explicitly uses nonstationary information to reveal metabolic fluxes and is therefore compatible even with autotrophic metabolism [26].

During INST-MFA, fluxes and pool sizes are estimated from measured labelling patterns and extracellular fluxes using an iterative fitting procedure. INST-MFA involves the minimization of the sum of squared residuals between simulated and experimental mass distribution vectors (MDVs) and pool sizes. INST-MFA requires an assumption of constant metabolic fluxes and pool sizes, with minimal perturbation by the introduction of the tracer. Cyanobacteria is grown in a bioreactor (PBR 101, Phenometrics, MI) on BG-11 PC medium [27]. Air was bubbled into the reactor, and the culture was stirred at 300 rpm. Temperature was maintained at 30 °C. The culture is grown until it reaches an OD730 of 0.6 to 1.2, representing mid to late exponential phase growth. Prior to the start of the experiment, triplicate samples were quenched to represent time zero data points. In the case of photoautotrophic cyanobacteria, ^{13}C labeled sodium bicarbonate ($NaH^{13}CO_3$) is a convenient tracer as it quickly equilibrates with CO_2 in an aqueous environment (a total concentration of 1 g/L is added to the bioreactor). Samples are rapidly quenched at time points of 0, 0.5, 1, 1.5, 2, 3, 5, 10 and 20 minutes in cold methanol in a dry ice and ethanol bath before extraction (2.2.2).

The isotopic labelling pattern of known metabolites were used to constrain the INST-MFA problem. Mass distribution vectors (MDV) represent the fraction of each isotopologue in vector form of a metabolite. As ^{13}C is integrated into the metabolome over time, there is a transient shift

in the relative amounts of each isotopomer (‘isotopic isomer’) for Calvin cycle intermediates. The rate of change of these isotopomer abundances can be correlated to the rate of each reaction. The model was fitted using INCA v1.7 or later [28] using the MATLAB computing environment. The resulting fit is only accepted if the $\chi 2$ test on the sum of squares is within the expected 95% confidence interval, as calculated based on the number of degrees of freedom in the model. As there is a possibility of finding a best fit solution within a local minima, this procedure is repeated multiple times ($n > 100$ for each experimental condition) with logistically perturbed initial estimates, and the best result is chosen to reduce the possibility that the iterative statistical procedure results in an nonoptimal local minimum.

Although it is technically possible to estimate the absolute concentrations of metabolites per mass of dry weight, there is also a possibility for some loss of metabolites during the quenching and extraction process [29]. While the INST-MFA problem can be constrained with pool sizes which would reduce the possibility of finding nonoptimal minima, we decided against constraining the search space with metabolite pool sizes due to the potential inaccuracy of the absolute measurements of metabolites. In comparison, the MDVs are essentially unaffected even during an inefficient extraction process.

2.2.4 LC-MS/MS measurements of metabolites

The LC-MS/MS protocol was adapted and slightly modified from prior literature [26], [30], [31] to quantify the majority of Calvin cycle intermediates. The phosphoketolase pathway intermediate acetyl phosphate (AP) was also included. Standards were procured from Sigma-Aldrich. LC-MS/MS parameters are listed in the appendix (Table A.1).

Chromatography was done using a HPLC-AD20 (Shimadzu, Columbia, MD) system. Separations was performed using a Polaris C18 column (150 x 2.0 mm, 5 µm, Agilent

Technologies, Santa Clara, CA) at 30 °C, 0.5 mL/min flow rate with a 20 µL injection volume. A combination of aqueous solvent A (11 mM TBA, 10 mM acetic acid, pH 4.9) and organic solvent B (100% methanol) was used as shown below (Figure 2.1). Under this flow profile, the majority of Calvin and TCA cycle metabolites will elute before 40 minutes, while the high amount of solvent B afterwards will help wash any remaining metabolites and impurities before the next run.

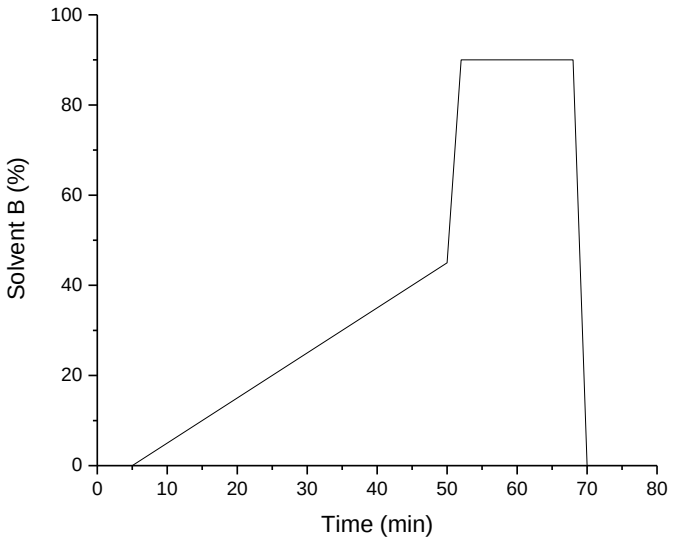

Figure 2.1 LC-MS/MS Flow Profile

Metabolites were profiled using a triple quadrupole mass spectrometer (QTrap 5500, AB Sciex, Redwood City, CA) under negative ion mode. The collision gas was set at 'Medium', curtain gas (CUR) was set at 30, ion spray voltage (IS) was set at -4500 V, temperature was set at 550 °C, ion source gas 1 (GS1) was set at 85, and ion source gas 2 (GS2) was set at 85.

2.2.5 Proteomics

Immediately prior to labelling experiments, a 20 mL aliquot of culture was withdrawn and pelleted for use in untargeted proteomics. Cell pellets were washed twice in 20 mM PBS and then

stored at -80 °C until sample preparation for proteomic analysis. Cell pellets were re-suspended in 400 µL of 100 mM ammonium bicarbonate containing 1 mM phenylmethylsulfonyl fluoride and homogenized at 6500 rpm for 90 seconds (Bertin Technologies SAS). Homogenate was transferred to new tubes and centrifuged at 13,500 rpm for 15 min at 4 °C. The supernatant was transferred to a new tube and treated as a soluble fraction, and the pellets were treated as insoluble fraction. Proteins in the soluble fractions were precipitated overnight at -20°C using 4 volume of cold (-20°C) acetone and precipitated proteins were pelleted by centrifugation at 13,500 rpm for 15 min at 4 °C. The soluble and insoluble fractions were dissolved in 8 M urea at room temperature for 1 h with continuous vortexing. The protein concentration was determined by Bicinchoninic Acid (BCA assay and 50 µg of the protein (equivalent volume) was used for proteomics sample preparation. Samples were incubated in 10 mM dithiothreitol at 37 °C for an hour for reduction followed by incubation in 20 mM iodoacetamide for an hour at room temperature in the dark for alkylation. Samples were digested using Trypsin/LysC protease mix at 1:25 (enzyme to substrate) ratio at 37°C. After 3 h of digestion, additional Trypsin/LysC protease mix was added at 1:50 (enzyme to substrate) ratio and digestion was allowed to proceed overnight at 37°C. Peptides were desalted using C18 micro spin desalting columns (The Nest Group, Inc.). Eluted peptides were dried and re-suspended in 3% acetonitrile/0.1% formic acid to a final concentration of 1 µg/µL and 1 µL (1 µg) was loaded used for LC-MS/MS analysis.

Peptides were analyzed in an Dionex UltiMate 3000 RSLC nano System coupled on-line to Q Exactive Orbitrap High Field Hybrid Quadrupole Mass Spectrometer (Thermo Fisher Scientific, Waltham, MA, USA) as described previously [32]. Briefly, reverse phase peptide separation was accomplished using a trap column (300 µm ID × 5 mm) packed with 5 µm 100 Å PepMap C18 medium coupled to a 50-cm long × 75 µm inner diameter analytical column packed

with 2 µm 100 Å PepMap C18 silica (Thermo Fisher Scientific). The column temperature was maintained at 50°C. Sample was loaded to the trap column at a flow rate of 5 µL/min and eluted from the analytical column at a flow rate of 300 nL/min using a 120-min LC gradient. The column was washed and equilibrated by using three 30 min LC gradient before injecting next sample. Precursor ion (MS1) scans were collected at a resolution of 120,000 and MS/MS scans at a resolution of 15,000 at 200 m/z in data dependent acquisition mode.

LC-MS/MS data were analyzed using MaxQuant (version 1.6.3.1) against the *Synechocystis* sp. PCC 6803 database downloaded from the NCBI (www.ncbi.nlm.nih.gov). We edited the following parameters for our search: precursor mass tolerance of 10 ppm; enzyme specificity of trypsin/Lys-C enzyme allowing up to 2 missed cleavages; oxidation of methionine (M) as a variable modification and carbamidomethylation (C) as a fixed modification. False discovery rate (FDR) of peptide spectral match (PSM) and protein identification was set to 0.01. Proteins with LFQ > 0 and MS/MS (spectral counts) ≥ 2 were considered as true identification and used for further downstream analysis. In total, 1,202 proteins were detected in at least one of the four tested conditions.

In total, 1,202 different proteins were identified in at least one of the four tested conditions (n=3). To compare data between different light conditions, the label free quantification (LFQ) intensities were used. The intensities of the soluble and insoluble fractions were combined for each replicate. InfernoRDN (omics.pnl.gov/software/infernordn) [33] was used to perform a Kruskal-Walis test to determine p-values and associated q-values to correct for background false discovery rate.

2.3 Results and Discussion

2.3.1 *Synechocystis* phenotypes across over several distinct light regimes

Measurement of *Synechocystis* growth rates under different light levels can reveal the different general phenotypical outcomes under different conditions [34]. Notably, under light limited conditions (40 and 80 µmol m^{-2} s^{-1}), simply increasing the light level almost linearly increases growth rate. Under light saturated growth (480 µmol m^{-2} s^{-1}), growth rate is maximized. Under light inhibited growth (960 µmol m^{-2} s^{-1}), the growth rate is slightly decreased because an excess of light generated radical oxygen species [35], [36]. As such, the growth profile as a function of light level typically results in a local maximum at light saturated growth (Figure 2.2).

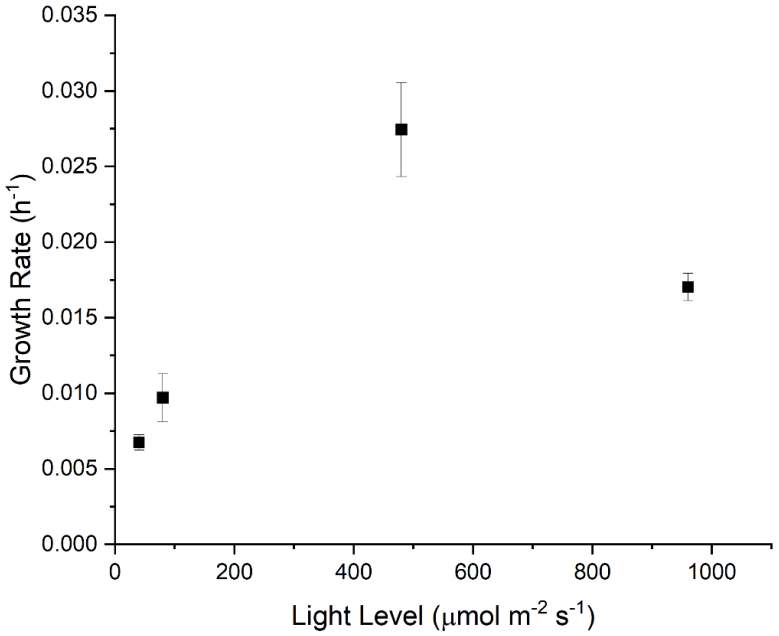

Figure 2.2 Measured growth rates (h^{-1}) as a function of light level (µmol m^{-2} s^{-1})

In a similar fashion, protein abundances both in and out of the Calvin cycle are shown to be partially light dependent. Although the overall total protein concentration of wild-type

cyanobacteria is thought to be relatively invariant [37], the individual enzyme levels of light harvesting complexes (LHC) and carbon fixation enzymes are not necessarily constant. For example, the relative abundances of LHC proteins detected appear to decrease as a function of light level (Figure A.1), corroborating prior proteomic studies [20], [34]. Contrastingly, the overall abundances of Calvin cycle enzymes tend to increase as a function of light level (Figure 2.3a), but this increase was not uniform across all enzymes.

A)

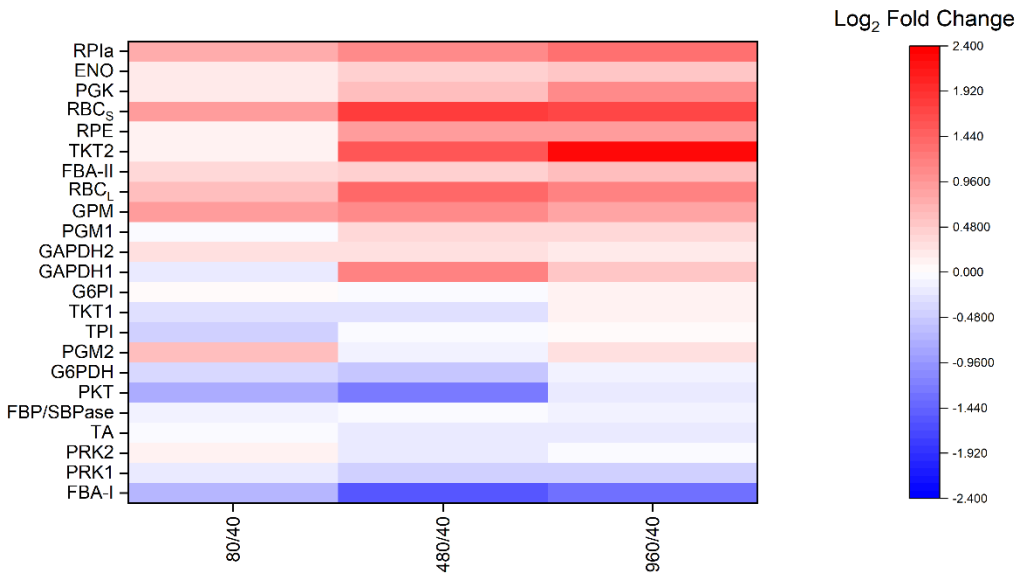

B)

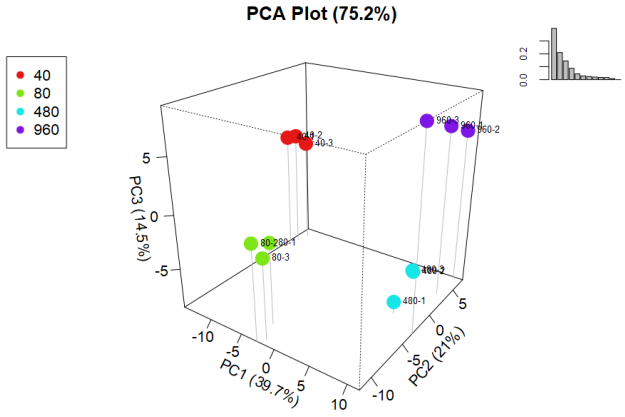

Figure 2.3 a) Average proteomic fold-change results relative to the 40 µmol m^{-2} s^{-1} condition for selected central carbon metabolism related enzymes, n = 3 for each light condition; b) Loadings for three dimensional principal component analysis

(Abbreviations: ENO, enolase; FBA-I/II, fructose-bisphosphate aldolase class I/II; FBP/SBPase, D-fructose 1,6-bisphosphatase class 2/sedoheptulose 1,7-bisphosphatase; G6PDH, glucose-6-phosphate 1-dehydrogenase; G6PI, glucose-6-phosphate isomerase; GAPDH, glyceraldehyde 3-phosphate dehydrogenase; GPM, phosphoglucomutase; PGK, phosphoglycerate kinase; PGM, phosphoglycerate mutase; PKT, phosphoketolase; PRK, phosphoribulokinase; RBCl, ribulose bisphosphate carboxylase large chain; RBCs, ribulose bisphosphate carboxylase small subunit; RPE, ribulose-phosphate 3-epimerase; RPIa, Ribose-5-phosphate isomerase A; TA, transaldolase; TKT, transketolase; TPI, triose-phosphate isomerase)

For isozymes, please refer to NCBI accession numbers: GAPDH1 (CAA60134.1), GAPDH2 (CAA60135.1), PRK1 (P37101.1), PRK2 (WP_010873279.1), TKT1 (WP_010871940.1), TKT2 (WP_010874098.1), PGM1 (WP_010871279.1), PGM2 (WP_010873603.1)

To enable visualization and aid in interpreting proteomic data, three-dimensional principal component analysis (PCA) was performed on the Calvin cycle enzymes. Under PCA, the close clustering of replicates (Figure 2.3b) can also be used as a general test of replicability.

While the majority of Calvin cycle enzymes did increase with respect to light level, at least some were insensitive or even decreased with respect to light level. This result largely corroborates previous proteomic studies [20], [34]. Enzymes such as RPIa, ENO, PGK, both subunits of RBC, RPE, TKT, FBA-II, GPM, PGM and GAPDH1 largely seem to be positively associated with light level and growth rate, which is expected in a light dependent carbon fixation pathway like the Calvin cycle. Additionally, the majority of detected abundances for photosystem subunits were negatively associated with light level, while TCA cycle enzyme abundances appeared to be largely unaffected (Figure A.1). G6PDH, FBA-I, and PKT are enzymes negatively associated with light level and growth rate. G6PDH, as the first step of the oxidative pentose phosphate pathway (OPPP), is known to be more active in the dark [8], [26]. Similarly, *Synechocystis* contains two FBA isozymes (Class I and Class II) [38], of which FBA-II is the dominant enzyme. This apparent dichotomy between FBA-I and FBA-II behavior is perhaps suggestive of the inherent plasticity of cyanobacterial metabolism, which in part relies on the differing efficacies of different protein isozymes under different conditions [39]. Finally, PKT which catalyzes an entry point into the tricarboxylic acid (TCA) cycle, is understandably negatively associated with light level because TCA cycle activity is minimal under photoautotrophic conditions [9], [26], which supports recent evidence that this pathway is inhibited by ATP, produced under light [40]. Previously, PKT was found to be non-essential, but slightly beneficial to growth rate during photoautotrophic conditions [9]. Interestingly, phosphoglycerate mutase (PGM) and enolase (ENO) do not share this behavior, despite also catalyzing an entry point into the TCA cycle. It was earlier speculated that PKT may

be able to improve the carbon efficiency since the phosphoketolase pathway requires a different stoichiometry that produces and requires slightly different amounts of cofactors [9]. The balance between the phosphoketolase-dependent pathway and the phosphoketolase-independent pathway may perhaps reflect a different ratio of cofactor production during different light levels.

To further quantify the relationship between metabolic fluxes and individual enzyme abundances, the Pearson correlation coefficient and associated p-value was calculated for each enzyme and its corresponding reaction (Table 1). Based on these results, the enzymes ENO, GAPDH1, RBC_L, PGM1, FBA-I, FBA-II, RPE and RBC_S have the highest correlations with their corresponding flux. In cases where a relationship between enzyme abundance and corresponding flux could be observed ($p < 0.1$), a "pseudo-flux control coefficient" (PFCC), $P^J_{E_i}$, was also calculated. In metabolic control analysis, a flux control coefficient, $C^J_{E_i}$, is the scaled infinitesimal change of flux, J, in response to some infinitesimal change in enzyme level, E_i, around a reference state [41].

$$P^J_{E_i} \approx C^J_{E_i} = \frac{dJ}{dE_i}\frac{E_i}{J}$$

Typically, a flux control coefficient is most accurate when only a single enzyme is perturbed and other enzyme abundances are held constant, a quality that is not met in these experimental conditions. Furthermore, due to a scarcity of data points, and because these experimental perturbations are not infinitesimal, these coefficient estimates are likely to be inaccurate [42]–[44], and do not abide by the summation or connectivity theorems typically applied in metabolic control analysis. As a result, we relied on an inexact approximation for the FCC, the PFCC, where these requirements are relaxed. PFCCs can be a useful way to determine if there is a strong relationship between flux and enzyme abundance around a reference state. In this case, the reference state was

chosen to be the 80 μmol m^{-2} s^{-1} steady state. The non-linear fitting method [45] was used to estimate the coefficients for each enzyme. In prior literature, enzymes with high flux control coefficients have been suggested as potential targets for overexpression [46], as they potentially offer high positive control over a pathway.

Table 2.1 Calculated Pearson R^2 and Pseudo-Flux Control Coefficients

Enzyme	Reaction	Pearson R^2	p	$P_{E_i}^J$
ENO	2PGA → PEP	0.99	0.01	3.0
GAPDH1	3PGA ↔GAP	0.98	0.02	1.6
RBC_L	RUBP + CO2 → 3PGA + 3PGA	0.96	0.04	1.6
PGM1	3PGA ↔ 2PGA	0.95	0.05	3.3
FBA-I	DHAP + GAP ↔ FBP	0.94	0.06	-0.9
FBA-II	DHAP + GAP ↔ FBP	0.93	0.07	2.1
RPE	RU5P ↔ X5P	0.90	0.10	2.6
RBC_S	RUBP + CO2 → 3PGA + 3PGA	0.90	0.10	1.1
TKT2	F6P ↔ E4P + EC2	0.85	0.15	
PRK1	RU5P → RUBP	0.85	0.15	
PRK2	RU5P → RUBP	0.83	0.17	
FBP/SBPase	FBP ↔ F6P	0.63	0.37	
RPIa	RU5P ↔ R5P	0.60	0.40	
PGK	3PGA ↔ GAP	0.51	0.49	
GAPDH2	3PGA ↔ GAP	0.50	0.50	
TKT2	S7P ↔ R5P + EC2	0.49	0.51	
G6PI	F6P ↔ G6P	0.47	0.53	
TPI	GAP ↔ DHAP	0.37	0.63	
TKT1	S7P ↔ R5P + EC2	0.36	0.64	
FBA-II	DHAP + E4P → SBP	0.24	0.76	
PGM2	S7P ↔ E4P + EC3	0.16	0.84	
FBP/SBPase	SBP → S7P	0.08	0.92	
TKT1	F6P ↔ E4P + EC2	0.04	0.96	

Of the selected enzymes, PGM1, ENO, RPE and FBA-II enzymes have the highest PFCCs, with FBA-II and both RBC subunits in particular corroborating experimental results which demonstrate enhanced growth rates in *Synechocystis* [47]. Interestingly, these PFCCs were often calculated to be above unity. In such cases, the flux increases proportionally more than the enzymatic abundance

around the reference state, indicating the presence of other confounding variables that positively affect flux. For instance, substrate concentrations may be altered after perturbation of light level, altering flux. Additionally, CBB cycle enzymes are known to adopt more active conformations as a result of redox-sensitive post-translational modifications [18], meaning that the same amount of enzyme concentration can support a larger flux under favorable reducing conditions. The flux control coefficient was not able to be calculated for enzymes where the correlation between enzyme abundance and flux were ambiguous or negligible (Table 1, $p > 0.1$), as it was not possible to perform any accurate non-linear fitting between *J* and *E*.

Based on correlation analysis, many enzyme abundances appear to be uncorrelated with their actual corresponding flux. Based on this data, the insensitivity of enzymes like GAPDH2, G6PI, TKT, TPI, FBP/SBPase, TA, and both isoforms of PRK may require further explanation. The isomerases (G6PI, TPI) have always been considered poor candidates for exerting control over the pathway based on kinetic parameters [48], having relatively favorable and rapid kinetics. The relatively insensitive behavior of GAPDH2 is also not unexpected when considering that the more photosynthetically active GAPDH1 isoform already exists and is positively associated with growth. However, TKT, FBP/SBPase and TA insensitivity are particularly unexplained results that imply that regulation of these reactions must not be controlled by enzymatic abundance. The effects of FBP/SBPase and TKT overexpression on *Synechocystis* metabolism is further explored in greater detail in a later chapter (3.3.1).

When there is little correlation between enzyme abundance and flux, PFCCs become difficult to meaningfully distinguish from zero, as the local slope around the reference steady state $\frac{dJ}{dE_i}$ can vary widely. One interpretation of uncorrelated or poorly correlated proteomic and fluxomic data is that these reactions are regulated at a post-translational level [49]. These results

appear to contradict previous results derived from kinetic models [16], [50] suggesting high flux control especially for PRK and FBP/SBPase, strongly implying that the control of these fluxes, at least in wild-type, are not based on enzyme abundances. Some alternative methods of regulation that could explain the changes in fluxes are discussed in the sections below (2.3.3-2.3.4).

The varying responses of enzymatic abundances to light level suggest that it is inaccurate to realistically model the Calvin cycle using only substrate changes as is common in earlier *in silico* kinetic models where Michaelis-Menten kinetics were sometimes employed with assumed constant V_{max} parameters [15], [17], [48]. These results also indicate that some enzymes are much more light-dependent than others despite being part of the same pathway, suggesting possible differences in regulatory behavior. In general, these results demonstrate an individualized enzyme abundance response to changes in light level. Rather than simply increasing the overall enzyme abundance across the board, this result is more consistent with a redistribution of enzyme abundances. These differences in sensitivity between CBB cycle enzymes and light level are not fully apparent when grouping enzymes broadly, as has been done in previous proteomic studies [20], [34].

2.3.2 Confirming the activity of the acetyl phosphate pathway under light

The acetyl phosphate (AP) pathway is a two step pathway connecting the Calvin cycle with the TCA cycle. It is well understood that carbon can enter the cyanobacterial TCA cycle through the conversion of pyruvate to acetyl-CoA through the NADPH-dependent pyruvate dehydrogenase complex, or with phosphoenolpyruvate carboxylase, which catalyzes the addition of bicarbonate with phosphoenolpyruvate to form oxaloacetate. Alternatively, the phosphoketolase (slr0453) pathway [9], which converts Calvin cycle intermediates X5P into GAP and AP or F6P into E4P and AP can also introduce carbon into the TCA cycle. AP is in a phosphate acetyltransferase

mediated equilibrium with acetyl-CoA. Previous literature has confirmed phosphoketolase pathway activity in heterotrophic or photomixotrophic conditions only, while its activity under photoautotrophic conditions was unconfirmed experimentally.

One straightforward application of a labelling experiment is to confirm the existence and activity of a pathway. As long as some labelling is observed, we can infer that the activity through the pathway is non-zero. We have included the phosphoketolase pathway in our photoautotrophic INST-MFA stoichiometric model after detecting isotopically labeled AP after the introduction of ^{13}C bicarbonate in photoautotrophic conditions (Figure 2.4). A phosphoketolase mutant (Δ0453) was simultaneously tested, from which we determined that while there was still labelling of acetyl phosphate, likely due to phosphate acetyltransferase activity, the measured pool size of acetyl phosphate was about an order of magnitude less. As a further negative control, a cyanobacteria thought to be lacking the phosphoketolase pathway, *Synechococcus* sp. PCC 7002 was also tested. No AP, labelled or otherwise, was measurably detected, as expected. It is likely that the presence of multiple pathways between the Calvin cycle and the TCA cycle provides additional plasticity [51] through which *Synechocystis* can maintain its metabolism. Notably, the phosphoketolase pathway does not produce any further energy in the form of ATP or NADPH, whereas the pyruvate

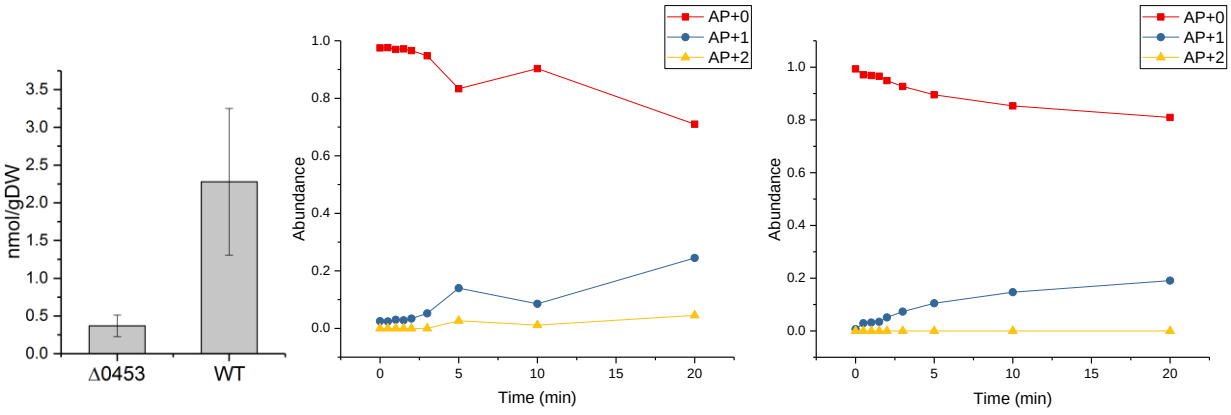

Figure 2.4 Measured AP pool sizes (left), and labeling dynamics under 80 μmol m^{-2} s^{-1} for WT (center) and Δ0453 (right)

dehydrogenase complex explicitly produces NADPH, while simultaneously losing a carbon in the form of CO_2. Depending on whether carbon or energy is more limited, having both pathways available provides the photosynthetic system a certain degree of metabolic flexibility.

The relatively slow labelling of AP suggests that the phosphoketolase pathway is largely inactivated in photoautotrophic conditions, but its non-zero labelling confirms this pathway's activity, nonetheless. To accommodate flux map comparisons between previous literature and newly obtained flux maps, a previously obtained photoautotrophic flux map [26] was refit with the newly added phosphoketolase reactions. However, the newly obtained wild type flux map was not significantly different because the predicted total flux through this pathway is near-zero. Thus, model stoichiometry was modified from prior literature to include phosphoketolase reactions [9], and a OgdA/SssA shunt which completes the cyanobacterial TCA cycle by conversion of α-ketoglutarate into succinate [52]. The previously hypothesized glyoxylate shunt [53] was excluded due to a lack of supporting evidence.

2.3.3 Thylakoid membrane localization of Calvin cycle enzymes can serve as an imperfect metabolite channel

Prior isotopic labelling studies have consistently found peculiar labelling kinetics where downstream metabolites in the Calvin cycle appear to be sometimes better labelled than their own precursors [26], [54]. A similar result was obtained in our own experiments across multiple light levels (Figure 2.5a). One likely explanation for this observation is that Calvin cycle appears to have some amount of metabolite channeling, a phenomenon where enzymes are organized into complexes or co-localized such that they can channel metabolites more directly to each other. When metabolite channeling occurs, the apparent local concentration of metabolites around enzymes can be higher than the bulk measured concentration, therefore increasing reaction rates

substantially [21]. On the other hand, metabolites generated throughout the Calvin cycle are also used in other pathways, so metabolites are not perfectly channeled directly into successive Calvin cycle enzymes.

In our own results, we found consistently lower ^{13}C labelling enrichments after 20 minutes between successive pairs of metabolites such as FBP and F6P, as well as RU5P and RUBP. These metabolites share the same carbons, so the observed result can only be reasonably explained if metabolite channeling exists. Metabolite channeling would result in a quickly labelled 'active' pool of metabolites representing those metabolites that are channeled, as well as a slowly labelled 'inactive' cytosolic pool that could dilute the overall labeling enrichment (Figure 2.5b). Mathematically, the presence of two different pools that are labelled at different rates can be accounted for in INST-MFA via the incorporation of dilution parameters to estimate the fractional size of the two pools [55]. This is mathematically analogous to having the same metabolite in two different compartments.

In summary, the formation of a metabolite channel can regulate flux for several reasons. Firstly, the local concentration of metabolites can be higher than the bulk concentration around the metabolite channel. Secondly, the kinetic parameters of thylakoid-bound enzymes can be significantly different from their soluble isoforms. Thirdly, a metabolite channel can result in separate cytosolic and thylakoid metabolite pools.

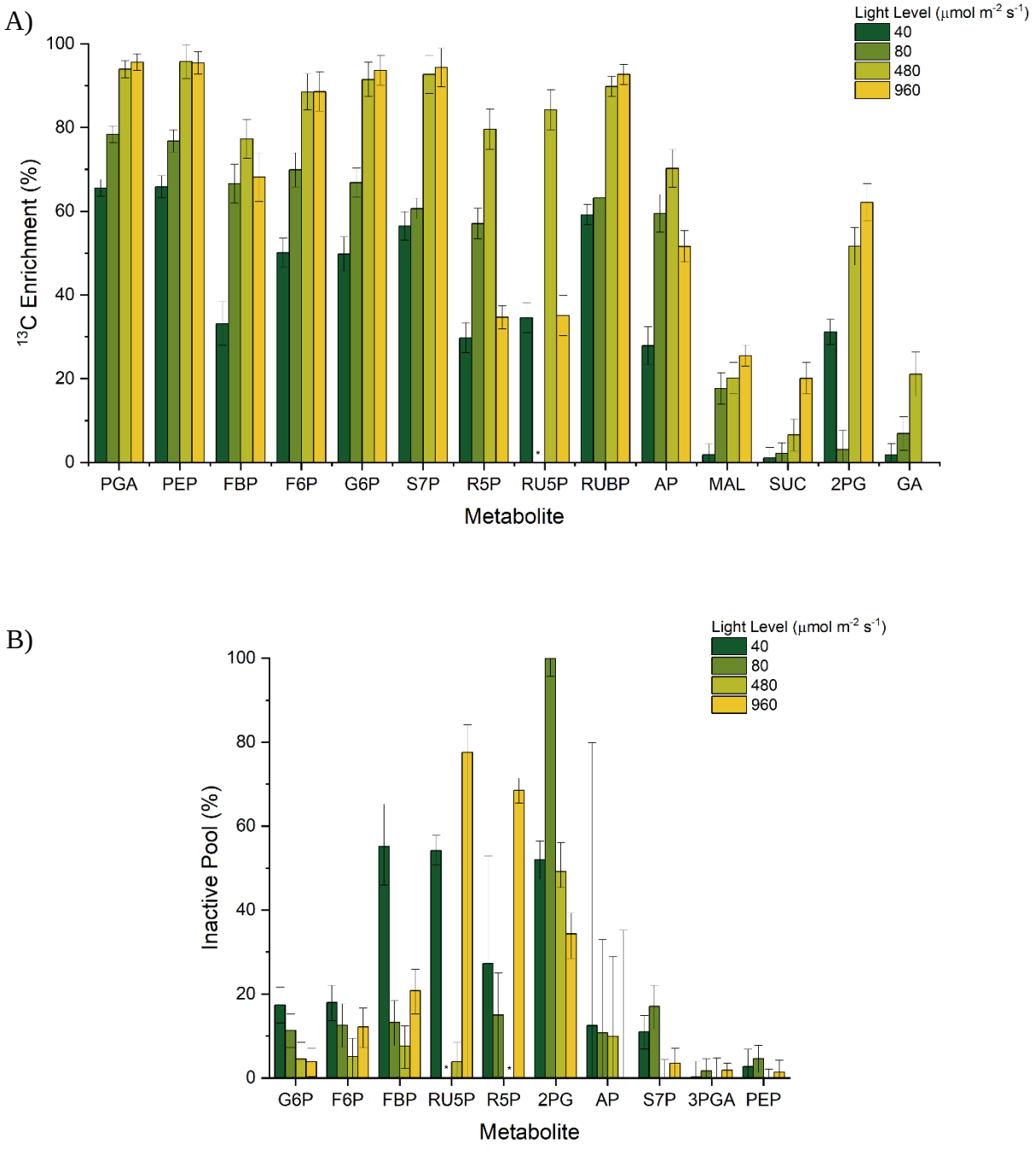

Figure 2.5 a) Measured ^{13}C enrichment 20 minutes after initial $NaH^{13}CO_3$ pulse, error bars represent standard error, and b) Estimated inactive pool sizes from INST-MFA, error bars represent the 95% confidence interval; * n.d.

A mechanistic explanation for metabolite channeling can be obtained by considering the localization of Calvin cycle enzymes around the thylakoid membranes as revealed by immunolabelling studies [56]–[58]. The thylakoid is an organelle present in both plants and cyanobacteria with high surface area where photosynthetic light dependent reactions typically occur. Specifically, both photosystems and the various pigments in photosynthetic organisms are localized to the thylakoid membrane, meaning that energetic cofactors like NADPH are generated around the thylakoid. As the Calvin cycle relies heavily on these cofactors, the localization of Calvin cycle enzymes on the thylakoid membrane helps to optimize these reactions by ensuring an abundance of cofactor availability. The localization of these enzymes can also help these enzymes interact quickly with the thioredoxin-ferredoxin system, allowing for quick transition between active and inactive post-translational states [18], an important trait that allows for quickly adapting to changing light conditions. The structural formation of these thylakoid membranes in both cyanobacteria and plants is interesting due to their tendency to stack themselves in parallel, forming a high surface area and low volume superstructure.

RPI, PRK, RuBisCO, PGK and GAPDH, which are five sequential enzymes in the Calvin cycle, were found to be preferentially localized on the exterior of the thylakoid membrane in *Synechocystis*. In a similar manner, aldolase, SBPase and FBPase were preferentially localized peripherally around the thylakoid membrane in pea leaves [59]–[62], even though these enzymes are also fully functional when tested *in vitro* without any membranes. We hypothesize that the stacked structure of these thylakoids, combined with the localization of these enzymes, can result in a diffusion limited condition where intermediates in the Calvin cycle are partially trapped, resulting in the observed ^{13}C enrichment pattern despite the fact that these substrates and enzymes are technically always contained in a single compartment.

Curiously, while our data indicated that metabolite channeling was likely to occur at all photoautotrophic conditions, the fractional size of the inactive pool is not constant across different light levels. In particular, the predicted inactive pool (Figure 2.5b) for RU5P is significantly higher at the light inhibiting condition (960 μmol m^{-2} s^{-1}) and slightly higher at the light limited conditions than at the light saturating condition (480 μmol m^{-2} s^{-1}), a result of the stark difference in RU5P enrichment (0.842 and 0.351 at 480 and 960 μmol m^{-2} s^{-1} respectively) even though the immediate product RUBP was similarly labelled (0.898 and 0.927 at 480 and 960 μmol m^{-2} s^{-1} respectively). To a lesser extent, this trend is also present for FBP and F6P enrichment. This result implies a movement of phosphoribulokinase (PRK) and FBP/SBPase to the cytosol to turn over the inactive cytosolic pool at highly reducing conditions. we infer from this data that the fractional active pool size is related to the redox environment of the cell. During light inhibiting conditions, the production of radical oxygen species can alter redox balance to favor oxidation [35]. Similarly, the lack of reducing cofactors during low light conditions also results in a non-optimal redox balance. It is only around the optimal light condition where redox conditions are ideal that PRK and FBP/SBPase most effectively turns over the pool of their respective substrates. Efforts to kinetically model the Calvin cycle should therefore incorporate these enzymes as isozymes, as thylakoid-bound enzymes likely have different kinetic parameters than their unbound forms.

2.3.4 Formation of the PRK/CP12/GAPDH complex further regulates the CBB cycle

PRK is notable for forming a multi-enzyme complex with GAPDH and the small protein CP12 [63]–[65]. This complex appears to be well conserved, appearing in both cyanobacteria and plants. This PRK/CP12/GAPDH complex is subject to a complicated redox regulation network [65] and forms under oxidizing conditions to inhibit both PRK and GAPDH activity. In *Synechocystis*, there exists two known GAPDH genes, *gap1* and *gap2*, with *gap2* being responsible for the largely

anabolic Calvin cycle activity, and *gap1* for the catabolic glycolytic activity [66]. On the other hand, our proteomic results suggest that both PRK and GAPDH2 abundance was counterintuitively insensitive to light level unlike the majority of Calvin cycle enzymes (Figure 2.3a), which is corroborated in another proteomic study [34]. Given that PRK and GAPDH fluxes are assuredly varying depending on the light level, we must conclude that the flux must be predominantly controlled by something other than enzymatic abundance. In general, these results suggested that the formation of PRK/CP12/GAPDH was a preferred way to regulate PRK and GAPDH activity.

During light-inhibiting conditions, the production of radical oxygen species becomes significant and may promote PRK/CP12/GAPDH formation similarly to a low light or dark condition, as reflected by a lower growth rate. Therefore, under light-inhibiting conditions where oxidative stress could be high, the formation of PRK/CP12/GAPDH complex can be an additional way to explain the reduced flux through PRK and GAPDH, because the PRK/CP12/GAPDH complex has much lowered activity as compared to the dimeric PRK or GAPDH alone [67]. Based on these findings, both the formation of metabolic channels and the formation of the PRK/CP12/GAPDH complex are coordinated by the redox environment (Figure 2.6).

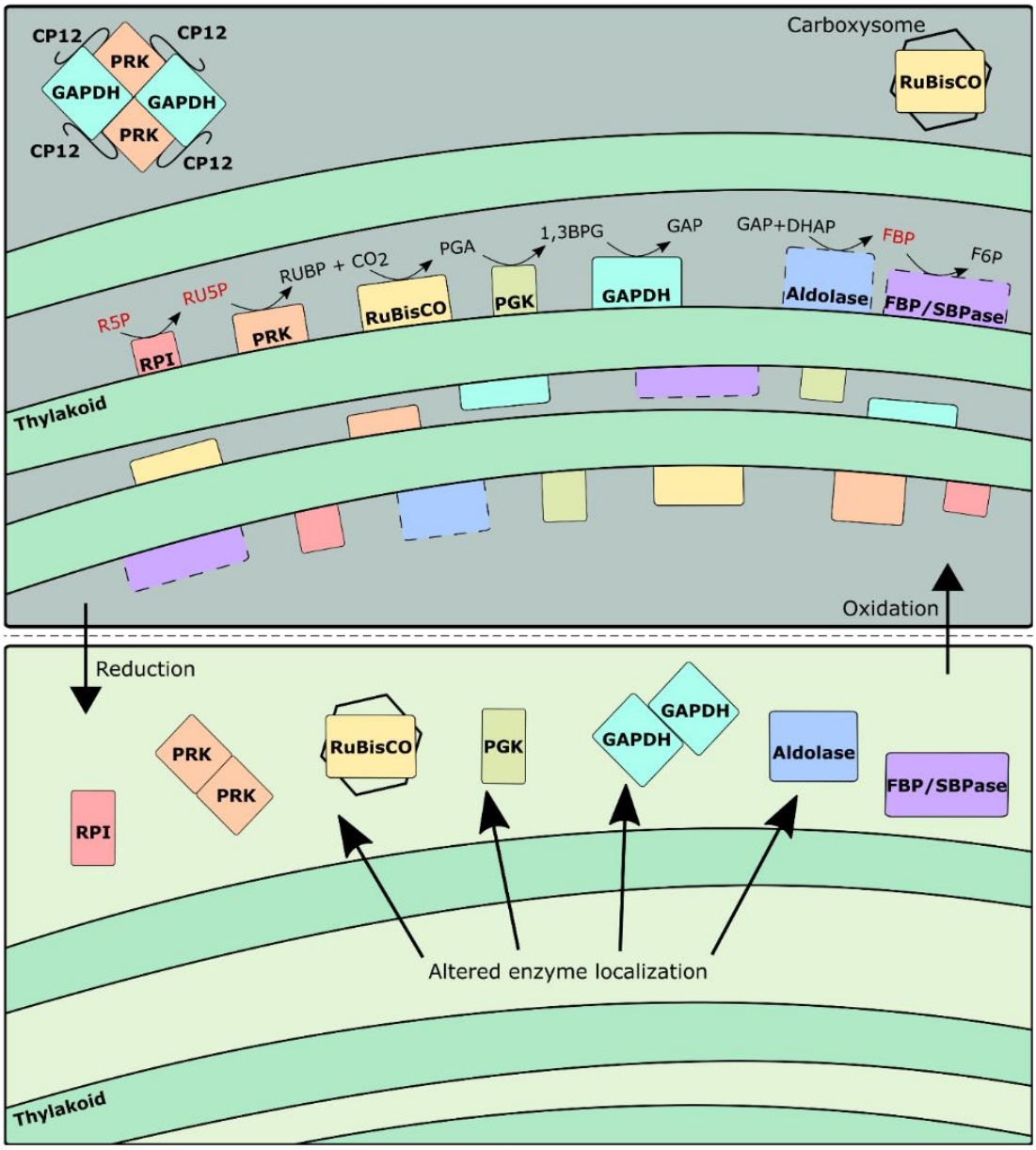

Figure 2.6 Schematic representing changes to enzyme localization and grouping as a function of redox environment. Dashed lines indicate enzymes not yet confirmed to be thylakoid-bound in *Synechocystis*. Metabolites in red indicate particularly large inactive pool fractions during oxidative conditions.

2.3.5 Carbon flux distribution varies slightly depending on light regime

It is possible to estimate fluxes in photosynthetic organisms using isotopic labelling approaches such as isotopically non-stationary metabolic flux analysis (INST-MFA) (2.2.3). The simplifying assumption that biomass composition is not significantly altered for WT cells under varying light levels was made. Unfortunately, the predicted relative flux distribution that was not statistically significantly different under different light conditions due to wide upper and lower bounds (Table 2.2 - Table 2.5).

Table 2.2 INST-MFA Estimated Fluxes for *Synechocystis* sp. PCC 6803 WT 40 µmol m^{-2} s^{-1}

SSR = 478.0 [408.1 527.7][a]

	Reaction	Value	LB [b]	UB [b]
CO2 net	CO2.x <-> CO2	102.5	102.5	102.5
RBC	RUBP.c + CO2 -> 3PGA.c + 3PGA.c + dummy	264.3	247.5	6241.7
GAPDH net	3PGA.c <-> GAP.c	552.5	480.6	11024.1
TPI net	GAP.c <-> DHAP.c	222.2	192.7	4418.6
FBP net	DHAP.c + GAP.c <-> FBP.c	214.8	182.4	4149.1
ALD	DHAP.c + E4P -> SBP.c	7.5	4.0	1235.5
PFK net	FBP.c <-> F6P.c	214.8	182.4	4149.1
SBP	SBP.c -> S7P.c	7.5	4.0	10.5
PGI net	F6P.c <-> G6P.c	10.2	6.2	21.5
G6PDH	G6P.c + dummy -> RU5P.c + CO2	4.0	0.0	15.4
TK1 net	X5P <-> GAP.c + EC2	-212.0	-4458.2	-187.3
TK2 net	F6P.c <-> E4P + EC2	107.3	94.7	2230.8
TK3 net	S7P.c <-> R5P.c + EC2	104.7	92.1	2218.1
TA1 net	F6P.c <-> GAP.c + EC3	97.3	N/A	1912.7
TA2 net	S7P.c <-> E4P + EC3	-97.3	-1912.7	N/A
PKT1	X5P -> GAP.c + AP.c	0.0	0.0	40498.0
PKT2	F6P.c -> E4P + AP.c	0.0	0.0	N/A
PTA net	AP.c <-> ACA	0.0	0.0	40140.8
PPE net	RU5P.c <-> X5P	-212.0	-230.4	-186.8
PPI net	RU5P.c <-> R5P.c	-101.0	-2226.1	-88.4
PRK	RU5P.c -> RUBP.c	317.1	275.0	6699.1
PGM net	3PGA.c <-> 2PGA	50.0	24.8	1968.5
ENO	2PGA -> PEP.c	50.0	24.8	1968.5
PK	PEP.c -> PYR	31.4	0.0	1968.9
PDH	PYR + dummy -> ACA + CO2	25.2	0.0	1943.7
CS	OAA + ACA -> CIT	6.4	6.4	1942.1
ACO net	CIT <-> ICI	6.4	6.4	1942.1
IDH	ICI + dummy -> AKG + CO2	6.4	6.4	1942.1
OGDA	AKG + dummy -> SSA + CO2	0.0	0.0	1935.7
SSAD	SSA -> SUC	0.0	0.0	1935.7
SDH net	SUC <-> FUM	0.0	0.0	1935.7
FUM net	FUM <-> MAL	3.5	3.5	1939.3
MDH net	MAL <-> OAA	3.5	-27.8	1937.1
ME	MAL + dummy -> PYR + CO2	0.0	0.0	1797.8
PPC	PEP.c + CO2 -> OAA + dummy	13.4	13.4	1811.2
RBOX	RUBP.c -> 3PGA.c + 2PG.c	52.8	27.5	70.6
PGP	2PG.c -> GLC	52.8	27.5	70.6
GDH	GLC -> GLY	52.8	27.5	70.6
GDC net	GLY + GLY + dummy <-> SER + CO2	25.5	12.8	34.3
SGA	SER -> GA	23.8	11.1	32.6

Table 2.2 continued

GK	GA -> 3PGA.c	23.8	11.1	32.6
Growth	0.715*R5P.c + 3.624*ACA + 1.191*G6P.c + 0.501*E4P + 0.511*3PGA.c + 1.002*PEP.c + 1.197*PYR + 2.039*OAA + 1.233*AKG + 0.133*GAP.c + 0.33*SER + 0.364*GLY + 1.017*dummy -> Biomass + 0.683*FUM	5.2	5.2	5.2
R1	dummy -> Sink	100.0	100.0	100.0
R22	G6P -> Sink	100.0	100.0	100.0
R2	F6P -> Sink	100.0	100.0	100.0
R3	FBP -> Sink	100.0	100.0	100.0
R4	GAP -> Sink	100.0	100.0	100.0
R5	DHAP -> Sink	100.0	100.0	100.0
R23	RU5P -> Sink	100.0	100.0	100.0
R6	R5P -> Sink	100.0	100.0	100.0
R7	2PG -> Sink	100.0	100.0	100.0
R26	AP -> Sink	100.0	100.0	100.0
R29	S7P -> Sink	100.0	100.0	100.0
R32	3PGA -> Sink	100.0	100.0	100.0
R35	PEP -> Sink	100.0	100.0	100.0
R38	RUBP -> Sink	100.0	100.0	100.0
R41	SBP -> Sink	100.0	100.0	100.0
R20	0*G6P.c -> G6P	82.6	78.4	86.9
R21	0*G6P.x -> G6P	17.4	13.1	21.6
R8	0*F6P.c -> F6P	82.0	78.0	86.4
R9	0*F6P.x -> F6P	18.0	13.6	22.0
R10	0*FBP.c -> FBP	44.9	34.8	54.1
R11	0*FBP.x -> FBP	55.1	45.9	65.2
R24	0*RU5P.c -> RU5P	45.8	42.2	49.2
R25	0*RU5P.x -> RU5P	54.2	50.8	57.8
R16	0*R5P.c -> R5P	72.7	47.1	100.0
R17	0*R5P.x -> R5P	27.3	0.0	52.9
R18	0*2PG.c -> 2PG	48.0	43.6	52.7
R19	0*2PG.x -> 2PG	52.0	47.3	56.4
R27	0*AP.c -> AP	87.5	20.2	100.0
R28	0*AP.x -> AP	12.5	0.0	79.8
R30	0*S7P.c -> S7P	89.0	85.1	93.1
R31	0*S7P.x -> S7P	11.0	6.9	14.9
R33	0*3PGA.c -> 3PGA	99.8	96.0	100.0
R34	0*3PGA.x -> 3PGA	0.2	0.0	4.0
R36	0*PEP.c -> PEP	97.3	93.2	100.0
R37	0*PEP.x -> PEP	2.7	0.0	6.8

Table 2.2 continued

R39	0*RUBP.c -> RUBP	5.5	0.0	100.0
R40	0*RUBP.x -> RUBP	94.5	0.0	100.0
R42	0*SBP.c -> SBP	76.7	0.0	100.0
R43	0*SBP.x -> SBP	23.3	0.0	100.0

[a] Sum of squared residuals (SSR), and the expected range in square brackets [$\chi^2_{a/2}$ (n – p), $\chi^2_{1-a/2}$ (n – p)]

[b] Lower bounds (LB) and upper bounds (UB) represent the 95% CI as determined via the parameter continuation method

Table 2.3 INST-MFA Estimated Fluxes for *Synechocystis* sp. PCC 6803 WT 80 µmol m^{-2} s^{-1}

SSR = 411.6 [375.4 490.4][a]

	Reaction	Value	LB [b]	UB [b]
CO2 net	CO2.x <-> CO2	330.4	330.4	330.4
RBC	RUBP.c + CO2 -> 3PGA.c + 3PGA.c + dummy	379.6	N/A	408.0
GAPDH net	3PGA.c <-> GAP.c	743.7	654.2	844.6
TPI net	GAP.c <-> DHAP.c	298.1	265.5	54264.9
FBP net	DHAP.c + GAP.c <-> FBP.c	294.3	252.9	342.4
ALD	DHAP.c + E4P -> SBP.c	3.8	0.0	10.4
PFK net	FBP.c <-> F6P.c	294.3	252.9	342.4
SBP	SBP.c -> S7P.c	3.8	0.0	10.4
PGI net	F6P.c <-> G6P.c	9.4	9.4	24.0
G6PDH	G6P.c + dummy -> RU5P.c + CO2	0.0	0.0	14.6
TK1 net	X5P <-> GAP.c + EC2	-288.7	-53865.2	-254.3
TK2 net	F6P.c <-> E4P + EC2	146.3	128.8	26871.0
TK3 net	S7P.c <-> R5P.c + EC2	142.4	125.3	27109.9
TA1 net	F6P.c <-> GAP.c + EC3	138.6	102.2	23278.6
TA2 net	S7P.c <-> E4P + EC3	-138.6	-23278.6	-102.2
PKT1	X5P -> GAP.c + AP.c	0.0	0.0	N/A
PKT2	F6P.c -> E4P + AP.c	0.0	0.0	N/A
PTA net	AP.c <-> ACA	0.0	0.0	N/A
PPE net	RU5P.c <-> X5P	-288.7	-321.1	N/A
PPI net	RU5P.c <-> R5P.c	-136.7	-26758.2	-119.8
PRK	RU5P.c -> RUBP.c	425.5	N/A	483.1
PGM net	3PGA.c <-> 2PGA	76.2	37.8	N/A
ENO	2PGA -> PEP.c	76.2	37.8	N/A
PK	PEP.c -> PYR	47.8	0.0	N/A
PDH	PYR + dummy -> ACA + CO2	38.4	0.0	N/A
CS	OAA + ACA -> CIT	9.7	9.7	26730.1
ACO net	CIT <-> ICI	9.7	9.7	26730.1
IDH	ICI + dummy -> AKG + CO2	9.7	9.7	26730.1
OGDA	AKG + dummy -> SSA + CO2	0.0	0.0	26720.4
SSAD	SSA -> SUC	0.0	0.0	26720.4
SDH net	SUC <-> FUM	0.0	0.0	26720.4
FUM net	FUM <-> MAL	5.4	5.4	26725.9
MDH net	MAL <-> OAA	5.4	-42.4	26723.0
ME	MAL + dummy -> PYR + CO2	0.0	0.0	17171.2
PPC	PEP.c + CO2 -> OAA + dummy	20.5	20.5	17191.5
RBOX	RUBP.c -> 3PGA.c + 2PG.c	45.9	12.5	85.8
PGP	2PG.c -> GLC	45.9	12.5	85.8
GDH	GLC -> GLY	45.9	12.5	85.8
GDC net	GLY + GLY + dummy <-> SER + CO2	21.5	4.8	41.4
SGA	SER -> GA	18.9	2.2	38.8
GK	GA -> 3PGA.c	18.9	2.2	38.8

Table 2.3 continued

Growth1	0.715*R5P.c + 3.624*ACA + 1.191*G6P.c + 0.501*E4P + 0.511*3PGA.c + 1.002*PEP.c + 1.197*PYR + 2.039*OAA + 1.233*AKG + 0.133*GAP.c + 0.33*SER + 0.364*GLY + 1.017*dummy -> Biomass + 0.683*FUM	7.9	7.9	7.9
R1	dummy -> Sink	100.0	100.0	100.0
R22	G6P -> Sink	100.0	100.0	100.0
R2	F6P -> Sink	100.0	100.0	100.0
R3	FBP -> Sink	100.0	100.0	100.0
R4	GAP -> Sink	100.0	100.0	100.0
R5	DHAP -> Sink	100.0	100.0	100.0
R23	RU5P -> Sink	100.0	100.0	100.0
R6	R5P -> Sink	100.0	100.0	100.0
R7	2PG -> Sink	100.0	100.0	100.0
R26	AP -> Sink	100.0	100.0	100.0
R29	S7P -> Sink	100.0	100.0	100.0
R32	3PGA -> Sink	100.0	100.0	100.0
R35	PEP -> Sink	100.0	100.0	100.0
R38	RUBP -> Sink	100.0	100.0	100.0
R41	SBP -> Sink	100.0	100.0	100.0
R20	0*G6P.c -> G6P	88.6	84.8	92.7
R21	0*G6P.x -> G6P	11.4	7.3	15.2
R8	0*F6P.c -> F6P	87.4	82.4	92.7
R9	0*F6P.x -> F6P	12.6	7.3	17.6
R10	0*FBP.c -> FBP	86.8	81.6	92.3
R11	0*FBP.x -> FBP	13.2	7.7	18.4
R24	0*RU5P.c -> RU5P	16.8	0.0	100.0
R25	0*RU5P.x -> RU5P	83.2	0.0	100.0
R16	0*R5P.c -> R5P	85.0	75.0	99.6
R17	0*R5P.x -> R5P	15.0	0.4	25.0
R18	0*2PG.c -> 2PG	0.0	0.0	4.3
R19	0*2PG.x -> 2PG	100.0	95.7	100.0
R27	0*AP.c -> AP	89.3	67.0	100.0
R28	0*AP.x -> AP	10.7	0.0	33.0
R30	0*S7P.c -> S7P	82.9	78.0	88.4
R31	0*S7P.x -> S7P	17.1	11.6	22.0
R33	0*3PGA.c -> 3PGA	98.3	95.4	100.0
R34	0*3PGA.x -> 3PGA	1.7	0.0	4.6
R36	0*PEP.c -> PEP	95.4	92.2	98.7
R37	0*PEP.x -> PEP	4.6	1.3	7.8
R39	0*RUBP.c -> RUBP	50.1	0.0	100.0

Table 2.3 continued

R40	0*RUBP.x -> RUBP	49.9	0.0	100.0
R42	0*SBP.c -> SBP	39.4	0.0	100.0
R43	0*SBP.x -> SBP	60.6	0.0	100.0

[a] Sum of squared residuals (SSR), and the expected range in square brackets [$\chi^2_{a/2}$ (n – p), $\chi^2_{1-a/2}$ (n – p)]

[b] Lower bounds (LB) and upper bounds (UB) represent the 95% CI as determined via the parameter continuation method

Table 2.4 INST-MFA Estimated Fluxes for *Synechocystis* sp. PCC 6803 WT 480 µmol m^{-2} s^{-1}

SSR = 424.6 [325.1 432.7][a]

	Reaction	Value	LB [b]	UB [b]
CO2 net	CO2.x <-> CO2	570.4	570.4	570.4
RBC	RUBP.c + CO2 -> 3PGA.c + 3PGA.c + dummy	1047.3	571.0	N/A
GAPDH net	3PGA.c <-> GAP.c	2078.9	1126.4	N/A
TPI net	GAP.c <-> DHAP.c	913.9	479.0	18697.1
FBP net	DHAP.c + GAP.c <-> FBP.c	491.3	191.0	86109.3
ALD	DHAP.c + E4P -> SBP.c	422.7	0.0	8710.5
PFK net	FBP.c <-> F6P.c	491.3	191.0	86109.3
SBP	SBP.c -> S7P.c	422.7	0.0	8738.9
PGI net	F6P.c <-> G6P.c	16.2	16.2	330.8
G6PDH	G6P.c + dummy -> RU5P.c + CO2	0.0	0.0	314.5
TK1 net	X5P <-> GAP.c + EC2	-699.0	-28604.0	-366.9
TK2 net	F6P.c <-> E4P + EC2	253.6	153.7	8921.4
TK3 net	S7P.c <-> R5P.c + EC2	445.4	213.2	43943.9
TA1 net	F6P.c <-> GAP.c + EC3	22.7	22.7	39864.9
TA2 net	S7P.c <-> E4P + EC3	-22.7	-39864.9	-22.7
PKT1	X5P -> GAP.c + AP.c	4.4	0.0	6649.3
PKT2	F6P.c -> E4P + AP.c	198.6	0.0	5069.1
PTA net	AP.c <-> ACA	203.0	0.0	6058.9
PPE net	RU5P.c <-> X5P	-694.7	-21707.6	-366.9
PPI net	RU5P.c <-> R5P.c	-435.7	-14270.9	-217.8
PRK	RU5P.c -> RUBP.c	1130.3	615.5	23070.4
PGM net	3PGA.c <-> 2PGA	126.2	65.3	10267.0
ENO	2PGA -> PEP.c	126.2	65.3	10267.0
PK	PEP.c -> PYR	28.9	0.0	6609.3
PDH	PYR + dummy -> ACA + CO2	60.9	0.0	10201.3
CS	OAA + ACA -> CIT	214.5	16.8	7889.7
ACO net	CIT <-> ICI	214.5	16.8	7889.7
IDH	ICI + dummy -> AKG + CO2	214.5	16.8	7889.7
OGDA	AKG + dummy -> SSA + CO2	197.7	0.0	7873.0
SSAD	SSA -> SUC	197.7	0.0	7873.0
SDH net	SUC <-> FUM	197.7	0.0	7873.0
FUM net	FUM <-> MAL	207.0	9.3	7882.5
MDH net	MAL <-> OAA	158.7	-66.2	36821.0
ME	MAL + dummy -> PYR + CO2	48.4	0.0	5269.3
PPC	PEP.c + CO2 -> OAA + dummy	83.7	35.3	5304.6
RBOX	RUBP.c -> 3PGA.c + 2PG.c	83.1	42.0	1126.9
PGP	2PG.c -> GLC	83.1	42.0	1126.9
GDH	GLC -> GLY	83.1	42.0	1126.9
GDC net	GLY + GLY + dummy <-> SER + CO2	39.1	18.5	561.0
SGA	SER -> GA	34.6	14.0	556.5
GK	GA -> 3PGA.c	34.6	14.0	556.5

Table 2.4 continued

Growth1	0.715*R5P.c + 3.624*ACA + 1.191*G6P.c + 0.501*E4P + 0.511*3PGA.c + 1.002*PEP.c + 1.197*PYR + 2.039*OAA + 1.233*AKG + 0.133*GAP.c + 0.33*SER + 0.364*GLY + 1.017*dummy -> Biomass + 0.683*FUM	13.6	13.6	13.6
R1	dummy -> Sink	100	100	100
R22	G6P -> Sink	100	100	100
R2	F6P -> Sink	100	100	100
R3	FBP -> Sink	100	100	100
R4	GAP -> Sink	100	100	100
R5	DHAP -> Sink	100	100	100
R23	RU5P -> Sink	100	100	100
R6	R5P -> Sink	100	100	100
R7	2PG -> Sink	100	100	100
R26	AP -> Sink	100	100	100
R29	S7P -> Sink	100	100	100
R32	3PGA -> Sink	100	100	100
R35	PEP -> Sink	100	100	100
R38	RUBP -> Sink	100	100	100
R41	SBP -> Sink	100	100	100
R20	0*G6P.c -> G6P	95.5	91.6	100
R21	0*G6P.x -> G6P	4.5	0	8.4
R8	0*F6P.c -> F6P	94.9	90.5	100
R9	0*F6P.x -> F6P	5.1	0	9.5
R10	0*FBP.c -> FBP	92.4	87.6	97.7
R11	0*FBP.x -> FBP	7.6	2.3	12.4
R24	0*RU5P.c -> RU5P	96.1	91.6	100
R25	0*RU5P.x -> RU5P	3.9	0	8.4
R16	0*R5P.c -> R5P	47.5	0	100
R17	0*R5P.x -> R5P	52.5	0	100
R18	0*2PG.c -> 2PG	50.8	44	54.7
R19	0*2PG.x -> 2PG	49.2	45.3	56
R27	0*AP.c -> AP	90.1	71.1	100
R28	0*AP.x -> AP	9.9	0	28.9
R30	0*S7P.c -> S7P	99.9	95.6	100
R31	0*S7P.x -> S7P	0.1	0	4.4
R33	0*3PGA.c -> 3PGA	100	95.3	100
R34	0*3PGA.x -> 3PGA	0.00E+00	0	4.7
R36	0*PEP.c -> PEP	100	97.9	100
R37	0*PEP.x -> PEP	0.00E+00	0	2.1
R39	0*RUBP.c -> RUBP	2.3	0	100

Table 2.4 continued

R40	0*RUBP.x -> RUBP	97.7	0	100
R42	0*SBP.c -> SBP	45	0	100
R43	0*SBP.x -> SBP	55	0	100

[a] Sum of squared residuals (SSR), and the expected range in square brackets [$\chi^2_{a/2}$ (n – p), $\chi^2_{1-a/2}$ (n – p)]

[b] Lower bounds (LB) and upper bounds (UB) represent the 95% CI as determined via the parameter continuation method

Table 2.5 INST-MFA Estimated Fluxes for *Synechocystis* sp. PCC 6803 WT 960 µmol m^{-2} s^{-1}

SSR = 460.0 [416.5 537.3][a]

	Reaction	Value	LB [b]	UB [b]
CO2 net	CO2.x <-> CO2	593.8	593.8	593.8
RBC	RUBP.c + CO2 -> 3PGA.c + 3PGA.c + dummy	664.9	638.5	7731.8
GAPDH net	3PGA.c <-> GAP.c	1250.5	1154.1	13501.3
TPI net	GAP.c <-> DHAP.c	501.5	479.9	5448.6
FBP net	DHAP.c + GAP.c <-> FBP.c	501.4	478.0	5278.5
ALD	DHAP.c + E4P -> SBP.c	0.1	0.0	12159.4
PFK net	FBP.c <-> F6P.c	501.4	478.0	5278.5
SBP	SBP.c -> S7P.c	0.1	0.0	12209.8
PGI net	F6P.c <-> G6P.c	16.9	16.9	48.1
G6PDH	G6P.c + dummy -> RU5P.c + CO2	0.0	0.0	31.2
TK1 net	X5P <-> GAP.c + EC2	-484.5	-5243.7	-463.0
TK2 net	F6P.c <-> E4P + EC2	245.8	235.1	2650.0
TK3 net	S7P.c <-> R5P.c + EC2	238.7	222.2	2613.2
TA1 net	F6P.c <-> GAP.c + EC3	238.7	222.0	2571.8
TA2 net	S7P.c <-> E4P + EC3	-238.7	-2571.8	-222.0
PKT1	X5P -> GAP.c + AP.c	0.1	0.0	263.2
PKT2	F6P.c -> E4P + AP.c	0.0	0.0	16.1
PTA net	AP.c <-> ACA	0.1	0.0	262.1
PPE net	RU5P.c <-> X5P	-484.4	-5369.1	-437.9
PPI net	RU5P.c <-> R5P.c	-228.6	-2639.0	-211.8
PRK	RU5P.c -> RUBP.c	712.9	667.6	7785.7
PGM net	3PGA.c <-> 2PGA	136.8	117.8	2322.4
ENO	2PGA -> PEP.c	136.8	117.8	2322.4
PK	PEP.c -> PYR	85.8	26.1	1174.3
PDH	PYR + dummy -> ACA + CO2	68.8	49.8	2254.4
CS	OAA + ACA -> CIT	17.5	17.5	2216.6
ACO net	CIT <-> ICI	17.5	17.5	2216.6
IDH	ICI + dummy -> AKG + CO2	17.5	17.5	2216.6
OGDA	AKG + dummy -> SSA + CO2	0.0	0.0	2199.1
SSAD	SSA -> SUC	0.0	0.0	2199.1
SDH net	SUC <-> FUM	0.0	0.0	2199.1
FUM net	FUM <-> MAL	9.7	9.7	2208.8
MDH net	MAL <-> OAA	9.7	-45.6	1183.6
ME	MAL + dummy -> PYR + CO2	0.0	0.0	1192.1
PPC	PEP.c + CO2 -> OAA + dummy	36.8	36.8	1228.9
RBOX	RUBP.c -> 3PGA.c + 2PG.c	48.1	14.5	370.7
PGP	2PG.c -> GLC	48.1	14.5	370.7
GDH	GLC -> GLY	48.1	14.5	370.7
GDC net	GLY + GLY + dummy <-> SER + CO2	21.5	4.7	182.8
SGA	SER -> GA	16.8	0.0	178.1
GK	GA -> 3PGA.c	16.8	0.0	178.1

Table 2.5 continued

Growth1	0.715*R5P.c + 3.624*ACA + 1.191*G6P.c + 0.501*E4P + 0.511*3PGA.c + 1.002*PEP.c + 1.197*PYR + 2.039*OAA + 1.233*AKG + 0.133*GAP.c + 0.33*SER + 0.364*GLY + 1.017*dummy -> Biomass + 0.683*FUM	14.2	14.2	14.2
R1	dummy -> Sink	100	100	100
R22	G6P -> Sink	100	100	100
R2	F6P -> Sink	100	100	100
R3	FBP -> Sink	100	100	100
R4	GAP -> Sink	100	100	100
R5	DHAP -> Sink	100	100	100
R23	RU5P -> Sink	100	100	100
R6	R5P -> Sink	100	100	100
R7	2PG -> Sink	100	100	100
R26	AP -> Sink	100	100	100
R29	S7P -> Sink	100	100	100
R32	3PGA -> Sink	100	100	100
R35	PEP -> Sink	100	100	100
R38	RUBP -> Sink	100	100	100
R41	SBP -> Sink	100	100	100
R20	0*G6P.c -> G6P	96.2	92.9	99.7
R21	0*G6P.x -> G6P	3.8	0.3	7.1
R8	0*F6P.c -> F6P	87.9	83.3	92.9
R9	0*F6P.x -> F6P	12.1	7.1	16.7
R10	0*FBP.c -> FBP	79.2	74.1	84.8
R11	0*FBP.x -> FBP	20.8	15.2	25.9
R24	0*RU5P.c -> RU5P	22.4	15.9	100
R25	0*RU5P.x -> RU5P	77.6	0	84.1
R16	0*R5P.c -> R5P	31.5	28.6	34.5
R17	0*R5P.x -> R5P	68.5	65.5	71.4
R18	0*2PG.c -> 2PG	65.7	60.7	71.5
R19	0*2PG.x -> 2PG	34.3	28.5	39.3
R27	0*AP.c -> AP	100	64.8	100
R28	0*AP.x -> AP	0.00E+00	0	35.2
R30	0*S7P.c -> S7P	96.5	92.9	100
R31	0*S7P.x -> S7P	3.5	0	7.1
R33	0*3PGA.c -> 3PGA	98.2	96.5	99.9
R34	0*3PGA.x -> 3PGA	1.8	0.1	3.5
R36	0*PEP.c -> PEP	98.6	95.8	100
R37	0*PEP.x -> PEP	1.4	0	4.2
R39	0*RUBP.c -> RUBP	73.7	0.00E+00	100

Table 2.5 continued

R40	0*RUBP.x -> RUBP	26.3	0	100
R42	0*SBP.c -> SBP	46.6	0	100
R43	0*SBP.x -> SBP	53.4	0	100

[a] Sum of squared residuals (SSR), and the expected range in square brackets [$\chi^2_{a/2}$ (n – p), $\chi^2_{1-a/2}$ (n – p)]

[b] Lower bounds (LB) and upper bounds (UB) represent the 95% CI as determined via the parameter continuation method

In comparison with earlier INST-MFA flux maps [26], [68], [69], these error bounds were much larger, likely due to the addition of more allowed inactive pools in the stoichiometric model. This contrasts with the estimated active and inactive fractional pool sizes of the metabolites themselves, which are frequently significantly different (Figure 2.5b). In general, it is difficult to statistically differentiate between small Calvin cycle fluxes due to relatively large error bounds. This indicates that relative carbon flux can be constantly regulated to partition itself into the different biomass components regardless of the light level.

This result implies a level of regulation inherent in the internal machinery of *Synechocystis*, consistent with the idea that Calvin cycle fluxes are well regulated [51]. Although slightly more flux was estimated for throughout the TCA cycle during light saturating conditions, even this difference is not significantly different. Similarly, a slight increase in labelling of the photorespiration intermediates 2PG and GA is observed at saturating and light inhibiting conditions, but photorespiration fluxes are again poorly resolved due to its relatively low values as compared to the CBB cycle. Such a result indirectly supports the notion that photorespiration may serve as a way to protect against oxidative stress [12]. We note that predicted photorespiration activity has non-zero lower bounds even under low light conditions, corroborating prior literature [70], [71]. Furthermore, as shown in flux maps [72] and in previous genome scale modeling [73], photorespiration can be beneficial for high light photosynthesis, and was also found to play an

important role during maximal *Synechococcus elongatus* UTEX 2973 growth [72], despite carbon loss.

It is additionally possible to estimate absolute flux values (Figure 2.7) by correlating carbon fixating reactions (specifically, RuBisCO and PPC reactions) to growth rate (h^{-1}), assuming 0.0412 mol C gDW^{-1} based on the WT biomass equation.

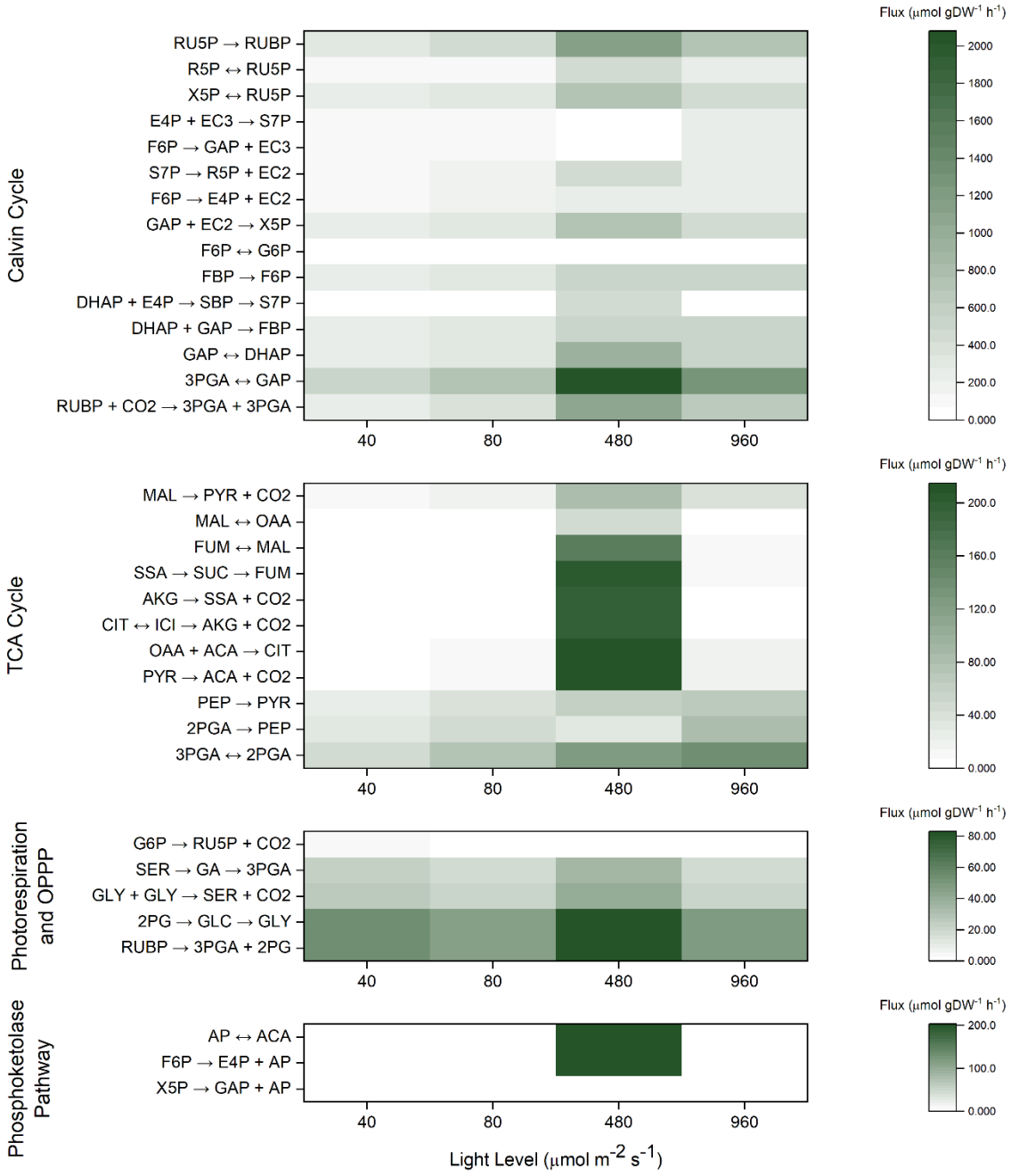

Figure 2.7 Heat map for best fit absolute flux values (µmol h^{-1}) across all four light levels

Therefore, even small changes in inactive pool sizes can result in large differences in absolute flux. Metabolomic studies confirm significant changes in intermediates across the diurnal

cycle to maximize growth during the day [74], [75]. The ability to modulate the fractional size of active intermediates during different light conditions provide an additional means to control the rate of CBB cycle reactions.

2.4 Conclusions

The abundance of many, but not all, Calvin cycle enzymes are well correlated with light levels. Therefore, not all reactions in the Calvin cycle are regulated by enzymatic abundance. The formation of metabolite channels is one potential additional method of regulation. Carbon enrichment data taken across different light levels indicate the presence of metabolite channeling within the Calvin cycle, especially for PRK and FBP/SBPase. Cyanobacteria possess the ability to localize Calvin cycle enzymes around the thylakoid membrane, potentially resulting in altered reaction kinetics and changes to the active pool sizes of Calvin cycle intermediates. The localization of Calvin cycle enzymes can easily influence the proportion of active and inactive metabolite pool sizes, and may help explain why kinetic models of the Calvin cycle often predict a set of stable fluxes even when metabolite pool sizes vary by several orders of magnitude [16].

While the exact mechanisms remain unclear, it is apparent that the fraction of the inactive pool is a variable factor that was minimized under high growth rates, and therefore may be a future target for metabolic engineering. For example, localization of enzymes onto membranes to form microdomains was able to enhance the production of N-acetylglucosamine in *Bacillus subtilus* [76]. Such a metabolic engineering approach is interesting because the spatial organization of these enzymes are orthogonal to other more typical genetic engineering approaches like overexpressions or knockdowns of genes. The localization of enzymes therefore represents an additional metabolic engineering lever that can contribute towards optimizing reaction rates within and without the Calvin cycle. This research provides an example of a combined multi-omic approach to

characterize biological mechanisms. In particular, the use of fluxomics and proteomics can reveal coordinated *in vivo* regulatory mechanisms like metabolite channeling that may not be observable when enzymes are characterized *in vitro* on a more individual basis. Both our proteomic data and our labelling data in combination with prior literature suggest a complex regulatory system where light availability can simultaneously influence enzyme activity, enzyme localization, and subsequent substrate localization.

3. MULTI-OMIC CHARACTERIZATION OF GENETICALLY ENGINEERED *SYNECHOCYSTIS*

3.1 Introduction

A natural way to attempt to improve the efficiency of the Calvin cycle is to overexpress existing enzymes within the pathway to further increase the rate of reaction. However, not every reaction within the Calvin cycle can be considered rate limiting.

To further characterize the Calvin cycle within cyanobacteria, we studied three different genetically modified strains of *Synechocystis*. First, a kanamycin resistant control strain (Km) was generated using an empty vector pPMQAK1, allowing the use of kanamycin as a selection marker. Secondly, a fructose-1,6-bisphosphatase belonging to *Synechococcus* sp. PCC 7002 was expressed on the vector pPMQAK1 to generate the strain 70glpX. Finally, a transketolase (*sll1070*) was expressed on pPMQAK1 to generate the strain tktA. Previous attempts to overexpress these Calvin cycle enzymes often result in disparate phenotypical responses [47]. For example, when the bifunctional FBP/SBPase was overexpressed in the 70glpX strain of *Synechocystis*, a faster growth rate was observed. On the other hand, when TKT was overexpressed in the tktA strain of *Synechocystis*, a chlorotic phenotype was observed outside of low light conditions. Consequently, to study the reason for these responses, the biomass composition of these strains was characterized. Metabolic flux analysis and untargeted proteomics were used to characterize the different strains and explain the different phenotypes. The following data and conclusions, along with related supplementary data, has been published and is available online [68].

3.2 Materials and Methods

3.2.1 Culturing Conditions

For growth measurements, Synechocystis sp. PCC 6803 cells were cultured in 50 mL BG-11 media in 250 mL shake flasks. Flasks were shaken at 200 rpm and kept at a constant temperature of 30 °C (Infors HT Minitron). Two different CO_2 conditions (high carbon, HC: 3%; low carbon, LC: 0.04% CO_2) and two different light conditions (low light, LL: 80 µmol m^{-2} s^{-1}; or high light, HL: 240 µmol m^{-2} s^{-1}) are used, for a total of four conditions (LLLC, HLLC, LLHC, HLHC). The control (Km), transketolase overexpressing (tktA) and fructose-1,6/seduheptulose-1,7-bisphosphatase overexpressing (70glpX) strains each containing a kanamycin resistant vector were grown with 25 µg/mL kanamycin as before [47].

3.2.2 Biomass Composition Measurements

For dry cell weight (DCW) measurement, 20 mL of late exponential growth culture were collected in pre-weighed plastic trays, which were dried at 80 °C for 24h afterwards. DCW was indicated as the weight difference of the trays with dried samples and the trays without dried samples. Chlorophyll α and carotenoid content were measured following previously published methods [77]. In brief, 100% methanol was used to extract the pigments under dark condition. Absorbance at wavelength 470 nm, 665 nm and 720 nm were recorded. The equations Chl α (µg/mL) = 12.9447*(OD665 − OD720) and carotenoids (µg/mL) = [1000*(OD470 − OD720) − 2.86*Chl α]/221 were used to calculate the pigment concentration. Crude protein extraction protocol was slightly modified from previous literature [78]. Phosphate-buffered saline (PBS) with 0.1% Triton-X 100 buffer was used as extraction buffer. Protein concentration was determined with DC protein assay (BIO-RAD). To extract the carbohydrate, cell paste was treated with 2.5 M

hydrochloric acid in 100°C water bath for 1 h. Afterwards, a mixture of sample extract (or glucose solution, which was used as standard), 5% phenol, and concentrated sulfuric acid (1:5:25) was incubated in a 25°C water bath for 30 minutes. The concentration of the glucose standard was between 10 to 100 μg mL^{-1}. Absorbance at 490 nm was measured [79], [80].

Lipids were measured after chloroform-methanol extraction [81]. In brief, 2:1 chloroform-methanol (v/v) mixture was added to cell paste in a glass centrifuge tube. A volume of at least 10 mL is recommended since a larger volume will increase the accuracy of the extraction measurements. The tubes were vigorously shaken until all the biomass dispersed in the solvent. 0.73% NaCl water solution was added in to form a final mixture of chloroform, methanol, and 0.73% NaCl water solution (10:5:4). The mixture was centrifuged (350 g for 2 min) to separate the phases. The lower phase was transferred to pre-weighed glass tubes. Samples in glass tubes were dried by overnight evaporation in a hood. The lipid weight was indicated by the weight differences between the tubes with dried samples and clean tubes. The phenol and chloroform method was used to extract RNA [82]. RNA concentration was determined with Nanodrop 2000 (Thermo Scientific). The remaining biomass is assumed to be composed of primarily DNA.

3.2.3 Isotopically Nonstationary Metabolic Flux Analysis

Isotopically nonstationary metabolic flux analysis (INST-MFA) is a technique to estimate the fluxes throughout a network using an isotopic tracer. The INST-MFA procedure was performed as shown previously (2.2.3).

As part of INST-MFA analysis, a biomass synthesis equation is required. The biomass synthesis equation for each genetically modified strain is slightly different than the WT biomass synthesis equation due to altered biomass composition (3.3.2), and therefore the coefficients must

be reformulated from the WT case obtained from previous literature [53] using the same methodology (Tables A.9-A.11).

3.2.4 LC-MS/MS measurements of metabolites

The LC-MS/MS protocol is the same as previously described (2.2.4).

3.2.5 Proteomics

Cultured cyanobacterial samples were first pelleted by centrifugation at 10000 rpm, and the supernatant removed. The resulting cell pellet was then lysed in a bead beater with silica beads in the presence of a detergent free buffer (50 mM HEPES/KOH pH 7.5, 50 mM KOAc, 2 mM Mg(OAc)2, 1 mM EDTA, 1 mM EGTA, 1 mM DTT, 2 mM PMSF in EtOH, 1% Protease Inhibitor Cocktail) and centrifuged. The resulting supernatant was transferred to a new tube and treated as a soluble protein fraction. The pellets were dissolved in 8 M urea and treated as insoluble protein fraction.

Proteins in the soluble and insoluble fractions were precipitated using 5 volume of cold (-20 °C) acetone overnight. Precipitated proteins were collected by centrifugation at 14,000 rpm for 15 min at 4 °C in (Eppendorf 5810R), and pellets were washed once with 80% cold (-20 °C) acetone. After drying briefly in CentriVap Concentrator (Labconco), pellets were dissolved in 50 µl of 8 M urea for 1 h at room temperature. Then, protein concentration in each fraction was determined by BCA assay using BSA as standard, and volume containing 100 µg of total protein was used for digestion. Samples were first reduced with 10 mM DTT at 60 °C for 45 min, and then cysteines alkylated with 20 mM IAA at room temperature in the dark for 45 min. Before digestion, the concentration of urea was brought down to 1.5 M by adding 25 mM ammonium bicarbonate. Digestion was performed at 37 °C overnight using mass spec grade trypsin and Lys-C mix from

Promega at a 1:25 (w/w) enzyme-to-substrate ratio. The digested peptides were desalted using Pierce C18 spin columns (Pierce Biotechnology, Rockford, IL) using the protocol provided by the manufacturer. Peptides were eluted using 80% acetonitrile containing 0.1% Formic Acid (FA) and dried in Centrivap. Peptides were re-suspended in 50 µl of the loading buffer (3% acetonitrile, 97% water and 0.1% FA), and 2 µl was used to determine peptide concentration in each sample using BCA assay. Peptide sample volume was adjusted to a final concentration of 0.2 µg/µL based on BCA assay and 5 µL (1 µg of total peptide) was loaded to the LC column for LC-MS/MS analysis.

Samples were analyzed by reverse-phase HPLC-ESI-MS/MS using the Dionex UltiMate 3000 RSLC nano System (Thermo Fisher Scientific) coupled to the Q-Exactive High Field (HF) Hybrid Quadrupole Orbitrap MS (Thermo Fisher Scientific) and a Nano- electrospray Flex ion source (Thermo Fisher Scientific). Purified peptides were loaded onto a trap column (300 µm ID x 5 mm) packed with 5 µm 100 Å PepMap C18 medium and washed using a flow rate of 5 µl/minute with 98% purified water/2% acetonitrile (ACN)/0.01% formic acid (FA). The trap column was then switched in-line with the analytical column after 5 minutes. Peptides were separated using a reverse phase Acclaim PepMap RSLC C18 (75 µm x 15 cm) analytical column using a 120 minutes method at a flow rate of 300 nl/minute. The analytical column was packed with 2 µm 100 Å PepMap C18 medium (Thermo Fisher Scientific). Mobile phase A consisted of 0.01% FA in water and a mobile phase B consisted of 0.01 % FA in 80% ACN. The linear gradient started at 5% B and reached 30% B in 80 minutes, 45% B in 91 minutes, and 100% B in 93 minutes. The column was held at 100% B for the next 5 minutes before being brought back to 5% B and held for 20 minutes. Sample was injected into the QE HF through the Nanospray Flex™ Ion Source fitted with an emission tip from Thermo Scientific. Column temperature was maintained at 35 °C.

MS data were acquired with a Top 20 data-dependent MS/MS scan method. The full scan MS spectra were collected over 300-1,650 m/z range with a maximum injection time of 100 milliseconds, a resolution of 120,000 at 200 m/z, spray voltage of 2 and AGC target of 1 ×106. Fragmentation of precursor ions was performed by high-energy C-trap dissociation (HCD) with the normalized collision energy of 27 eV. MS/MS scans were acquired at a resolution of 30,000 at m/z. The dynamic exclusion was set at 20 s to avoid repeated scanning of identical peptides. Instrument optimization and recalibration was carried out at the start of each batch run using Pierce calibration solution. The sensitivity of the instrument was also monitored using E. coli digest at the start of the sample run.

LC-MS/MS data were searched using MaxQuant software (v. 1.5.3.28) [83], [84] with its built-in Andromeda search engine [85] for protein identification and label free MS1 quantitation. The MS/MS spectra were searched against the *Synechocystis* sp. PCC 6803 protein database downloaded from the NCBI. The minimal length of six amino acids was required in the database search. The database search was performed with the precursor mass tolerance set to 10 ppm and MS/MS fragment ions tolerance was set to 20 ppm. Database search was performed with enzyme specificity for trypsin, allowing up to two missed cleavages. Oxidation of methionine was defined as a variable modification, and carbamidomethylation of cysteine was defined as a fixed modification. The 'unique plus razor peptides' were used for peptide quantitation. Razor peptides are the non-unique peptides assigned to the protein group with the most other peptides. The false discovery rate (FDR) of peptides and proteins identification was set at 1%.

All the raw LC-MS/MS data are submitted to MassIVE (massive.ucsd.edu) and are publicly available as dataset ID MSV000084011.

3.3 Results and Discussion

3.3.1 Genetically engineered *Synechocystis* result in disparate responses to changing CO_2 conditions

Previous literature suggested that when tktA and 70glpX were cultivated under low light (15 µmol m^{-2} s^{-1}), they both outperformed the kanamycin resistant control strain (Km) [47]. Yet, when these strains were grown under 100 µmol m^{-2} s^{-1}, the tktA strain was chlorotic and growth inhibited. To further investigate these strains, we grew these strains at a moderate 80 µmol m^{-2} s^{-1} light level and atmospheric carbon (LLLC) and at a 80 µmol m^{-2} s^{-1} and 3% CO_2 (v/v) (LLHC) in shake flasks. We also confirmed the phenotypical similarity in growth rates between the *Synechocystis* wild-type and Km strain.

Curiously, while both wild-type and 70glpX grew faster under LLHC conditions as compared to LLLC, this was not true for tktA, which did not grow significantly faster (Figure 3.1). We therefore hypothesized a rate limitation unrelated to the carbon concentrating mechanisms of the carboxylase activity of RuBisCO, which normally benefit from elevated CO_2 levels [23].

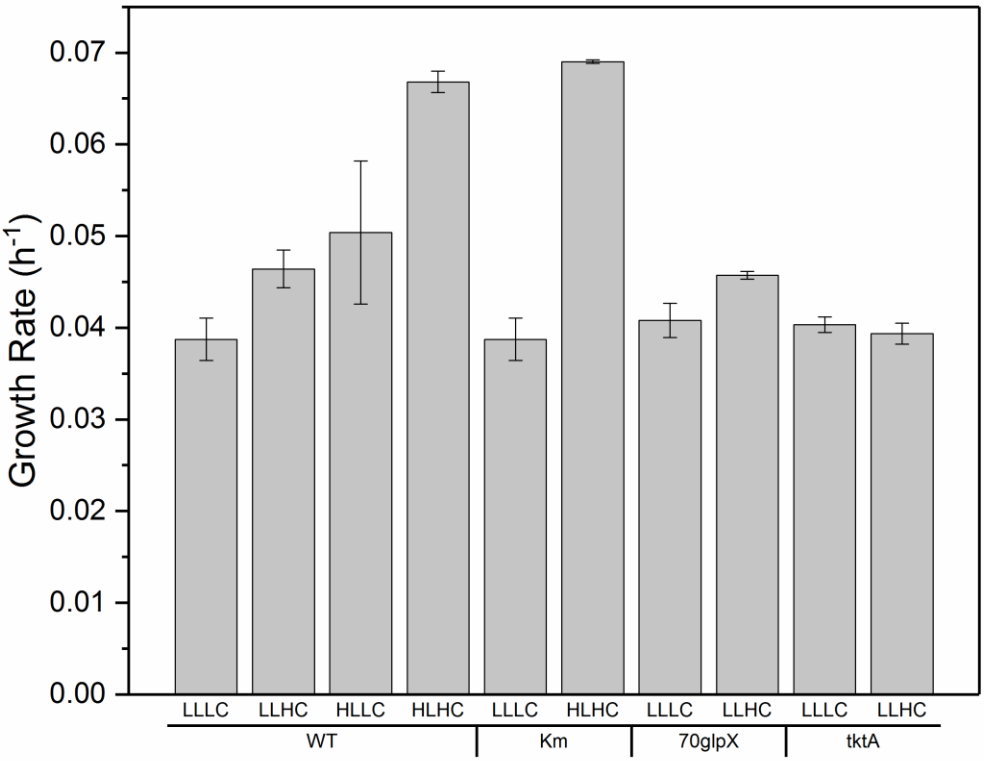

Figure 3.1 Growth rates of WT, Km, 70glpX and tktA strains of *Synechocystis* sp. PCC 6803 cultured in 50 mL BG-11 in shake flasks at 30°C, 200 rpm, measured over approximately three days (n = 3). (Abbreviations: LL = 80 μmol $m^{-2}s^{-1}$, HL = 240 μmol $m^{-2}s^{-1}$, LC = 0.04% (v/v) CO_2, HC = 3% (v/v) CO_2)

From growth data alone, it is unclear why tktA did not benefit from the increase in CO_2, as transketolase is not known to be allosterically controlled by CO_2. Therefore, we relied on more comprehensive such as fluxomics and proteomics to investigate these responses.

3.3.2 Biomass characterization of genetically engineered *Synechocystis* strains

INST-MFA requires, in part, a characterization of the biomass components in different strains of *Synechocystis* due to the possibility that the introduction of newly expressed enzymes

result in an altered biomass composition. The relative distribution of different macromolecules define the so-called biomass equation, which is needed to form the negative component of the mass balance equations during INST-MFA fitting.

We observed a statistically significant increase in protein concentration and a smaller decrease in lipid concentration in the 70glpX strain compared to the Km strain. The carbohydrate concentrations were not statistically different. We observed a statistically significant increase in protein, carbohydrate and lipid concentrations despite a slower overall growth rate (Figure 3.2).

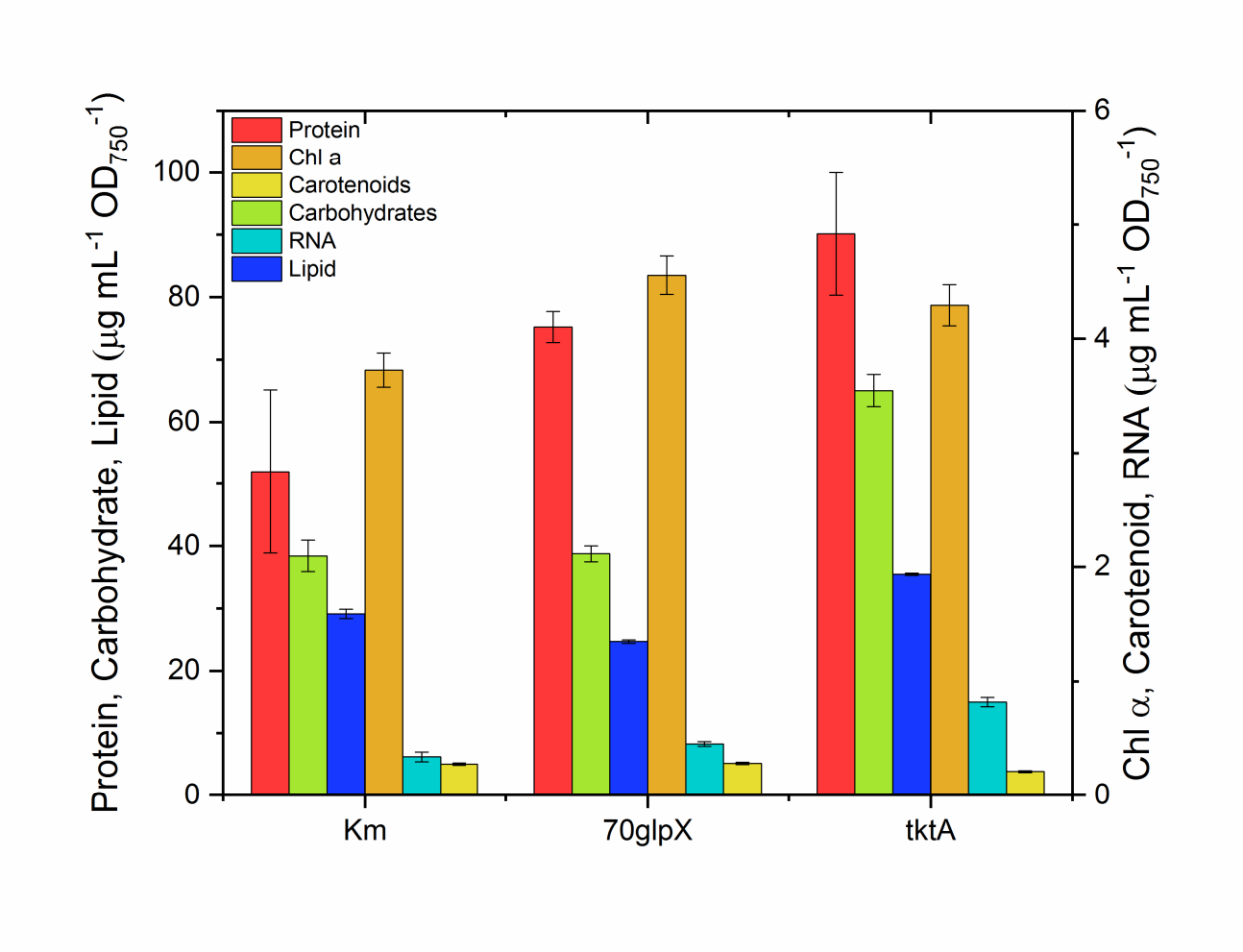

Figure 3.2 Absolute concentrations of biomass components as normalized to OD_{750} in *Synechocystis* sp. PCC 6803 control (Km), fructose-1,6/sedoheptulose-1,7-bisphosphatase overexpressing (70glpX) and transketolase overexpressing (tktA) strains

The fractional carbohydrate content in the 70glpX strain is significantly less than either the Km or tktA strains (Figure 3.3). The remainder of the biomass is assumed to be nucleic acids.

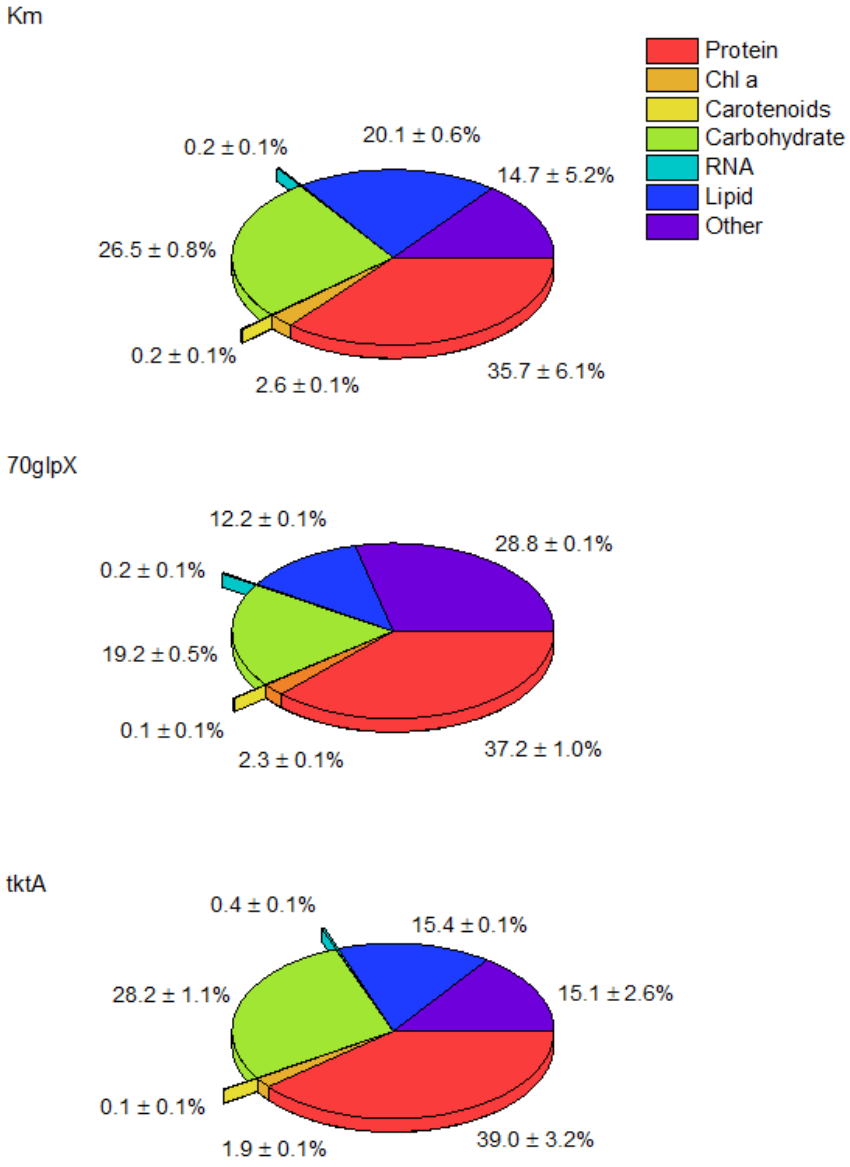

Figure 3.3 Biomass composition of *Synechocystis* sp. PCC 6803 control (Km), fructose-1,6/sedoheptulose-1,7-bisphosphatase overexpressing (70glpX) and transketolase overexpressing (tktA) strains grown under air at 55 ± 5 µmol m^{-2} s^{-1}. ± indicates standard deviation.

3.3.3 INST-MFA in 70glpX reveals a more efficient carbon cycle

INST-MFA was performed on the Km, 70glpX and tktA strains, each cultured at 55 µmol m^{-2} s^{-1} at 30 °C. Under this light limited condition, both strains were expected to grow at least as fast as the control. The resulting flux fit strongly suggested a difference in oxidative pentose phosphate pathway (OPPP) activity in both 70glpX and tktA, with the results being particularly noticeable in 70glpX (Figure 3.5). These results are a consequence of the observed difference in R5P and RU5P labelling in different strains (Figure 3.4). The nature of the Calvin cycle is such that RU5P can be generated either through the normal set of Calvin reactions, or through the OPPP which utilizes G6P. However, a crucial difference is that the Calvin cycle simultaneously generates other five carbon sugars R5P and X5P. In the Km strain, the labelling of R5P is significantly less than the labeling of RU5P, a metabolite that is downstream of R5P. This therefore implies that a significant portion of labelled carbon in RU5P must come from G6P instead. In comparison, this observed disparity between R5P and RU5P is much less in tktA and close to zero in 70glpX.

This result also challenges the assumptions posited by several earlier kinetic models of the Calvin cycle which assume that RPI is under equilibrium and therefore defined by a single equilibrium rate constant [15], [17], [48]. In actuality, the observed differences in both concentration and the unequal distribution of carbon labels between R5P and RU5P strongly suggest that a more complex kinetic equation may be appropriate.

Per unit of carbon fixated, the Calvin cycle requires 3 ATP and 2 NADPH as energy input. The OPPP releases CO_2 while generating two units of NADPH, which therefore results in a futile cycle, a lowered carbon fixation efficiency, and is one reason why both strains have been observed to conditionally grow slightly faster than the control. While the OPPP is typically considered insignificant under most photoautotrophic conditions [25], [26], [69], [72], the OPPP has also been observed under low light conditions, and under heterotrophic or photomixotrophic conditions [8].

This partial activity is likely due to the incomplete inactivation of OPPP enzymes. This observed decreased in flux is complemented by proteomic results which demonstrate decreases in OPPP enzymes such as 6-phosphogluconolactonase, 6-phosphogluconate dehydrogenase, and glucose-6-phosphate dehydrogenase in 70glpX and tktA (Table 3.1).

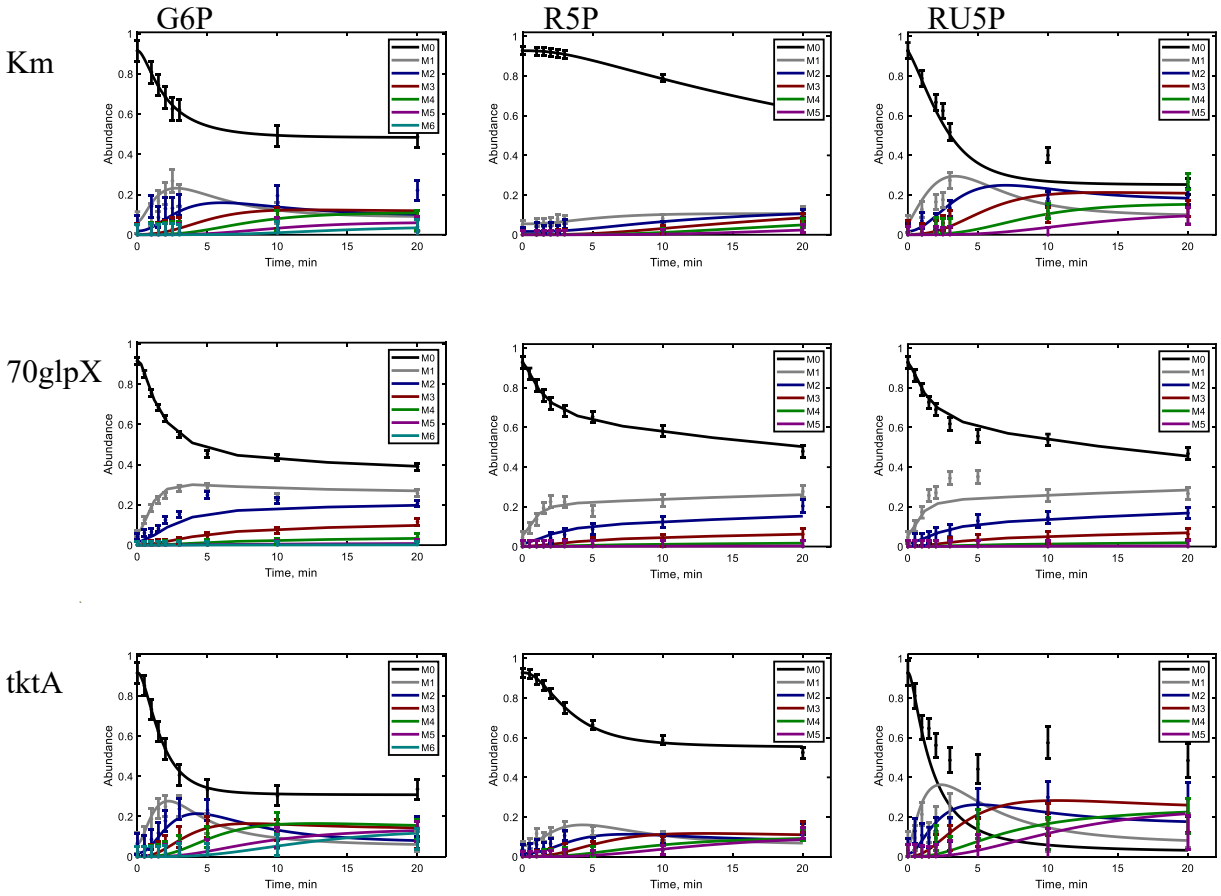

Figure 3.4 Selected labelling dynamics for G6P (left column), R5P (center column) and RU5P (right column) for Km, 70glpX and tktA strains under photoautotrophic growth (55 µmol m^{-2} s^{-1}, 30 °C)

We also observed a preference for SBP over FBP as the substrate in FBP/SBPase activity in 70glpX when compared to the control. While the bifunctional cyanobacterial FBP/SBPase has

been characterized to have a more favorable K_m and k_{cat} for FBP than SBP, both reactions also operate under Hill kinetics due to having multiple binding sites with positive cooperativity [86]. The Hill coefficient for SBP is significantly larger than that of FBP (3.4 and 1.9, respectively), which may explain the increase in SBPase flux in 70glpX (i.e. FBP/SBPase is sensitive to even a slight change in substrate balance).

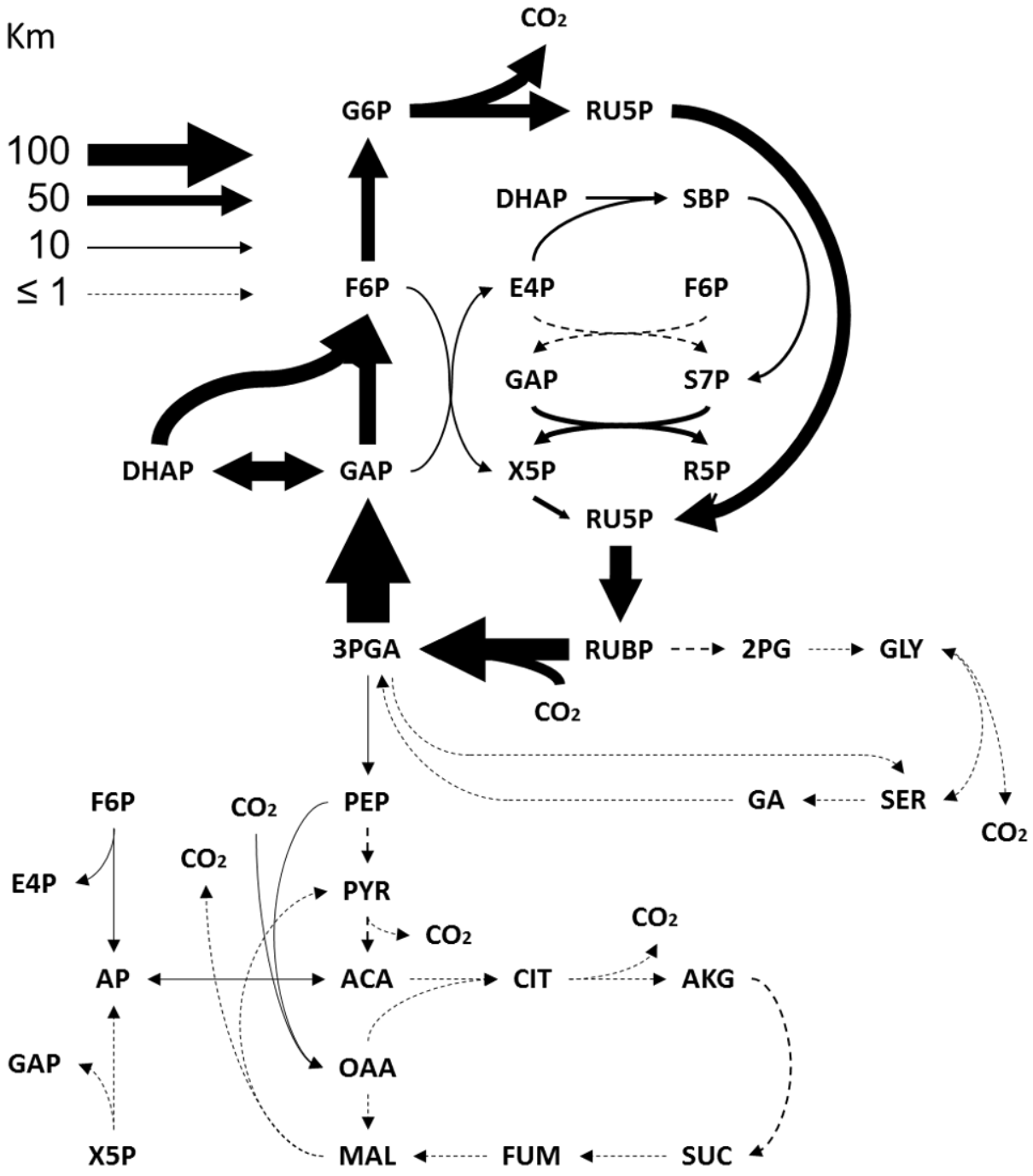

Figure 3.5 Net fluxes for Km, tktA and 70glpX under photoautotrophic growth (55 µmol m^{-2} s^{-1}, 30 °C) normalized to a net RuBisCO uptake rate of 100. Arrow thickness is proportional to net flux. Enzymatic fold-changes are listed in green (if FC > 1.20), red (if FC < 0.8), or black otherwise. Overexpressed enzymes are **bolded** and repeated enzymes are isozymes.

Figure 3.5 continued

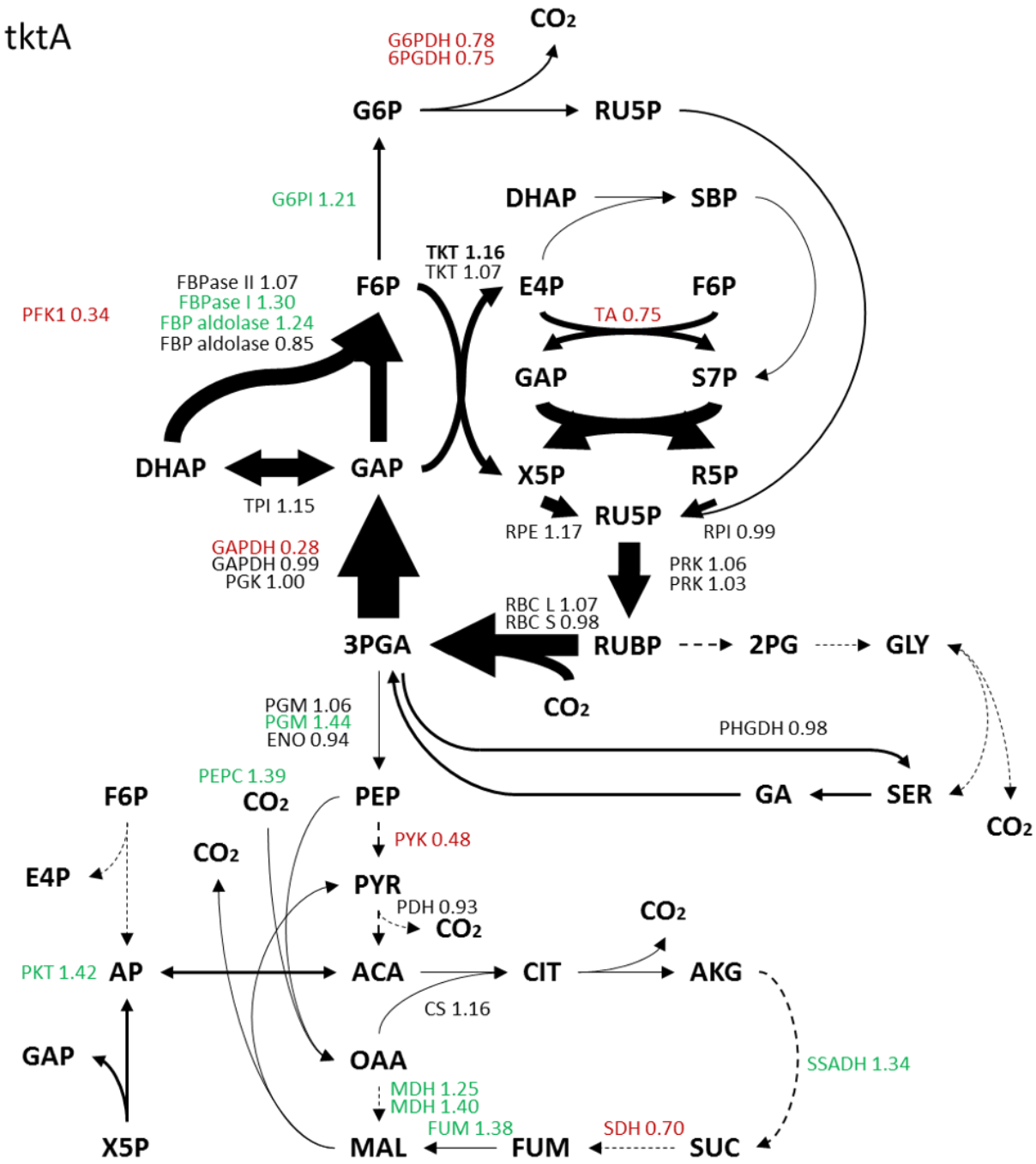

Figure 3.5 continued

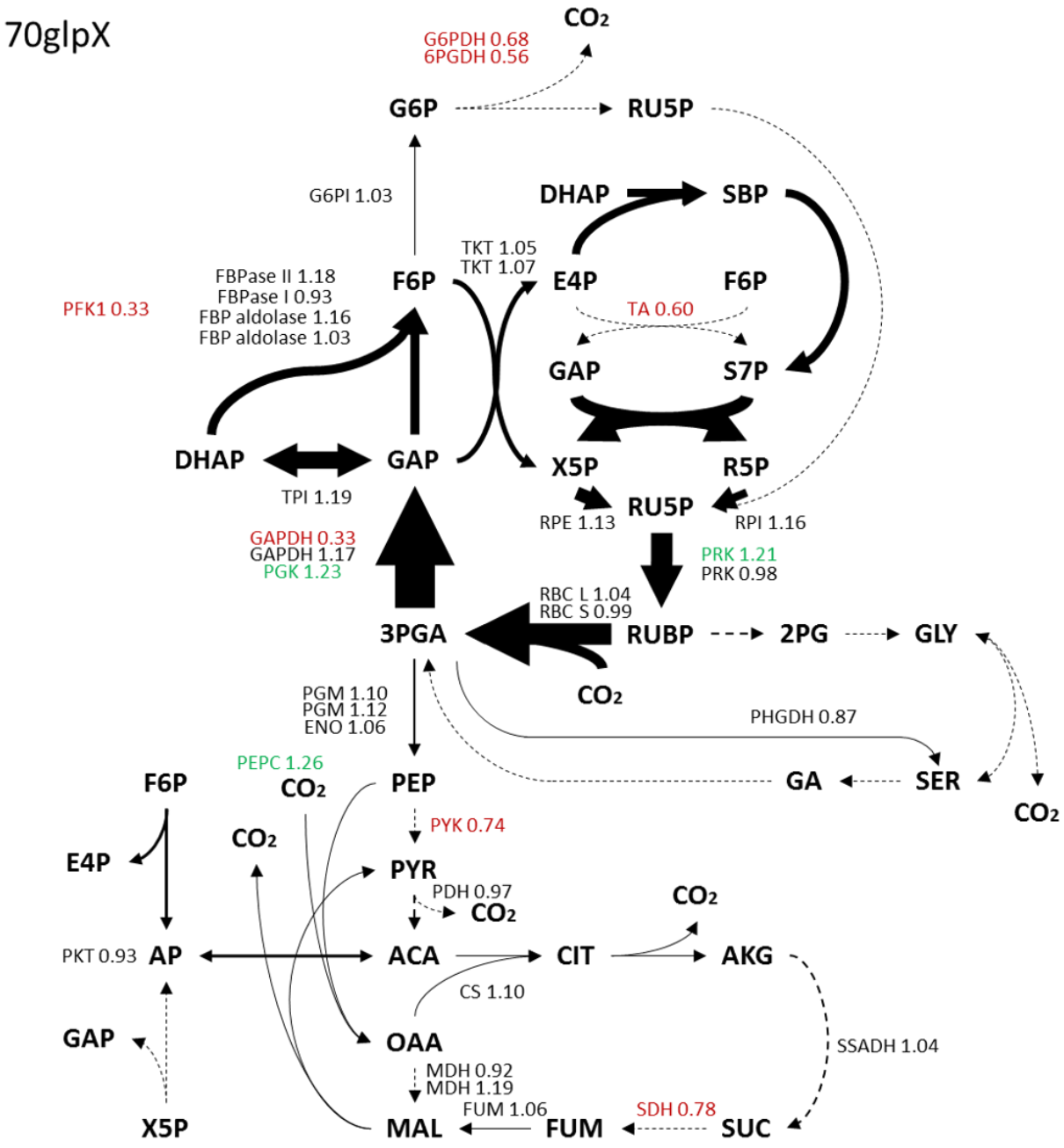

3.3.4 Transketolase overexpression leads to oxidative stress and pigment degradation under high light

Transketolase overexpression in *Synechocystis* outside of low light conditions resulted in chlorosis and retarded growth consistent with oxidative stress. This result was not entirely unexpected because similar results were observed when transketolase was overexpressed in tobacco plants [87]. It was found that pigment degradation was induced in tobacco plants due to a thiamine deficiency, and that growth could be recovered under thiamine supplemented growth. Thiamine synthesis notably shares some precursors with the transketolase reaction, and thiamine diphosphate is additionally a cofactor in transketolase activity. Among other functions, thiamine has an important role in managing oxidative stress [88].

Proteomic results revealed a particularly strong increase in the enzyme dihydroorotate oxidase (DHOD) abundance in tktA as opposed to both Km and 70glpX (Table 3.1). DHOD is a critical enzyme in the biosynthesis of pyrimidine rings which are a component of thiamine pyrophosphates [89], which we hypothesized to be a compensating response to altered precursor availability. DHOD is also known as iron-stress induced chlorophyll binding protein (isiA), which has been found to protect cyanobacteria from photooxidative stress [90]. This increase is accompanied also by an increase in the stress induced redox carrier flavodoxin (FldA) [91], [92], which also plays a role in thiamine synthesis and redox envrionment [93]. Therefore, these proteomic results indicated a perturbed and inefficient thiamine biosynthesis pathway and a subsequently altered redox environment that decreases growth rates particularly at high light levels.

Table 3.1 Proteomic Fold-Changes (FC) in *Synechocystis* sp. PCC 6803 70glpX and tktA as compared to Km strain

Accession Number[a]	**Name**[b]	**q**[c]	**Log_2 (FC) (70glpX/Km)**[d]	**Log_2 (FC) (tktA/Km)**[d]
CALVIN-BENSON-BASSHAM CYCLE				
ALJ67312.1	glyceraldehyde-3-phosphate dehydrogenase	0.0000	**-1.613**	**-1.815**
ALJ66581.1	transaldolase	0.0000	-0.727	-0.415
ALJ68409.1	fructose-1,6-bisphosphate aldolase	0.0001	0.037	-0.231
ALJ68417.1	ribulose 1,5-bisphosphate carboxylase small subunit	0.0105	-0.002	-0.063
ALJ69060.1	glyceraldehyde-3-phosphate dehydrogenase	0.0012	0.226	-0.017
ALJ68624.1	ribose 5-phosphate isomerase	0.0002	0.216	-0.015
ALJ68155.1	phosphoglycerate kinase	0.0002	0.293	-0.003
ALJ68287.1	phosphoribulokinase	0.0029	-0.025	0.036
ALJ68099.1	phosphoribulokinase	0.0069	0.270	0.083
ALJ66435.1	phosphoglycerate mutase	0.0001	0.140	0.086
ALJ67669.1	fructose 1,6-bisphosphatase	0.0177	0.245	0.101
ALJ69043.1	transketolase	0.0097	0.077	0.102
ALJ68415.1	ribulose 1,5-bisphosphate carboxylase	0.0368	0.061	0.113
ALJ68375.1	triosephosphate isomerase	0.0082	0.257	0.206
ALJ67042.1	transketolase	0.0058	0.073	0.216
ALJ67800.1	ribulose phosphate epimerase	0.0193	0.172	0.228
ALJ67832.1	glucose-6-phosphate isomerase	0.0084	0.047	0.279
ALJ68049.1	fructose-1,6-bisphosphate aldolase	0.0257	0.212	0.315
ALJ68064.1	fructose 1,6-bisphosphatase	0.0000	-0.110	0.380
ALJ69229.1	phosphoketolase	0.0000	-0.102	0.509
ALJ68591.1	phosphoglycerate mutase	0.0011	0.167	0.526

Table 3.1 continued

GLYCOLYSIS				
ALJ66612.1	6-phosphofructokinase	0.0002	**-1.617**	**-1.574**
ALJ69176.1	phosphoglucomutase	0.0193	-0.045	-0.177
OXIDATIVE PENTOSE PHOSPHATE PATHWAY				
P74618.3	6-phosphogluconolactonase	0.0002	**-1.008**	-0.946
ALJ69507.1	6-phosphogluconate dehydrogenase	0.0000	-0.827	-0.415
ALJ67168.1	glucose-6-phosphate dehydrogenase	0.0001	-0.557	-0.356
PYRIMIDINE BIOSYNTHESIS				
ALJ68314.1	orotate phosphoribosyltransferase	0.0138	-0.485	-0.686
ALJ69052.1	dihydroorotate dehydrogenase (quinone)	0.0076	-0.828	-0.263
ALJ67951.1	CTP synthase	0.0061	-0.026	0.085
ALJ69529.1	carbamoyl phosphate synthase large subunit	0.0048	-0.010	0.213
ALJ69587.1	carbamoyl phosphate synthase small subunit	0.0138	-0.012	0.264
ALJ68228.1	nucleoside diphosphate kinase	0.0014	0.197	0.285
ALJ66676.1	carbamoyl phosphate synthase large subunit	0.0095	-0.231	0.380
ALJ66712.1	dihydroorotase	0.0334	0.254	0.506
ALJ67628.1	dihydroorotate oxidase	0.0000	0.403	**5.165**
TRICARBOXYLIC ACID CYCLE				
ALJ67462.1	succinate dehydrogenase	0.0062	-0.359	-0.510
ALJ67226.1	fumarate reductase	0.0004	-0.310	-0.294
ALJ69108.1	aconitate hydratase	0.0007	-0.080	-0.259
ALJ68418.1	pyruvate/2-oxoglutarate dehydrogenase complex	0.0001	0.009	-0.225
ALJ68224.1	pyruvate dehydrogenase	0.0270	-0.048	-0.098
ALJ66604.1	isocitrate dehydrogenase	0.0089	0.098	0.128
ALJ68479.1	citrate synthase	0.0110	0.137	0.216

Table 3.1 continued

ALJ66446.1	malate dehydrogenase	0.0026	-0.127	0.319
ALJ68325.1	succinate-semialdehyde dehydrogenase	0.0000	0.051	0.422
ALJ69511.1	fumarate hydratase	0.0234	0.086	0.460
ALJ68038.1	phosphoenolpyruvate carboxylase	0.0057	0.329	0.470
ALJ69534.1	malate dehydrogenase	0.0022	0.251	0.483
THIAMINE SYNTHESIS				
ALJ68568.1	thiazole synthase	0.0001	-0.058	-0.427
ALJ66831.1	1-deoxy-D-xylulose-5-phosphate synthase	0.0027	-0.297	-0.374
ALJ67350.1	thiamine biosynthesis protein ThiJ	0.0023	-0.049	-0.261
ALJ67799.1	thiamine biosynthesis protein ThiS	0.0134	-0.013	0.170
ALJ66743.1	thiamine-phosphate pyrophosphorylase	0.0107	0.269	0.356
ALJ68841.1	thiamine biosynthesis protein ThiC	0.0002	0.233	0.642
OTHER				
ALJ68948.1	pyruvate-flavodoxin oxidoreductase	0.0010	-0.915	-0.921
ALJ69241.1	glucose-1-phosphate adenylyltransferase	0.0014	0.132	0.386
ALJ66926.1	acetate kinase	0.0052	0.137	0.537
ALJ66456.1	glycerol dehydrogenase	0.0004	0.688	**1.500**
ALJ67627.1	flavodoxin FldA	0.0000	-0.147	**4.076**

[a] NCBI GenBank
[b] Repeated enzyme names are isozymes
[c] Enzymes were filtered by FDR-adjusted statistical significance ($q < 0.05$ by ANOVA), n = 3 replicates for each strain
[d] Fold-change results are **bolded** for emphasis for $Log_2(FC) > 1$ or $Log_2(FC) < -1$

3.4 Conclusions

Two Calvin cycle enzymes, FBP/SBPase and TKT, were separately overexpressed in *Synechocystis*. In addition to growth rates, fluxomic and proteomic data were combined to investigate the Calvin cycle and photoautotrophic metabolism.

Although the bifunctional cyanobacterial FBP/SBPase show little homology with either the FBPase or SBPase common in higher plants [94], overexpression of cyanobacterial FBP/SBPase in both tobacco plants and in *Synechococcus* sp. PCC 7002 resulted in increases in growth rates [94]–[96]. This result is also corroborated with *in silico* kinetic modeling which previously have implicated FBP/SBPase as an enzyme with substantial flux control coefficient [48]. Our own results for 70glpX indicate that an increase in growth rate which we attributed to a less active OPPP flux at the tested light level. Similarly, a concomitant proteomic study revealed decreases in the majority of OPPP enzmyes, including glucose-6-phosphate dehydrogenase, 6-phosphogluconate dehydrogenase, and 6-phosphogluconolactonase (Table 3.1).

Our results also suggest a slight preference for SBPase activity over FBPase activity. While F6P can be rapidly isomerized into G6P which can form glycogen or enter the OPPP, S7P only participates in the Calvin cycle. The presence of the dedicated FBPase and SBPase within higher order plants suggests some evolutionary pressure that favors monofunctional activity or plasticity. For example, carbon flow can be effectively cycle through the Calvin cycle when SBPase activity is dominant, or alternatively carbon can be sequested as glycogen when FBPase activity is dominant. This imbalanced substrate preference in the bifunctional FBP/SBPase might accomplish a similar bifurcation by favoring SBPase activity when substrate concentrations are high (i.e. the amount of carbon is not very limited, so the need to sequester carbon as glycogen is potentially less).

In contrast to 70glpX, we observed that the overexpression of TKT in tktA resulted in retarded growth rates at high light levels. Chlorosis, as well as carbohydrate accumulation, are commonly seen in nutrient starved wild-type cultures [97], but we observed the chlrorotic phenotype even under nutrient replete conditions. Thus, the observed phycobilisome degradation was more likely to be triggered by perturbations in metabolite concentration or redox imbalance instead. In particular, the increase in DHOD and FldA levels that overexpression of transketolase can divert carbon away from pyrimidine and thiamine synthesis, resulting in overall increased photosensitivity in this strain. On the other hand, we also observed that, similar to 70glpX, the activity of the OPPP and the abundance of the associated enzymes in the OPPP was much decreased, which may explain the increase in biomass accumulation.

Both 70glpX and tktA resulted in altered biomass distributions and decreases in OPPP activity, resulting in an improved efficiency of carbon fixation. Depending on the conditions being tested, the efficiency of the Calvin cycle appears to be variable, especially for tktA. This work underlines the need for individual optimization of different strains by testing across a wider variety of external conditions. In addition, this work demonstrates how multiple omic-level techniques can be combined together to strengthen and arrive at more complex conclusions than would be possible with either fluxomics or proteomics alone.

4. CONCLUSIONS AND FUTURE DIRECTIONS

4.1 Conclusions

The potential of cyanobacteria and other photosynthetic microorganisms as sustainable alternatives to existing industrial processes remains a subject of active research and investigation. Based on the work presented in this work, the utilization of multi-omics technologies is one way in which regulatory processes within cyanobacteria can be probed. In particular, the use of untargeted proteomics and fluxomics has revealed insight into how internal perturbations within the genome of *Synechocystis*, and external perturbations in the form of light level, can result in both anticipated and unanticipated changes in cyanobacterial metabolism. For example, changes in patterns within labelling dynamics, combined with information from proteomics, suggested that enzyme localization within cyanobacteria is more flexible than previously understood. Overexpressing the enzymes FBP/SBPase and transketolase in the Calvin cycle additionally has resulted in measurable changes within the OPPP, changing the efficiency of the carbon fixation cycle. These insights were obtained only by combining the information gleaned from both fluxomics and untargeted proteomics, as either method alone would not have provided sufficient information to make many of the conclusions presented in this work. These experiments additionally provide successful examples of exploratory research, which reveal many relationships between different variables, and provide potential avenues for future work.

4.2 Future Directions

4.2.1 Characterization of thylakoid-bound enzymes

Previous kinetic models of the Calvin cycle have typically lumped many reactions within the Calvin cycle [14], [16], [17], [48], even when there exist multiple isozymes that facilitate the same reaction, which may reduce model accuracy [39]. The potential for Calvin cycle enzymes to localize on the periphery of the thylakoid membrane represents an additional level of complexity, because these thylakoid-bound enzymes are likely to have different kinetic parameters, and whose reactions would be best represented by separate kinetic equations. Therefore, an incremental improvement to existing kinetic models can be made by characterizing the kinetic parameters of these thylakoid-bound enzymes. *In vitro* experiments of purified thylakoid-bound enzymes would enable estimation of these kinetic parameters. Importantly, this implies that even when proteomic or transcriptomic analyses only find one enzyme, the apparent behavior of these enzymes with changing localization can resemble the behavior of two isozymes.

Additionally, a more quantitative understanding of the split between cytosolic and thylakoid-membrane fractions of various enzymes under different light conditions can be established by taking advantage of non-aqueous fractionation, which enables differentiation between different subcellular compartments [98], combined with proteomics.

4.2.2 Taking advantage of metabolite channeling in cyanobacteria

Recent studies have indicated the potential of synthetic metabolite channels as a way to significantly enhance reaction efficiency [76]. As inferred from our data and previous literature, cyanobacteria have an intrinsic way to form metabolite channels, potentially in a highly inducible manner, as metabolite channels preferentially form in cyanobacteria during sub-optimal light

conditions. When taking advantage of the availability of natural light, cyanobacteria that are grown outdoors are often exposed to sub-optimal lighting. Therefore, taking advantage of this intrinsic mechanism can be a way to enhance production of specific products of interest during such sub-optimal conditions. With some level of protein engineering, the addition of thylakoid-binding domains to enzymes outside of the Calvin cycle would be one theoretical way to divert Calvin cycle substrates into specific pathways.

4.2.3 Further investigating the Calvin cycle under diurnal conditions

Our experiments on FBP/SBPase and transketolase overexpressing strains of *Synechocystis* revealed that the advantage provided by these genetic modifications was more significant under low light conditions than during higher light conditions. Moreover, the data collated from the wild-type experiments under different light levels revealed strong regulatory changes. These changes were present when cyanobacteria were grown under steady and unchanging light levels. Therefore, these experiments are unable to clearly determine if these results were a result of short- or long-term mechanisms. Together, these data strongly underline the need for additional experiments done under changing light conditions. To clearly identify the type and magnitude of response, diurnal experiments involving realistic day-night light levels are needed.

APPENDIX

Table A.1 LC-MS/MS Ion Transitions and Parameters

Q1	Q3	Metabolite	DP (v)	EP (v)	CE (v)	CXP (v)
259	97	G6P/F6P+0	-25	-11	-21	-10
260	97	G6P/F6P+1	-25	-11	-21	-10
261	97	G6P/F6P+2	-25	-11	-21	-10
262	97	G6P/F6P+3	-25	-11	-21	-10
263	97	G6P/F6P+4	-25	-11	-21	-10
264	97	G6P/F6P+5	-25	-11	-21	-10
265	97	G6P/F6P+6	-25	-11	-21	-10
169	97	DHAP+0	-40	-5	-16	-23
170	97	DHAP+1	-40	-5	-16	-23
171	97	DHAP+2	-40	-5	-16	-23
172	97	DHAP+3	-40	-5	-16	-23
289	97	S7P+0	-26	-3	-30	-6
290	97	S7P+1	-26	-3	-30	-6
291	97	S7P+2	-26	-3	-30	-6
292	97	S7P+3	-26	-3	-30	-6
293	97	S7P+4	-26	-3	-30	-6
294	97	S7P+5	-26	-3	-30	-6
295	97	S7P+6	-26	-3	-30	-6
296	97	S7P+7	-26	-3	-30	-6
229	97	P5P+0	-28	-7	-19	-5
230	97	P5P+1	-28	-7	-19	-5
231	97	P5P+2	-28	-7	-19	-5
232	97	P5P+3	-28	-7	-19	-5
233	97	P5P+4	-28	-7	-19	-5
234	97	P5P+5	-28	-7	-19	-5
87	43	PYR+0	-24	-7	-13	-3
117	73	SUC+0	-41	-10	-18.5	-2
118	73	SUC+1	-41	-10	-18.5	-2
118	74	SUC+1_2	-41	-10	-18.5	-2
119	74	SUC+2	-41	-10	-18.5	-2
119	75	SUC+2_2	-41	-10	-18.5	-2
120	75	SUC+3	-41	-10	-18.5	-2
120	76	SUC+3_2	-41	-10	-18.5	-2
121	76	SUC+4	-41	-10	-18.5	-2
133	115	MAL+0	-30	-10	-18	-4
134	116	MAL+1	-30	-10	-18	-4
135	117	MAL+2	-30	-10	-18	-4
136	118	MAL+3	-30	-10	-18	-4

Table A.1 continued

137	119	MAL+4	-30	-10	-18	-4
145	101	AKG+0	-29	-5	-14	-7
146	101	AKG+1	-29	-5	-14	-7
146	102	AKG+1_2	-29	-5	-14	-7
147	102	AKG+2	-29	-5	-14	-7
147	103	AKG+2_2	-29	-5	-14	-7
148	103	AKG+3	-29	-5	-14	-7
148	104	AKG+3_2	-29	-5	-14	-7
149	104	AKG+4	-29	-5	-14	-7
149	105	AKG+4_2	-29	-5	-14	-7
150	105	AKG+5	-29	-5	-14	-7
115	71	FUM+0	-32	-8	-13	-3
116	71	FUM+1	-32	-8	-13	-3
116	72	FUM+1_2	-32	-8	-13	-3
117	72	FUM+2	-32	-8	-13	-3
117	73	FUM+2_2	-32	-8	-13	-3
118	73	FUM+3	-32	-8	-13	-3
118	74	FUM+3_2	-32	-8	-13	-3
119	74	FUM+4	-32	-8	-13	-3
185	79	PGA+0	-35	-10	-44	-3
186	79	PGA+1	-35	-10	-44	-3
187	79	PGA+2	-35	-10	-44	-3
188	79	PGA+3	-35	-10	-44	-3
339	97	FBP+0	-37	-10	-25	-5
340	97	FBP+1	-37	-10	-25	-5
341	97	FBP+2	-37	-10	-25	-5
342	97	FBP+3	-37	-10	-25	-5
343	97	FBP+4	-37	-10	-25	-5
344	97	FBP+5	-37	-10	-25	-5
345	97	FBP+6	-37	-10	-25	-5
309	97	RUBP+0	-28	-10	-31	-16
310	97	RUBP+1	-28	-10	-31	-16
311	97	RUBP+2	-28	-10	-31	-16
312	97	RUBP+3	-28	-10	-31	-16
313	97	RUBP+4	-28	-10	-31	-16
314	97	RUBP+5	-28	-10	-31	-16
167	79	PEP+0	-37	-8	-22	-6
168	79	PEP+1	-37	-8	-22	-6
169	79	PEP+2	-37	-8	-22	-6
170	79	PEP+3	-37	-8	-22	-6
155	79	2PG+0	-35	-10	-20	-5
156	79	2PG+1	-35	-10	-20	-5
157	79	2PG+2	-35	-10	-20	-5

Table A.1 continued

259	79	G1P+0	-27	-9	-58	-5
260	79	G1P+1	-27	-9	-58	-5
261	79	G1P+2	-27	-9	-58	-5
262	79	G1P+3	-27	-9	-58	-5
263	79	G1P+4	-27	-9	-58	-5
264	79	G1P+5	-27	-9	-58	-5
265	79	G1P+6	-27	-9	-58	-5
173	85	ACO+0	-35	-10	-17	-5
174	85	ACO+1	-35	-10	-17	-5
174	86	ACO+1_2	-35	-10	-17	-5
175	85	ACO+2	-35	-10	-17	-5
175	86	ACO+2_2	-35	-10	-17	-5
175	87	ACO+2_3	-35	-10	-17	-5
176	86	ACO+3	-35	-10	-17	-5
176	87	ACO+3_2	-35	-10	-17	-5
176	88	ACO+3_3	-35	-10	-17	-5
177	87	ACO+4	-35	-10	-17	-5
177	88	ACO+4_2	-35	-10	-17	-5
177	89	ACO+4_3	-35	-10	-17	-5
178	88	ACO+5	-35	-10	-17	-5
178	89	ACO+5_2	-35	-10	-17	-5
179	89	ACO+6	-35	-10	-17	-5
139	79	AP+0	-10	-5	-25	-10
140	79	AP+1	-10	-5	-25	-10
141	79	AP+2	-10	-5	-25	-10
73	45	GLX+0	-50	-9	-11.2	-5
74	45	GLX+1_1	-50	-9	-11.2	-5
74	46	GLX+1_2	-50	-9	-11.2	-5
75	46	GLX+2	-50	-9	-11.2	-5
199	97	E4P+0	-55	-10	-14	-5
200	97	E4P+1	-55	-10	-14	-5
201	97	E4P+2	-55	-10	-14	-5
202	97	E4P+3	-55	-10	-14	-5
203	97	E4P+4	-55	-10	-14	-5
105	75	GA+0	-40	-3.8	-14	-3.8
106	75	GA+1	-40	-3.8	-14	-3.8
107	75	GA+2	-40	-3.8	-14	-3.8
108	75	GA+3	-40	-3.8	-14	-3.8

A)

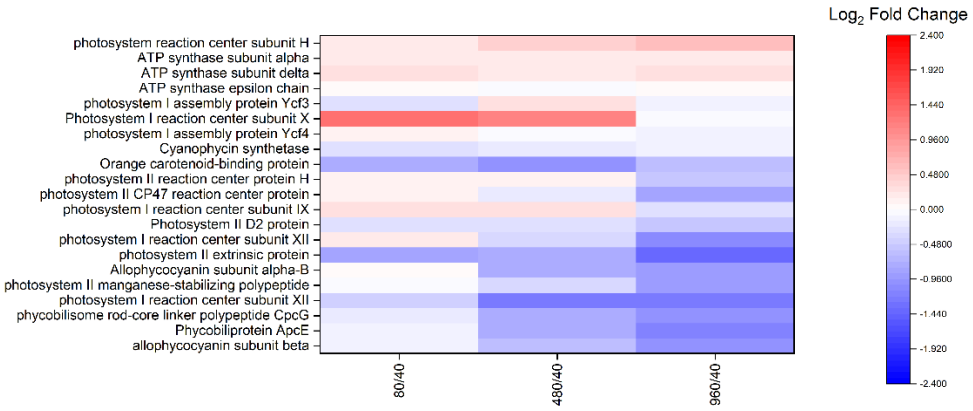

B)

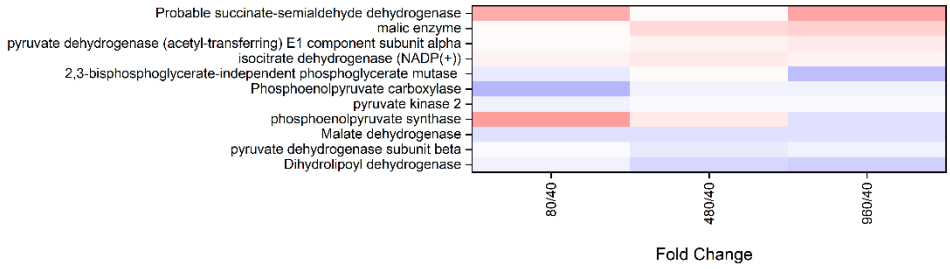

Figure A.1 Average proteomic $\log_2$ fold-change results relative to the 40 µmol m^{-2} s^{-1} condition for selected a) photosystems, pigments and ATP synthase subunits, and b) TCA cycle related enzymes, n = 3 for each light condition

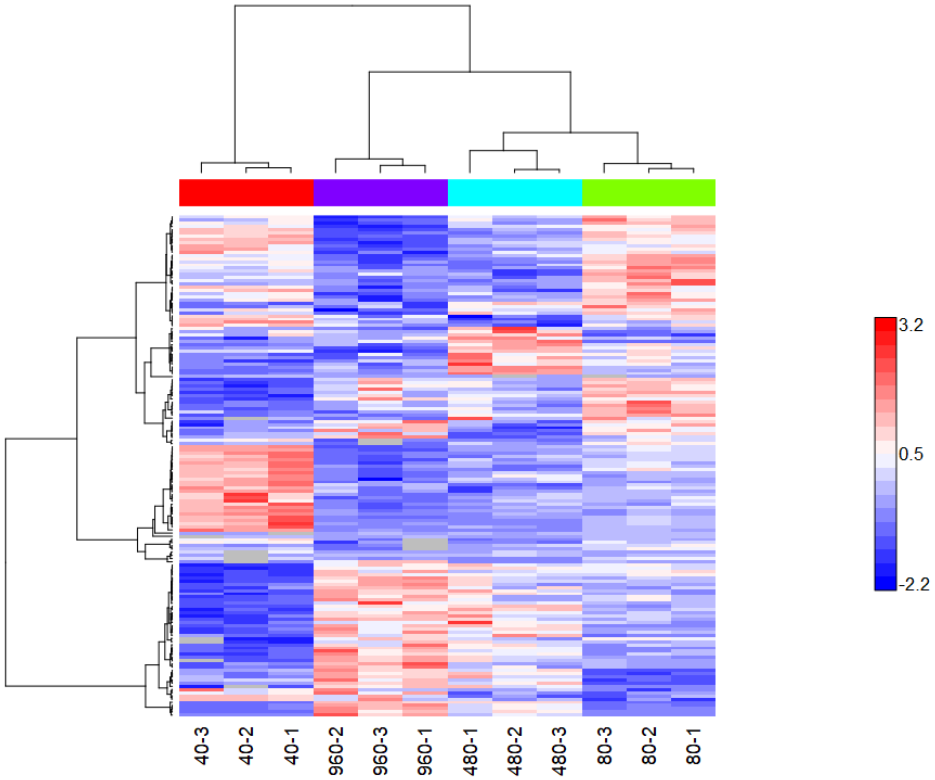

Figure A.2 Clustered proteomic heat map using Ward's aggregation method and Pearson distance metric for filtered proteomic results ($p < 0.05$ and at least 2 data points per light level)

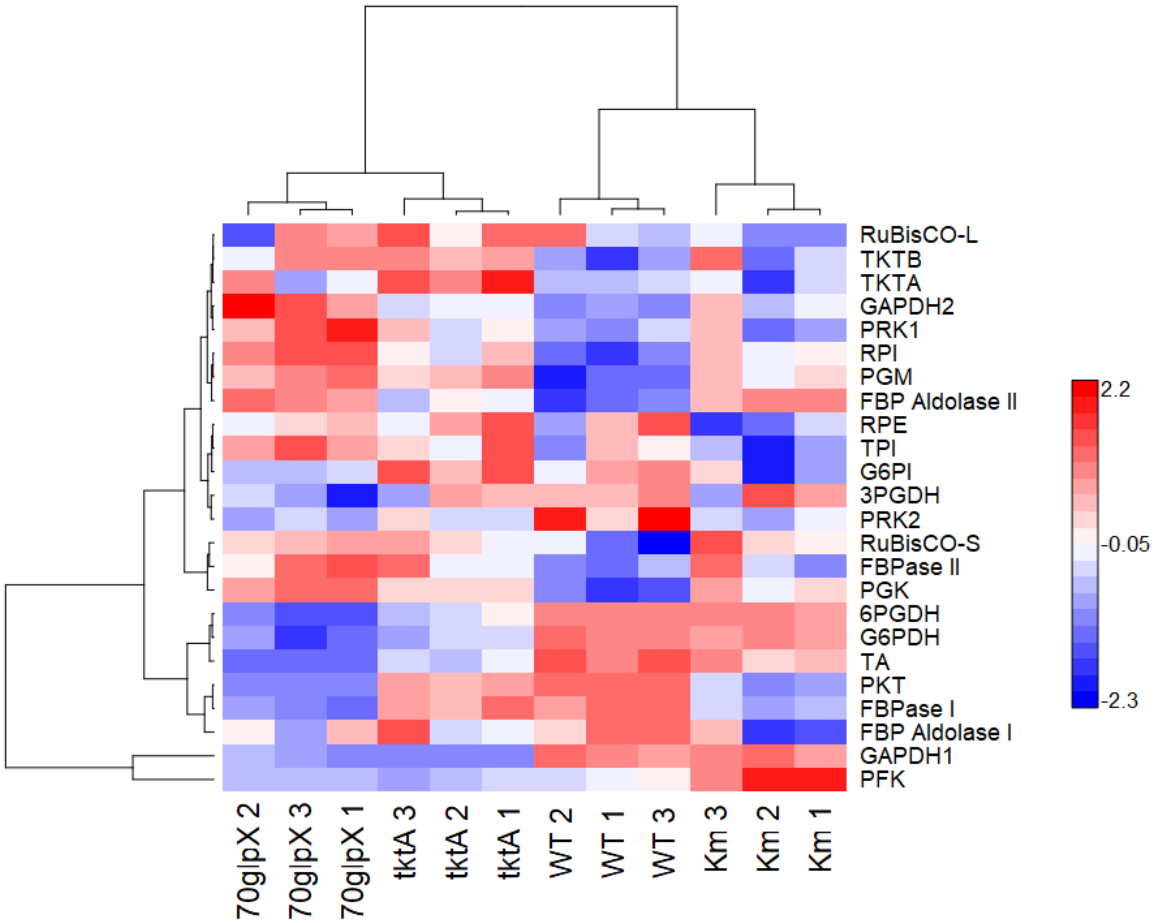

Figure A.3 Row-scaled heat map of Calvin cycle enzymes for triplicate samples of *Synechocystis* Km, 70glpX and tktA strains clustered by Pearson's correlation coefficient. Values represent normalized z-scores.

Table A.2 Measured MDVs and Standard Error for *Synechocystis* sp. PCC 6803 WT, 40 µmol m^{-2} s^{-1}

	Time (min)																	
2PG	**0**		**1**		**1.5**		**2**		**2.5**		**3**		**5**		**10**		**20**	
+0	0.973	0.020	0.965	0.020	0.961	0.020	0.915	0.020	0.903	0.020	0.838	0.020	0.780	0.020	0.708	0.020	0.605	0.020
+1	0.027	0.020	0.035	0.020	0.039	0.020	0.085	0.020	0.084	0.020	0.129	0.020	0.130	0.020	0.156	0.020	0.166	0.020
+2	0.000	0.020	0.000	0.020	0.000	0.020	0.000	0.020	0.013	0.020	0.034	0.020	0.090	0.020	0.135	0.020	0.229	0.020
AKG	**0**		**1**		**1.5**		**2**		**2.5**		**3**		**5**		**10**		**20**	
+0	0.966	0.025	0.988	0.025	0.983	0.025	0.988	0.025	0.989	0.025	0.981	0.025	0.979	0.025	0.985	0.025	0.984	0.025
+1	0.034	0.025	0.012	0.025	0.017	0.025	0.012	0.025	0.011	0.025	0.019	0.025	0.021	0.025	0.015	0.025	0.016	0.025
+2	0.000	0.025	0.000	0.025	0.000	0.025	0.000	0.025	0.000	0.025	0.000	0.025	0.000	0.025	0.000	0.025	0.000	0.025
+3	0.000	0.025	0.000	0.025	0.000	0.025	0.000	0.025	0.000	0.025	0.000	0.025	0.000	0.025	0.000	0.025	0.000	0.025
+4	0.000	0.025	0.000	0.025	0.000	0.025	0.000	0.025	0.000	0.025	0.000	0.025	0.000	0.025	0.000	0.025	0.000	0.025
+5	0.000	0.025	0.000	0.025	0.000	0.025	0.000	0.025	0.000	0.025	0.000	0.025	0.000	0.025	0.000	0.025	0.000	0.025
AP	**0**		**1**		**1.5**		**2**		**2.5**		**3**		**5**		**10**		**20**	
+0	0.899	0.030	0.912	0.030	0.848	0.030	0.894	0.030	0.882	0.030	0.874	0.030	0.823	0.030	0.752	0.030	0.683	0.030
+1	0.012	0.030	0.012	0.030	0.030	0.030	0.020	0.030	0.033	0.030	0.032	0.030	0.076	0.030	0.064	0.030	0.075	0.030
+2	0.089	0.030	0.076	0.030	0.121	0.030	0.086	0.030	0.085	0.030	0.095	0.030	0.101	0.030	0.184	0.030	0.241	0.030
F6P	**0**		**1**		**1.5**		**2**		**2.5**		**3**		**5**		**10**		**20**	
+0	0.936	0.030	0.901	0.030	0.793	0.030	0.645	0.030	0.516	0.030	0.453	0.030	0.255	0.030	0.188	0.030	0.156	0.030
+1	0.064	0.030	0.099	0.030	0.207	0.030	0.220	0.030	0.241	0.030	0.230	0.030	0.221	0.030	0.135	0.030	0.092	0.030
+2	0.000	0.030	0.000	0.030	0.000	0.030	0.101	0.030	0.176	0.030	0.183	0.030	0.275	0.030	0.233	0.030	0.185	0.030
+3	0.000	0.030	0.000	0.030	0.000	0.030	0.026	0.030	0.054	0.030	0.095	0.030	0.128	0.030	0.159	0.030	0.122	0.030
+4	0.000	0.030	0.000	0.030	0.000	0.030	0.009	0.030	0.013	0.030	0.034	0.030	0.083	0.030	0.164	0.030	0.177	0.030
+5	0.000	0.030	0.000	0.030	0.000	0.030	0.000	0.030	0.000	0.030	0.005	0.030	0.025	0.030	0.061	0.030	0.135	0.030
+6	0.000	0.030	0.000	0.030	0.000	0.030	0.000	0.030	0.000	0.030	0.000	0.030	0.014	0.030	0.060	0.030	0.132	0.030
FBP	**0**		**1**		**1.5**		**2**		**2.5**		**3**		**5**		**10**		**20**	
+0	0.733	0.045	0.685	0.045	0.660	0.045	0.580	0.045	0.602	0.045	0.594	0.045	0.531	0.045	0.456	0.045	0.488	0.045
+1	0.081	0.045	0.114	0.045	0.062	0.045	0.144	0.045	0.136	0.045	0.124	0.045	0.126	0.045	0.052	0.045	0.058	0.045
+2	0.053	0.045	0.061	0.045	0.061	0.045	0.081	0.045	0.075	0.045	0.053	0.045	0.106	0.045	0.081	0.045	0.037	0.045
+3	0.058	0.045	0.045	0.045	0.121	0.045	0.053	0.045	0.059	0.045	0.068	0.045	0.087	0.045	0.119	0.045	0.107	0.045
+4	0.041	0.045	0.050	0.045	0.035	0.045	0.033	0.045	0.059	0.045	0.048	0.045	0.056	0.045	0.109	0.045	0.087	0.045
+5	0.033	0.045	0.045	0.045	0.060	0.045	0.109	0.045	0.069	0.045	0.113	0.045	0.093	0.045	0.137	0.045	0.147	0.045

+6	0.000	0.045	0.000	0.045	0.000	0.045	0.000	0.045	0.000	0.045	0.000	0.045	0.000	0.045	0.046	0.045	0.075	0.045
G6P	**0**		**1**		**1.5**		**2**		**2.5**		**3**		**5**		**10**		**20**	
+0	0.838	0.035	0.738	0.035	0.572	0.035	0.517	0.035	0.433	0.035	0.368	0.035	0.258	0.035	0.155	0.035	0.154	0.035
+1	0.058	0.035	0.092	0.035	0.157	0.035	0.258	0.035	0.212	0.035	0.241	0.035	0.185	0.035	0.112	0.035	0.093	0.035
+2	0.103	0.035	0.170	0.035	0.271	0.035	0.195	0.035	0.312	0.035	0.305	0.035	0.321	0.035	0.294	0.035	0.204	0.035
+3	0.000	0.035	0.000	0.035	0.000	0.035	0.027	0.035	0.035	0.035	0.057	0.035	0.130	0.035	0.153	0.035	0.119	0.035
+4	0.000	0.035	0.000	0.035	0.000	0.035	0.004	0.035	0.008	0.035	0.026	0.035	0.080	0.035	0.148	0.035	0.156	0.035
+5	0.000	0.035	0.000	0.035	0.000	0.035	0.000	0.035	0.000	0.035	0.004	0.035	0.017	0.035	0.081	0.035	0.136	0.035
+6	0.000	0.035	0.000	0.035	0.000	0.035	0.000	0.035	0.000	0.035	0.000	0.035	0.010	0.035	0.057	0.035	0.138	0.035
GA	**0**		**1**		**1.5**		**2**		**2.5**		**3**		**5**		**10**		**20**	
+0	0.986	0.020	0.983	0.020	0.990	0.020	0.984	0.020	0.984	0.020	0.978	0.020	0.949	0.020	0.935	0.020	0.972	0.020
+1	0.014	0.020	0.017	0.020	0.010	0.020	0.016	0.020	0.016	0.020	0.022	0.020	0.024	0.020	0.024	0.020	0.012	0.020
+2	0.000	0.020	0.000	0.020	0.000	0.020	0.000	0.020	0.000	0.020	0.000	0.020	0.017	0.020	0.020	0.020	0.006	0.020
+3	0.000	0.020	0.000	0.020	0.000	0.020	0.000	0.020	0.000	0.020	0.000	0.020	0.010	0.020	0.022	0.020	0.010	0.020
MAL	**0**		**1**		**1.5**		**2**		**2.5**		**3**		**5**		**10**		**20**	
+0	0.942	0.020	0.942	0.020	0.921	0.020	0.917	0.020	0.923	0.020	0.944	0.020	0.905	0.020	0.837	0.020	0.938	0.020
+1	0.044	0.020	0.046	0.020	0.062	0.020	0.064	0.020	0.059	0.020	0.047	0.020	0.064	0.020	0.069	0.020	0.050	0.020
+2	0.014	0.020	0.012	0.020	0.017	0.020	0.019	0.020	0.018	0.020	0.009	0.020	0.031	0.020	0.070	0.020	0.011	0.020
+3	0.000	0.020	0.000	0.020	0.000	0.020	0.000	0.020	0.000	0.020	0.000	0.020	0.000	0.020	0.024	0.020	0.001	0.020
+4	0.000	0.020	0.000	0.020	0.000	0.020	0.000	0.020	0.000	0.020	0.000	0.020	0.000	0.020	0.000	0.020	0.000	0.020
PEP	**0**		**1**		**1.5**		**2**		**2.5**		**3**		**5**		**10**		**20**	
+0	0.963	0.020	0.887	0.020	0.751	0.020	0.668	0.020	0.584	0.020	0.452	0.020	0.248	0.020	0.165	0.020	0.129	0.020
+1	0.032	0.020	0.108	0.020	0.234	0.020	0.305	0.020	0.365	0.020	0.447	0.020	0.518	0.020	0.413	0.020	0.223	0.020
+2	0.005	0.020	0.004	0.020	0.015	0.020	0.021	0.020	0.040	0.020	0.078	0.020	0.149	0.020	0.191	0.020	0.193	0.020
+3	0.000	0.020	0.000	0.020	0.000	0.020	0.006	0.020	0.012	0.020	0.024	0.020	0.085	0.020	0.231	0.020	0.455	0.020
PGA	**0**		**1**		**1.5**		**2**		**2.5**		**3**		**5**		**10**		**20**	
+0	0.952	0.015	0.827	0.015	0.691	0.015	0.618	0.015	0.514	0.015	0.376	0.015	0.230	0.015	0.130	0.015	0.105	0.015
+1	0.037	0.015	0.157	0.015	0.275	0.015	0.334	0.015	0.413	0.015	0.489	0.015	0.523	0.015	0.391	0.015	0.249	0.015
+2	0.010	0.015	0.012	0.015	0.027	0.015	0.041	0.015	0.060	0.015	0.100	0.015	0.153	0.015	0.214	0.015	0.221	0.015
+3	0.001	0.015	0.003	0.015	0.007	0.015	0.008	0.015	0.013	0.015	0.035	0.015	0.094	0.015	0.265	0.015	0.425	0.015
R5P	**0**		**1**		**1.5**		**2**		**2.5**		**3**		**5**		**10**		**20**	
+0	0.937	0.030	0.929	0.030	0.905	0.030	0.906	0.030	0.884	0.030	0.837	0.030	0.793	0.030	0.661	0.030	0.473	0.030

+1	0.055	0.030	0.062	0.030	0.081	0.030	0.068	0.030	0.084	0.030	0.101	0.030	0.126	0.030	0.134	0.030	0.126	0.030
+2	0.008	0.030	0.008	0.030	0.013	0.030	0.024	0.030	0.027	0.030	0.046	0.030	0.048	0.030	0.087	0.030	0.106	0.030
+3	0.000	0.030	0.000	0.030	0.000	0.030	0.002	0.030	0.005	0.030	0.011	0.030	0.025	0.030	0.071	0.030	0.123	0.030
+4	0.000	0.030	0.000	0.030	0.000	0.030	0.000	0.030	0.000	0.030	0.004	0.030	0.007	0.030	0.027	0.030	0.082	0.030
+5	0.000	0.030	0.000	0.030	0.000	0.030	0.000	0.030	0.000	0.030	0.000	0.030	0.002	0.030	0.019	0.030	0.090	0.030
RU5P	**0**		**1**		**1.5**		**2**		**2.5**		**3**		**5**		**10**		**20**	
+0	0.900	0.030	0.782	0.030	0.606	0.030	0.600	0.030	0.571	0.030	0.583	0.030	0.462	0.030	0.624	0.030	0.382	0.030
+1	0.053	0.030	0.098	0.030	0.221	0.030	0.208	0.030	0.229	0.030	0.191	0.030	0.191	0.030	0.094	0.030	0.066	0.030
+2	0.047	0.030	0.120	0.030	0.173	0.030	0.132	0.030	0.134	0.030	0.130	0.030	0.181	0.030	0.124	0.030	0.266	0.030
+3	0.000	0.030	0.000	0.030	0.000	0.030	0.061	0.030	0.065	0.030	0.068	0.030	0.116	0.030	0.068	0.030	0.105	0.030
+4	0.000	0.030	0.000	0.030	0.000	0.030	0.000	0.030	0.000	0.030	0.028	0.030	0.033	0.030	0.063	0.030	0.091	0.030
+5	0.000	0.030	0.000	0.030	0.000	0.030	0.000	0.030	0.000	0.030	0.000	0.030	0.017	0.030	0.026	0.030	0.090	0.030
S7P	**0**		**1**		**1.5**		**2**		**2.5**		**3**		**5**		**10**		**20**	
+0	0.913	0.030	0.809	0.030	0.595	0.030	0.487	0.030	0.399	0.030	0.256	0.030	0.160	0.030	0.084	0.030	0.080	0.030
+1	0.062	0.030	0.153	0.030	0.296	0.030	0.291	0.030	0.311	0.030	0.279	0.030	0.182	0.030	0.114	0.030	0.092	0.030
+2	0.025	0.030	0.038	0.030	0.108	0.030	0.163	0.030	0.195	0.030	0.247	0.030	0.246	0.030	0.142	0.030	0.120	0.030
+3	0.000	0.030	0.000	0.030	0.000	0.030	0.048	0.030	0.075	0.030	0.149	0.030	0.218	0.030	0.175	0.030	0.133	0.030
+4	0.000	0.030	0.000	0.030	0.000	0.030	0.009	0.030	0.014	0.030	0.043	0.030	0.110	0.030	0.168	0.030	0.124	0.030
+5	0.000	0.030	0.000	0.030	0.000	0.030	0.003	0.030	0.006	0.030	0.018	0.030	0.054	0.030	0.180	0.030	0.143	0.030
+6	0.000	0.030	0.000	0.030	0.000	0.030	0.000	0.030	0.000	0.030	0.006	0.030	0.019	0.030	0.090	0.030	0.150	0.030
+7	0.000	0.030	0.000	0.030	0.000	0.030	0.000	0.030	0.000	0.030	0.003	0.030	0.010	0.030	0.048	0.030	0.159	0.030
SUC	**0**		**1**		**1.5**		**2**		**2.5**		**3**		**5**		**10**		**20**	
+0	0.957	0.020	0.957	0.020	0.961	0.020	0.955	0.020	0.963	0.020	0.957	0.020	0.953	0.020	0.958	0.020	0.955	0.020
+1	0.043	0.020	0.043	0.020	0.039	0.020	0.045	0.020	0.037	0.020	0.043	0.020	0.047	0.020	0.042	0.020	0.045	0.020
+2	0.000	0.020	0.000	0.020	0.000	0.020	0.000	0.020	0.000	0.020	0.000	0.020	0.000	0.020	0.000	0.020	0.000	0.020
+3	0.000	0.020	0.000	0.020	0.000	0.020	0.000	0.020	0.000	0.020	0.000	0.020	0.000	0.020	0.000	0.020	0.000	0.020
+4	0.000	0.020	0.000	0.020	0.000	0.020	0.000	0.020	0.000	0.020	0.000	0.020	0.000	0.020	0.000	0.020	0.000	0.020
RUBP[a]	**0**		**1**		**1.5**		**2**		**2.5**		**3**		**5**		**10**		**20**	
+0	0.913	0.020	0.833	0.020	0.558	0.020	0.532	0.020	0.443	0.020	0.380	0.020	0.231	0.020	0.171	0.020	0.143	0.020
+1	0.037	0.020	0.093	0.020	0.126	0.020	0.283	0.020	0.312	0.020	0.300	0.020	0.301	0.020	0.153	0.020	0.083	0.020
+2	0.049	0.020	0.074	0.020	0.257	0.020	0.132	0.020	0.184	0.020	0.242	0.020	0.229	0.020	0.253	0.020	0.163	0.020
+3	0.000	0.020	0.000	0.020	0.059	0.020	0.053	0.020	0.061	0.020	0.078	0.020	0.148	0.020	0.223	0.020	0.169	0.020

+4	0.000	0.020	0.000	0.020	0.000	0.020	0.000	0.020	0.000	0.020	0.000	0.020	0.061	0.020	0.113	0.020	0.170	0.020
+5	0.000	0.020	0.000	0.020	0.000	0.020	0.000	0.020	0.000	0.020	0.000	0.020	0.031	0.020	0.087	0.020	0.272	0.020

[a] Not included in INCA fitting due to one or more possible interfering peaks or low signals

Table A.3 Measured MDVs and Standard Error for *Synechocystis* sp. PCC 6803 WT, 80 µmol m^{-2} s^{-1}

	Time (min)																	
2PG	**0**		**0.5**		**1**		**1.5**		**2**		**3**		**5**		**10**		**20**	
+0	0.977	0.030	0.978	0.030	0.976	0.030	0.972	0.030	0.970	0.030	0.971	0.030	0.971	0.030	0.959	0.030	0.938	0.030
+1	0.023	0.030	0.022	0.030	0.024	0.030	0.028	0.030	0.030	0.030	0.029	0.030	0.029	0.030	0.041	0.030	0.062	0.030
+2	0.000	0.030	0.000	0.030	0.000	0.030	0.000	0.030	0.000	0.030	0.000	0.030	0.000	0.030	0.000	0.030	0.000	0.030
AKG	**0**		**0.5**		**1**		**1.5**		**2**		**3**		**5**		**10**		**20**	
+0	0.989	0.020	0.993	0.020	0.988	0.020	0.987	0.020	0.988	0.020	0.992	0.020	0.992	0.020	0.986	0.020	0.990	0.020
+1	0.011	0.020	0.007	0.020	0.012	0.020	0.013	0.020	0.012	0.020	0.008	0.020	0.008	0.020	0.014	0.020	0.010	0.020
+2	0.000	0.020	0.000	0.020	0.000	0.020	0.000	0.020	0.000	0.020	0.000	0.020	0.000	0.020	0.000	0.020	0.000	0.020
+3	0.000	0.020	0.000	0.020	0.000	0.020	0.000	0.020	0.000	0.020	0.000	0.020	0.000	0.020	0.000	0.020	0.000	0.020
+4	0.000	0.020	0.000	0.020	0.000	0.020	0.000	0.020	0.000	0.020	0.000	0.020	0.000	0.020	0.000	0.020	0.000	0.020
+5	0.000	0.020	0.000	0.020	0.000	0.020	0.000	0.020	0.000	0.020	0.000	0.020	0.000	0.020	0.000	0.020	0.000	0.020
AP	**0**		**0.5**		**1**		**1.5**		**2**		**3**		**5**		**10**		**20**	
+0	1.000	0.030	0.907	0.030	0.852	0.030	0.818	0.030	0.743	0.030	0.727	0.030	0.650	0.030	0.551	0.030	0.318	0.030
+1	0.000	0.030	0.068	0.030	0.070	0.030	0.074	0.030	0.124	0.030	0.105	0.030	0.113	0.030	0.104	0.030	0.174	0.030
+2	0.000	0.030	0.025	0.030	0.078	0.030	0.108	0.030	0.134	0.030	0.168	0.030	0.237	0.030	0.345	0.030	0.508	0.030
F6P	**0**		**0.5**		**1**		**1.5**		**2**		**3**		**5**		**10**		**20**	
+0	0.918	0.035	0.740	0.035	0.699	0.035	0.611	0.035	0.413	0.035	0.318	0.035	0.222	0.035	0.129	0.035	0.080	0.035
+1	0.064	0.035	0.161	0.035	0.230	0.035	0.277	0.035	0.247	0.035	0.223	0.035	0.116	0.035	0.105	0.035	0.065	0.035
+2	0.000	0.035	0.000	0.035	0.000	0.035	0.000	0.035	0.196	0.035	0.102	0.035	0.126	0.035	0.053	0.035	0.067	0.035
+3	0.000	0.035	0.038	0.035	0.044	0.035	0.082	0.035	0.089	0.035	0.133	0.035	0.159	0.035	0.121	0.035	0.090	0.035
+4	0.000	0.035	0.000	0.035	0.000	0.035	0.000	0.035	0.023	0.035	0.136	0.035	0.132	0.035	0.228	0.035	0.132	0.035
+5	0.008	0.035	0.023	0.035	0.015	0.035	0.011	0.035	0.023	0.035	0.062	0.035	0.134	0.035	0.119	0.035	0.198	0.035
+6	0.010	0.035	0.038	0.035	0.011	0.035	0.019	0.035	0.010	0.035	0.026	0.035	0.110	0.035	0.246	0.035	0.367	0.035
FBP	**0**		**0.5**		**1**		**1.5**		**2**		**3**		**5**		**10**		**20**	
+0	0.658	0.040	0.589	0.040	0.480	0.040	0.369	0.040	0.297	0.040	0.195	0.040	0.140	0.040	0.136	0.040	0.084	0.040
+1	0.077	0.040	0.131	0.040	0.153	0.040	0.192	0.040	0.196	0.040	0.121	0.040	0.128	0.040	0.079	0.040	0.075	0.040
+2	0.056	0.040	0.061	0.040	0.087	0.040	0.122	0.040	0.198	0.040	0.168	0.040	0.163	0.040	0.076	0.040	0.075	0.040
+3	0.084	0.040	0.086	0.040	0.108	0.040	0.149	0.040	0.144	0.040	0.191	0.040	0.218	0.040	0.168	0.040	0.130	0.040
+4	0.063	0.040	0.046	0.040	0.065	0.040	0.073	0.040	0.082	0.040	0.185	0.040	0.155	0.040	0.209	0.040	0.147	0.040
+5	0.042	0.040	0.063	0.040	0.074	0.040	0.060	0.040	0.044	0.040	0.084	0.040	0.096	0.040	0.125	0.040	0.141	0.040

+6	0.020	0.040	0.024	0.040	0.034	0.040	0.035	0.040	0.038	0.040	0.055	0.040	0.099	0.040	0.208	0.040	0.348	0.040
G6P	**0**		**0.5**		**1**		**1.5**		**2**		**3**		**5**		**10**		**20**	
+0	0.858	0.030	0.748	0.030	0.576	0.030	0.411	0.030	0.369	0.030	0.202	0.030	0.158	0.030	0.123	0.030	0.081	0.030
+1	0.059	0.030	0.108	0.030	0.169	0.030	0.261	0.030	0.240	0.030	0.189	0.030	0.118	0.030	0.060	0.030	0.051	0.030
+2	0.003	0.030	0.006	0.030	0.163	0.030	0.175	0.030	0.205	0.030	0.212	0.030	0.212	0.030	0.068	0.030	0.115	0.030
+3	0.019	0.030	0.046	0.030	0.046	0.030	0.074	0.030	0.103	0.030	0.116	0.030	0.165	0.030	0.144	0.030	0.091	0.030
+4	0.050	0.030	0.069	0.030	0.035	0.030	0.067	0.030	0.069	0.030	0.202	0.030	0.220	0.030	0.246	0.030	0.183	0.030
+5	0.003	0.030	0.007	0.030	0.005	0.030	0.005	0.030	0.009	0.030	0.040	0.030	0.066	0.030	0.146	0.030	0.151	0.030
+6	0.009	0.030	0.016	0.030	0.007	0.030	0.007	0.030	0.005	0.030	0.039	0.030	0.061	0.030	0.214	0.030	0.328	0.030
GA	**0**		**0.5**		**1**		**1.5**		**2**		**3**		**5**		**10**		**20**	
+0	0.991	0.030	0.983	0.030	0.984	0.030	0.969	0.030	0.977	0.030	0.978	0.030	0.960	0.030	0.915	0.030	0.917	0.030
+1	0.009	0.030	0.013	0.030	0.013	0.030	0.014	0.030	0.015	0.030	0.015	0.030	0.021	0.030	0.019	0.030	0.016	0.030
+2	0.000	0.030	0.004	0.030	0.003	0.030	0.004	0.030	0.006	0.030	0.003	0.030	0.007	0.030	0.009	0.030	0.010	0.030
+3	0.000	0.030	0.000	0.030	0.000	0.030	0.014	0.030	0.002	0.030	0.004	0.030	0.012	0.030	0.056	0.030	0.057	0.030
MAL	**0**		**0.5**		**1**		**1.5**		**2**		**3**		**5**		**10**		**20**	
+0	0.955	0.030	0.948	0.030	0.942	0.030	0.943	0.030	0.942	0.030	0.903	0.030	0.890	0.030	0.738	0.030	0.739	0.030
+1	0.042	0.030	0.045	0.030	0.048	0.030	0.047	0.030	0.047	0.030	0.071	0.030	0.063	0.030	0.066	0.030	0.061	0.030
+2	0.003	0.030	0.007	0.030	0.010	0.030	0.010	0.030	0.012	0.030	0.021	0.030	0.039	0.030	0.105	0.030	0.062	0.030
+3	0.000	0.030	0.000	0.030	0.000	0.030	0.000	0.030	0.000	0.030	0.004	0.030	0.005	0.030	0.033	0.030	0.030	0.030
+4	0.000	0.030	0.000	0.030	0.000	0.030	0.000	0.030	0.000	0.030	0.000	0.030	0.002	0.030	0.058	0.030	0.108	0.030
PEP	**0**		**0.5**		**1**		**1.5**		**2**		**3**		**5**		**10**		**20**	
+0	0.960	0.020	0.850	0.020	0.689	0.020	0.552	0.020	0.449	0.020	0.335	0.020	0.195	0.020	0.099	0.020	0.090	0.020
+1	0.033	0.020	0.138	0.020	0.279	0.020	0.380	0.020	0.435	0.020	0.454	0.020	0.416	0.020	0.253	0.020	0.139	0.020
+2	0.006	0.020	0.011	0.020	0.024	0.020	0.049	0.020	0.081	0.020	0.126	0.020	0.176	0.020	0.174	0.020	0.148	0.020
+3	0.001	0.020	0.002	0.020	0.009	0.020	0.019	0.020	0.035	0.020	0.085	0.020	0.212	0.020	0.474	0.020	0.623	0.020
PGA	**0**		**0.5**		**1**		**1.5**		**2**		**3**		**5**		**10**		**20**	
+0	0.954	0.015	0.790	0.015	0.605	0.015	0.505	0.015	0.390	0.015	0.267	0.015	0.165	0.015	0.090	0.015	0.073	0.015
+1	0.036	0.015	0.183	0.015	0.325	0.015	0.400	0.015	0.467	0.015	0.503	0.015	0.426	0.015	0.266	0.015	0.143	0.015
+2	0.007	0.015	0.019	0.015	0.045	0.015	0.066	0.015	0.095	0.015	0.138	0.015	0.175	0.015	0.167	0.015	0.144	0.015
+3	0.002	0.015	0.008	0.015	0.025	0.015	0.030	0.015	0.047	0.015	0.092	0.015	0.233	0.015	0.477	0.015	0.640	0.015
R5P	**0**		**0.5**		**1**		**1.5**		**2**		**3**		**5**		**10**		**20**	
+0	0.880	0.030	0.879	0.030	0.831	0.030	0.837	0.030	0.812	0.030	0.704	0.030	0.597	0.030	0.371	0.030	0.217	0.030

+1	0.056	0.030	0.060	0.030	0.075	0.030	0.093	0.030	0.103	0.030	0.149	0.030	0.136	0.030	0.120	0.030	0.077	0.030
+2	0.045	0.030	0.052	0.030	0.081	0.030	0.056	0.030	0.064	0.030	0.101	0.030	0.098	0.030	0.123	0.030	0.107	0.030
+3	0.010	0.030	0.003	0.030	0.008	0.030	0.009	0.030	0.017	0.030	0.036	0.030	0.067	0.030	0.143	0.030	0.160	0.030
+4	0.000	0.030	0.000	0.030	0.000	0.030	0.000	0.030	0.000	0.030	0.000	0.030	0.084	0.030	0.134	0.030	0.118	0.030
+5	0.009	0.030	0.006	0.030	0.005	0.030	0.005	0.030	0.005	0.030	0.010	0.030	0.018	0.030	0.110	0.030	0.322	0.030
S7P	**0**		**0.5**		**1**		**1.5**		**2**		**3**		**5**		**10**		**20**	
+0	0.751	0.035	0.630	0.035	0.592	0.035	0.484	0.035	0.372	0.035	0.294	0.035	0.204	0.035	0.156	0.035	0.116	0.035
+1	0.064	0.035	0.129	0.035	0.186	0.035	0.209	0.035	0.208	0.035	0.152	0.035	0.119	0.035	0.076	0.035	0.061	0.035
+2	0.068	0.035	0.132	0.035	0.119	0.035	0.166	0.035	0.170	0.035	0.197	0.035	0.149	0.035	0.086	0.035	0.092	0.035
+3	0.001	0.035	0.006	0.035	0.029	0.035	0.058	0.035	0.101	0.035	0.146	0.035	0.154	0.035	0.113	0.035	0.104	0.035
+4	0.000	0.035	0.000	0.035	0.000	0.035	0.000	0.035	0.078	0.035	0.118	0.035	0.149	0.035	0.133	0.035	0.111	0.035
+5	0.020	0.035	0.024	0.035	0.014	0.035	0.021	0.035	0.028	0.035	0.035	0.035	0.120	0.035	0.172	0.035	0.121	0.035
+6	0.059	0.035	0.050	0.035	0.039	0.035	0.040	0.035	0.023	0.035	0.034	0.035	0.068	0.035	0.104	0.035	0.129	0.035
+7	0.036	0.035	0.028	0.035	0.020	0.035	0.022	0.035	0.020	0.035	0.023	0.035	0.038	0.035	0.160	0.035	0.266	0.035
SUC	**0**		**0.5**		**1**		**1.5**		**2**		**3**		**5**		**10**		**20**	
+0	0.951	0.020	0.952	0.020	0.948	0.020	0.946	0.020	0.946	0.020	0.955	0.020	0.947	0.020	0.954	0.020	0.936	0.020
+1	0.044	0.020	0.042	0.020	0.047	0.020	0.049	0.020	0.048	0.020	0.041	0.020	0.048	0.020	0.038	0.020	0.050	0.020
+2	0.005	0.020	0.005	0.020	0.005	0.020	0.005	0.020	0.005	0.020	0.003	0.020	0.005	0.020	0.006	0.020	0.009	0.020
+3	0.000	0.020	0.000	0.020	0.000	0.020	0.000	0.020	0.000	0.020	0.000	0.020	0.000	0.020	0.001	0.020	0.002	0.020
+4	0.000	0.020	0.000	0.020	0.000	0.020	0.000	0.020	0.000	0.020	0.000	0.020	0.000	0.020	0.001	0.020	0.003	0.020
RUBP[a]	**0**		**0.5**		**1**		**1.5**		**2**		**3**		**5**		**10**		**20**	
+0	1.000	N/A	0.804	N/A	0.698	N/A	0.642	N/A	0.610	N/A	0.556	N/A	0.439	N/A	0.177	N/A	0.143	N/A
+1	0.000	N/A	0.142	N/A	0.221	N/A	0.259	N/A	0.181	N/A	0.157	N/A	0.167	N/A	0.102	N/A	0.069	N/A
+2	0.000	N/A	0.054	N/A	0.082	N/A	0.099	N/A	0.103	N/A	0.165	N/A	0.164	N/A	0.110	N/A	0.044	N/A
+3	0.000	N/A	0.000	N/A	0.000	N/A	0.000	N/A	0.107	N/A	0.123	N/A	0.229	N/A	0.236	N/A	0.296	N/A
+4	0.000	N/A	0.000	N/A	0.000	N/A	0.000	N/A	0.000	N/A	0.000	N/A	0.000	N/A	0.109	N/A	0.126	N/A
+5	0.000	N/A	0.000	N/A	0.000	N/A	0.000	N/A	0.000	N/A	0.000	N/A	0.000	N/A	0.266	N/A	0.322	N/A

[a] Not included in INCA fitting due to one or more possible interfering peaks or low signals

Table A.4 Measured MDVs and Standard Error for *Synechocystis* sp. PCC 6803 WT, 480 µmol m^{-2} s^{-1}

	Time (min)																	
2PG	**0**		**0.5**		**1**		**1.5**		**2**		**3**		**5**		**10**		**20**	
+0	0.967	0.030	0.942	0.030	0.887	0.030	0.844	0.030	0.766	0.030	0.729	0.030	0.574	0.030	0.575	0.030	0.461	0.030
+1	0.026	0.030	0.043	0.030	0.082	0.030	0.102	0.030	0.110	0.030	0.106	0.030	0.080	0.030	0.030	0.030	0.045	0.030
+2	0.008	0.030	0.015	0.030	0.031	0.030	0.054	0.030	0.124	0.030	0.165	0.030	0.346	0.030	0.394	0.030	0.493	0.030
AKG	**0**		**0.5**		**1**		**1.5**		**2**		**3**		**5**		**10**		**20**	
+0	0.926	0.020	0.945	0.020	0.952	0.020	0.931	0.020	0.941	0.020	0.973	0.020	0.858	0.020	0.852	0.020	0.821	0.020
+1	0.074	0.020	0.055	0.020	0.048	0.020	0.069	0.020	0.059	0.020	0.027	0.020	0.105	0.020	0.132	0.020	0.141	0.020
+2	0.000	0.020	0.000	0.020	0.000	0.020	0.000	0.020	0.000	0.020	0.000	0.020	0.037	0.020	0.016	0.020	0.038	0.020
+3	0.000	0.020	0.000	0.020	0.000	0.020	0.000	0.020	0.000	0.020	0.000	0.020	0.000	0.020	0.000	0.020	0.000	0.020
+4	0.000	0.020	0.000	0.020	0.000	0.020	0.000	0.020	0.000	0.020	0.000	0.020	0.000	0.020	0.000	0.020	0.000	0.020
+5	0.000	0.020	0.000	0.020	0.000	0.020	0.000	0.020	0.000	0.020	0.000	0.020	0.000	0.020	0.000	0.020	0.000	0.020
AP	**0**		**0.5**		**1**		**1.5**		**2**		**3**		**5**		**10**		**20**	
+0	0.925	0.030	0.880	0.030	0.878	0.030	0.811	0.030	0.689	0.030	0.527	0.030	0.457	0.030	0.334	0.030	0.269	0.030
+1	0.024	0.030	0.036	0.030	0.075	0.030	0.102	0.030	0.145	0.030	0.177	0.030	0.120	0.030	0.066	0.030	0.058	0.030
+2	0.051	0.030	0.085	0.030	0.046	0.030	0.087	0.030	0.165	0.030	0.296	0.030	0.423	0.030	0.601	0.030	0.673	0.030
F6P	**0**		**0.5**		**1**		**1.5**		**2**		**3**		**5**		**10**		**20**	
+0	0.820	0.037	0.383	0.037	0.288	0.037	0.162	0.037	0.134	0.037	0.131	0.037	0.030	0.037	0.006	0.037	0.021	0.037
+1	0.050	0.037	0.185	0.037	0.227	0.037	0.193	0.037	0.095	0.037	0.058	0.037	0.017	0.037	0.009	0.037	0.006	0.037
+2	0.126	0.037	0.404	0.037	0.354	0.037	0.371	0.037	0.278	0.037	0.292	0.037	0.226	0.037	0.101	0.037	0.061	0.037
+3	0.004	0.037	0.028	0.037	0.079	0.037	0.147	0.037	0.184	0.037	0.151	0.037	0.097	0.037	0.043	0.037	0.016	0.037
+4	0.000	0.037	0.000	0.037	0.045	0.037	0.102	0.037	0.263	0.037	0.245	0.037	0.252	0.037	0.126	0.037	0.064	0.037
+5	0.000	0.037	0.000	0.037	0.007	0.037	0.025	0.037	0.046	0.037	0.090	0.037	0.146	0.037	0.136	0.037	0.111	0.037
+6	0.000	0.037	0.000	0.037	0.000	0.037	0.000	0.037	0.000	0.037	0.034	0.037	0.232	0.037	0.580	0.037	0.721	0.037
G6P	**0**		**0.5**		**1**		**1.5**		**2**		**3**		**5**		**10**		**20**	
+0	0.808	0.035	0.425	0.035	0.263	0.035	0.152	0.035	0.137	0.035	0.135	0.035	0.044	0.035	0.030	0.035	0.019	0.035
+1	0.058	0.035	0.182	0.035	0.305	0.035	0.236	0.035	0.112	0.035	0.071	0.035	0.015	0.035	0.006	0.035	0.004	0.035
+2	0.090	0.035	0.317	0.035	0.294	0.035	0.312	0.035	0.320	0.035	0.238	0.035	0.127	0.035	0.014	0.035	0.024	0.035
+3	0.004	0.035	0.026	0.035	0.086	0.035	0.168	0.035	0.183	0.035	0.179	0.035	0.098	0.035	0.026	0.035	0.016	0.035
+4	0.016	0.035	0.042	0.035	0.040	0.035	0.098	0.035	0.184	0.035	0.215	0.035	0.269	0.035	0.123	0.035	0.058	0.035
+5	0.004	0.035	0.004	0.035	0.008	0.035	0.024	0.035	0.035	0.035	0.087	0.035	0.167	0.035	0.147	0.035	0.117	0.035

+6	0.019	0.035	0.004	0.035	0.005	0.035	0.011	0.035	0.029	0.035	0.075	0.035	0.279	0.035	0.653	0.035	0.762	0.035
PEP	**0**		**0.5**		**1**		**1.5**		**2**		**3**		**5**		**10**		**20**	
+0	0.936	0.030	0.590	0.030	0.379	0.030	0.251	0.030	0.142	0.030	0.067	0.030	0.025	0.030	0.014	0.030	0.000	0.030
+1	0.041	0.030	0.374	0.030	0.508	0.030	0.540	0.030	0.551	0.030	0.458	0.030	0.264	0.030	0.084	0.030	0.031	0.030
+2	0.011	0.030	0.029	0.030	0.084	0.030	0.136	0.030	0.162	0.030	0.195	0.030	0.162	0.030	0.098	0.030	0.066	0.030
+3	0.012	0.030	0.006	0.030	0.029	0.030	0.073	0.030	0.145	0.030	0.280	0.030	0.549	0.030	0.805	0.030	0.903	0.030
PGA	**0**		**0.5**		**1**		**1.5**		**2**		**3**		**5**		**10**		**20**	
+0	0.926	0.015	0.502	0.015	0.313	0.015	0.214	0.015	0.124	0.015	0.085	0.015	0.035	0.015	0.022	0.015	0.019	0.015
+1	0.049	0.015	0.442	0.015	0.505	0.015	0.486	0.015	0.527	0.015	0.371	0.015	0.256	0.015	0.089	0.015	0.033	0.015
+2	0.013	0.015	0.046	0.015	0.126	0.015	0.178	0.015	0.176	0.015	0.183	0.015	0.170	0.015	0.103	0.015	0.062	0.015
+3	0.012	0.015	0.011	0.015	0.056	0.015	0.123	0.015	0.173	0.015	0.361	0.015	0.539	0.015	0.786	0.015	0.887	0.015
R5P	**0**		**0.5**		**1**		**1.5**		**2**		**3**		**5**		**10**		**20**	
+0	0.876	0.040	0.664	0.040	0.517	0.040	0.264	0.040	0.232	0.040	0.215	0.040	0.217	0.040	0.162	0.040	0.129	0.040
+1	0.054	0.040	0.225	0.040	0.261	0.040	0.291	0.040	0.204	0.040	0.137	0.040	0.075	0.040	0.035	0.040	0.019	0.040
+2	0.070	0.040	0.098	0.040	0.170	0.040	0.255	0.040	0.284	0.040	0.219	0.040	0.122	0.040	0.113	0.040	0.053	0.040
+3	0.000	0.040	0.014	0.040	0.052	0.040	0.134	0.040	0.168	0.040	0.214	0.040	0.209	0.040	0.116	0.040	0.053	0.040
+4	0.000	0.040	0.000	0.040	0.000	0.040	0.044	0.040	0.087	0.040	0.137	0.040	0.167	0.040	0.122	0.040	0.036	0.040
+5	0.000	0.040	0.000	0.040	0.000	0.040	0.014	0.040	0.025	0.040	0.078	0.040	0.209	0.040	0.452	0.040	0.710	0.040
RU5P	**0**		**0.5**		**1**		**1.5**		**2**		**3**		**5**		**10**		**20**	
+0	0.892	0.040	0.533	0.040	0.381	0.040	0.182	0.040	0.068	0.040	0.056	0.040	0.052	0.040	0.041	0.040	0.053	0.040
+1	0.053	0.040	0.323	0.040	0.370	0.040	0.297	0.040	0.215	0.040	0.101	0.040	0.055	0.040	0.027	0.040	0.000	0.040
+2	0.022	0.040	0.122	0.040	0.191	0.040	0.325	0.040	0.306	0.040	0.228	0.040	0.115	0.040	0.098	0.040	0.078	0.040
+3	0.033	0.040	0.022	0.040	0.059	0.040	0.129	0.040	0.212	0.040	0.289	0.040	0.274	0.040	0.124	0.040	0.057	0.040
+4	0.000	0.040	0.000	0.040	0.000	0.040	0.053	0.040	0.161	0.040	0.211	0.040	0.229	0.040	0.193	0.040	0.177	0.040
+5	0.000	0.040	0.000	0.040	0.000	0.040	0.014	0.040	0.038	0.040	0.115	0.040	0.274	0.040	0.518	0.040	0.635	0.040
S7P	**0**		**0.5**		**1**		**1.5**		**2**		**3**		**5**		**10**		**20**	
+0	0.871	0.040	0.445	0.040	0.171	0.040	0.082	0.040	0.037	0.040	0.008	0.040	0.011	0.040	0.009	0.040	0.006	0.040
+1	0.070	0.040	0.350	0.040	0.311	0.040	0.181	0.040	0.106	0.040	0.037	0.040	0.015	0.040	0.005	0.040	0.005	0.040
+2	0.019	0.040	0.160	0.040	0.286	0.040	0.265	0.040	0.214	0.040	0.107	0.040	0.040	0.040	0.017	0.040	0.006	0.040
+3	0.039	0.040	0.045	0.040	0.165	0.040	0.253	0.040	0.279	0.040	0.214	0.040	0.100	0.040	0.035	0.040	0.019	0.040
+4	0.000	0.040	0.000	0.040	0.063	0.040	0.134	0.040	0.194	0.040	0.242	0.040	0.090	0.040	0.022	0.040	0.017	0.040
+5	0.000	0.040	0.000	0.040	0.000	0.040	0.062	0.040	0.113	0.040	0.210	0.040	0.267	0.040	0.159	0.040	0.063	0.040

+6	0.000	0.040	0.000	0.040	0.004	0.040	0.017	0.040	0.042	0.040	0.119	0.040	0.215	0.040	0.177	0.040	0.154	0.040
+7	0.000	0.040	0.000	0.040	0.000	0.040	0.006	0.040	0.015	0.040	0.063	0.040	0.262	0.040	0.576	0.040	0.730	0.040
SUC	**0**		**0.5**		**1**		**1.5**		**2**		**3**		**5**		**10**		**20**	
+0	0.940	0.030	0.946	0.030	0.931	0.030	0.924	0.030	0.946	0.030	0.943	0.030	0.920	0.030	0.910	0.030	0.904	0.030
+1	0.054	0.030	0.049	0.030	0.061	0.030	0.068	0.030	0.047	0.030	0.048	0.030	0.055	0.030	0.047	0.030	0.025	0.030
+2	0.006	0.030	0.005	0.030	0.007	0.030	0.008	0.030	0.007	0.030	0.008	0.030	0.016	0.030	0.019	0.030	0.018	0.030
+3	0.000	0.030	0.000	0.030	0.000	0.030	0.000	0.030	0.000	0.030	0.001	0.030	0.003	0.030	0.007	0.030	0.009	0.030
+4	0.000	0.030	0.000	0.030	0.000	0.030	0.000	0.030	0.000	0.030	0.000	0.030	0.005	0.030	0.017	0.030	0.043	0.030
RUBP[a]	**0**		**0.5**		**1**		**1.5**		**2**		**3**		**5**		**10**		**20**	
+0	0.910	0.020	0.615	0.020	0.316	0.020	0.212	0.020	0.157	0.020	0.122	0.020	0.117	0.020	0.119	0.020	0.000	0.020
+1	0.070	0.020	0.301	0.020	0.422	0.020	0.352	0.020	0.280	0.020	0.254	0.020	0.073	0.020	0.038	0.020	0.000	0.020
+2	0.019	0.020	0.069	0.020	0.175	0.020	0.226	0.020	0.302	0.020	0.284	0.020	0.103	0.020	0.039	0.020	0.073	0.020
+3	0.001	0.020	0.013	0.020	0.070	0.020	0.156	0.020	0.169	0.020	0.199	0.020	0.245	0.020	0.118	0.020	0.107	0.020
+4	0.000	0.020	0.001	0.020	0.013	0.020	0.040	0.020	0.057	0.020	0.075	0.020	0.163	0.020	0.117	0.020	0.078	0.020
+5	0.000	0.020	0.000	0.020	0.004	0.020	0.014	0.020	0.035	0.020	0.066	0.020	0.300	0.020	0.569	0.020	0.742	0.020
FBP[a]	**0**		**0.5**		**1**		**1.5**		**2**		**3**		**5**		**10**		**20**	
+0	0.793	0.040	0.449	0.040	0.239	0.040	0.119	0.040	0.122	0.040	0.120	0.040	0.082	0.040	0.095	0.040	0.061	0.040
+1	0.059	0.040	0.352	0.040	0.356	0.040	0.262	0.040	0.177	0.040	0.104	0.040	0.049	0.040	0.022	0.040	0.025	0.040
+2	0.047	0.040	0.128	0.040	0.252	0.040	0.320	0.040	0.264	0.040	0.180	0.040	0.096	0.040	0.039	0.040	0.082	0.040
+3	0.030	0.040	0.030	0.040	0.096	0.040	0.164	0.040	0.184	0.040	0.147	0.040	0.128	0.040	0.091	0.040	0.110	0.040
+4	0.026	0.040	0.019	0.040	0.036	0.040	0.092	0.040	0.135	0.040	0.256	0.040	0.243	0.040	0.141	0.040	0.062	0.040
+5	0.034	0.040	0.013	0.040	0.012	0.040	0.028	0.040	0.063	0.040	0.099	0.040	0.158	0.040	0.127	0.040	0.093	0.040
+6	0.012	0.040	0.009	0.040	0.010	0.040	0.015	0.040	0.055	0.040	0.095	0.040	0.245	0.040	0.484	0.040	0.568	0.040
GA[a]	**0**		**0.5**		**1**		**1.5**		**2**		**3**		**5**		**10**		**20**	
+0	0.989	0.040	0.979	0.040	0.950	0.040	0.927	0.040	0.962	0.040	0.936	0.040	0.745	0.040	0.823	0.040	0.783	0.040
+1	0.011	0.040	0.017	0.040	0.032	0.040	0.034	0.040	0.020	0.040	0.017	0.040	0.023	0.040	0.009	0.040	0.009	0.040
+2	0.000	0.040	0.004	0.040	0.009	0.040	0.015	0.040	0.000	0.040	0.000	0.040	0.024	0.040	0.008	0.040	0.000	0.040
+3	0.000	0.040	0.001	0.040	0.009	0.040	0.024	0.040	0.018	0.040	0.047	0.040	0.208	0.040	0.160	0.040	0.208	0.040
MAL[a]	**0**		**0.5**		**1**		**1.5**		**2**		**3**		**5**		**10**		**20**	
+0	0.943	0.030	0.892	0.030	0.906	0.030	0.801	0.030	0.844	0.030	0.842	0.030	0.718	0.030	0.879	0.030	0.759	0.030
+1	0.047	0.030	0.076	0.030	0.067	0.030	0.106	0.030	0.076	0.030	0.067	0.030	0.056	0.030	0.048	0.030	0.038	0.030
+2	0.010	0.030	0.030	0.030	0.024	0.030	0.074	0.030	0.061	0.030	0.060	0.030	0.110	0.030	0.020	0.030	0.016	0.030

+3	0.000	0.030	0.002	0.030	0.002	0.030	0.014	0.030	0.012	0.030	0.015	0.030	0.043	0.030	0.008	0.030	0.012	0.030
+4	0.000	0.030	0.000	0.030	0.001	0.030	0.005	0.030	0.007	0.030	0.015	0.030	0.072	0.030	0.044	0.030	0.174	0.030

[a] Not included in INCA fitting due to one or more possible interfering peaks or low signals

Table A.5 Measured MDVs and Standard Error for *Synechocystis* sp. PCC 6803 WT, 960 µmol m^{-2} s^{-1}

	Time (min)																	
2PG	**0**		**0.5**		**1**		**1.5**		**2**		**3**		**5**		**10**		**20**	
+0	0.976	0.030	0.939	0.030	0.930	0.030	0.848	0.030	0.749	0.030	0.742	0.030	0.732	0.030	0.445	0.030	0.355	0.030
+1	0.024	0.030	0.061	0.030	0.070	0.030	0.110	0.030	0.126	0.030	0.113	0.030	0.073	0.030	0.071	0.030	0.047	0.030
+2	0.000	0.030	0.000	0.030	0.000	0.030	0.042	0.030	0.125	0.030	0.145	0.030	0.196	0.030	0.484	0.030	0.597	0.030
AKG	**0**		**0.5**		**1**		**1.5**		**2**		**3**		**5**		**10**		**20**	
+0	0.992	0.020	0.985	0.020	0.990	0.020	0.988	0.020	0.991	0.020	0.990	0.020	0.992	0.020	0.990	0.020	0.990	0.020
+1	0.008	0.020	0.015	0.020	0.010	0.020	0.012	0.020	0.009	0.020	0.010	0.020	0.008	0.020	0.010	0.020	0.010	0.020
+2	0.000	0.020	0.000	0.020	0.000	0.020	0.000	0.020	0.000	0.020	0.000	0.020	0.000	0.020	0.000	0.020	0.000	0.020
+3	0.000	0.020	0.000	0.020	0.000	0.020	0.000	0.020	0.000	0.020	0.000	0.020	0.000	0.020	0.000	0.020	0.000	0.020
+4	0.000	0.020	0.000	0.020	0.000	0.020	0.000	0.020	0.000	0.020	0.000	0.020	0.000	0.020	0.000	0.020	0.000	0.020
+5	0.000	0.020	0.000	0.020	0.000	0.020	0.000	0.020	0.000	0.020	0.000	0.020	0.000	0.020	0.000	0.020	0.000	0.020
AP	**0**		**0.5**		**1**		**1.5**		**2**		**3**		**5**		**10**		**20**	
+0	0.961	0.025	0.853	0.025	0.887	0.025	0.828	0.025	0.796	0.025	0.762	0.025	0.822	0.025	0.653	0.025	0.471	0.025
+1	0.021	0.025	0.037	0.025	0.041	0.025	0.069	0.025	0.074	0.025	0.073	0.025	0.038	0.025	0.030	0.025	0.025	0.025
+2	0.018	0.025	0.110	0.025	0.072	0.025	0.103	0.025	0.130	0.025	0.165	0.025	0.140	0.025	0.317	0.025	0.503	0.025
F6P	**0**		**0.5**		**1**		**1.5**		**2**		**3**		**5**		**10**		**20**	
+0	0.884	0.040	0.646	0.040	0.493	0.040	0.321	0.040	0.258	0.040	0.193	0.040	0.286	0.040	0.103	0.040	0.052	0.040
+1	0.054	0.040	0.196	0.040	0.189	0.040	0.229	0.040	0.141	0.040	0.063	0.040	0.041	0.040	0.016	0.040	0.007	0.040
+2	0.062	0.040	0.120	0.040	0.223	0.040	0.228	0.040	0.264	0.040	0.213	0.040	0.117	0.040	0.044	0.040	0.031	0.040
+3	0.000	0.040	0.025	0.040	0.055	0.040	0.107	0.040	0.127	0.040	0.125	0.040	0.081	0.040	0.018	0.040	0.012	0.040
+4	0.000	0.040	0.012	0.040	0.031	0.040	0.083	0.040	0.134	0.040	0.224	0.040	0.176	0.040	0.113	0.040	0.050	0.040
+5	0.000	0.040	0.002	0.040	0.007	0.040	0.022	0.040	0.050	0.040	0.088	0.040	0.097	0.040	0.089	0.040	0.081	0.040
+6	0.000	0.040	0.000	0.040	0.003	0.040	0.010	0.040	0.025	0.040	0.094	0.040	0.202	0.040	0.619	0.040	0.768	0.040
FBP	**0**		**0.5**		**1**		**1.5**		**2**		**3**		**5**		**10**		**20**	
+0	0.745	0.050	0.404	0.050	0.291	0.050	0.182	0.050	0.175	0.050	0.264	0.050	0.175	0.050	0.153	0.050	0.136	0.050
+1	0.080	0.050	0.300	0.050	0.260	0.050	0.205	0.050	0.137	0.050	0.072	0.050	0.062	0.050	0.051	0.050	0.046	0.050
+2	0.054	0.050	0.146	0.050	0.198	0.050	0.237	0.050	0.196	0.050	0.124	0.050	0.072	0.050	0.067	0.050	0.063	0.050
+3	0.064	0.050	0.079	0.050	0.142	0.050	0.172	0.050	0.216	0.050	0.188	0.050	0.138	0.050	0.134	0.050	0.112	0.050
+4	0.057	0.050	0.071	0.050	0.066	0.050	0.115	0.050	0.137	0.050	0.173	0.050	0.190	0.050	0.122	0.050	0.098	0.050
+5	0.000	0.050	0.000	0.050	0.034	0.050	0.057	0.050	0.070	0.050	0.068	0.050	0.122	0.050	0.092	0.050	0.086	0.050

+6	0.000	0.050	0.000	0.050	0.010	0.050	0.032	0.050	0.069	0.050	0.111	0.050	0.241	0.050	0.380	0.050	0.460	0.050
G6P	**0**		**0.5**		**1**		**1.5**		**2**		**3**		**5**		**10**		**20**	
+0	0.885	0.030	0.477	0.030	0.305	0.030	0.144	0.030	0.103	0.030	0.056	0.030	0.083	0.030	0.026	0.030	0.013	0.030
+1	0.067	0.030	0.307	0.030	0.303	0.030	0.240	0.030	0.155	0.030	0.051	0.030	0.017	0.030	0.004	0.030	0.003	0.030
+2	0.042	0.030	0.173	0.030	0.246	0.030	0.273	0.030	0.265	0.030	0.180	0.030	0.096	0.030	0.026	0.030	0.019	0.030
+3	0.001	0.030	0.032	0.030	0.091	0.030	0.168	0.030	0.161	0.030	0.169	0.030	0.069	0.030	0.020	0.030	0.009	0.030
+4	0.005	0.030	0.010	0.030	0.043	0.030	0.132	0.030	0.208	0.030	0.308	0.030	0.244	0.030	0.100	0.030	0.046	0.030
+5	0.000	0.030	0.001	0.030	0.009	0.030	0.030	0.030	0.064	0.030	0.125	0.030	0.142	0.030	0.136	0.030	0.093	0.030
+6	0.000	0.030	0.000	0.030	0.002	0.030	0.013	0.030	0.045	0.030	0.112	0.030	0.351	0.030	0.687	0.030	0.816	0.030
MAL	**0**		**0.5**		**1**		**1.5**		**2**		**3**		**5**		**10**		**20**	
+0	0.950	0.020	0.932	0.020	0.936	0.020	0.805	0.020	0.809	0.020	0.902	0.020	0.900	0.020	0.827	0.020	0.705	0.020
+1	0.040	0.020	0.055	0.020	0.050	0.020	0.116	0.020	0.097	0.020	0.050	0.020	0.054	0.020	0.046	0.020	0.039	0.020
+2	0.008	0.020	0.011	0.020	0.012	0.020	0.063	0.020	0.072	0.020	0.032	0.020	0.026	0.020	0.029	0.020	0.016	0.020
+3	0.002	0.020	0.001	0.020	0.001	0.020	0.011	0.020	0.014	0.020	0.008	0.020	0.008	0.020	0.012	0.020	0.010	0.020
+4	0.000	0.020	0.000	0.020	0.000	0.020	0.005	0.020	0.007	0.020	0.008	0.020	0.011	0.020	0.087	0.020	0.230	0.020
PEP	**0**		**0.5**		**1**		**1.5**		**2**		**3**		**5**		**10**		**20**	
+0	0.947	0.020	0.560	0.020	0.376	0.020	0.233	0.020	0.156	0.020	0.066	0.020	0.061	0.020	0.015	0.020	0.011	0.020
+1	0.042	0.020	0.392	0.020	0.500	0.020	0.485	0.020	0.480	0.020	0.412	0.020	0.212	0.020	0.061	0.020	0.023	0.020
+2	0.009	0.020	0.040	0.020	0.083	0.020	0.157	0.020	0.180	0.020	0.176	0.020	0.128	0.020	0.072	0.020	0.058	0.020
+3	0.002	0.020	0.009	0.020	0.040	0.020	0.125	0.020	0.184	0.020	0.346	0.020	0.599	0.020	0.852	0.020	0.908	0.020
PGA	**0**		**0.5**		**1**		**1.5**		**2**		**3**		**5**		**10**		**20**	
+0	0.943	0.015	0.433	0.015	0.328	0.015	0.204	0.015	0.126	0.015	0.066	0.015	0.050	0.015	0.015	0.015	0.014	0.015
+1	0.042	0.015	0.488	0.015	0.484	0.015	0.439	0.015	0.457	0.015	0.380	0.015	0.159	0.015	0.046	0.015	0.020	0.015
+2	0.011	0.015	0.061	0.015	0.104	0.015	0.187	0.015	0.186	0.015	0.160	0.015	0.128	0.015	0.053	0.015	0.050	0.015
+3	0.004	0.015	0.018	0.015	0.084	0.015	0.169	0.015	0.230	0.015	0.394	0.015	0.662	0.015	0.886	0.015	0.916	0.015
R5P	**0**		**0.5**		**1**		**1.5**		**2**		**3**		**5**		**10**		**20**	
+0	0.877	0.023	0.764	0.023	0.758	0.023	0.657	0.023	0.682	0.023	0.640	0.023	0.646	0.023	0.624	0.023	0.590	0.023
+1	0.062	0.023	0.113	0.023	0.095	0.023	0.121	0.023	0.087	0.023	0.077	0.023	0.069	0.023	0.045	0.023	0.039	0.023
+2	0.061	0.023	0.061	0.023	0.054	0.023	0.090	0.023	0.083	0.023	0.053	0.023	0.041	0.023	0.041	0.023	0.031	0.023
+3	0.000	0.023	0.014	0.023	0.030	0.023	0.058	0.023	0.070	0.023	0.083	0.023	0.058	0.023	0.029	0.023	0.010	0.023
+4	0.000	0.023	0.047	0.023	0.059	0.023	0.060	0.023	0.059	0.023	0.102	0.023	0.098	0.023	0.059	0.023	0.050	0.023
+5	0.000	0.023	0.000	0.023	0.004	0.023	0.013	0.023	0.020	0.023	0.045	0.023	0.088	0.023	0.203	0.023	0.280	0.023

RU5P	**0**		**0.5**		**1**		**1.5**		**2**		**3**		**5**		**10**		**20**	
+0	0.894	0.040	0.805	0.040	0.789	0.040	0.758	0.040	0.756	0.040	0.637	0.040	0.764	0.040	0.757	0.040	0.551	0.040
+1	0.055	0.040	0.093	0.040	0.081	0.040	0.107	0.040	0.078	0.040	0.061	0.040	0.057	0.040	0.053	0.040	0.050	0.040
+2	0.052	0.040	0.045	0.040	0.045	0.040	0.059	0.040	0.070	0.040	0.128	0.040	0.060	0.040	0.050	0.040	0.049	0.040
+3	0.000	0.040	0.008	0.040	0.020	0.040	0.041	0.040	0.030	0.040	0.063	0.040	0.036	0.040	0.026	0.040	0.029	0.040
+4	0.000	0.040	0.047	0.040	0.061	0.040	0.028	0.040	0.058	0.040	0.079	0.040	0.033	0.040	0.045	0.040	0.085	0.040
+5	0.000	0.040	0.003	0.040	0.004	0.040	0.008	0.040	0.007	0.040	0.032	0.040	0.051	0.040	0.070	0.040	0.236	0.040
S7P	**0**		**0.5**		**1**		**1.5**		**2**		**3**		**5**		**10**		**20**	
+0	0.905	0.040	0.332	0.040	0.132	0.040	0.073	0.040	0.069	0.040	0.034	0.040	0.072	0.040	0.030	0.040	0.016	0.040
+1	0.075	0.040	0.309	0.040	0.255	0.040	0.165	0.040	0.084	0.040	0.038	0.040	0.010	0.040	0.003	0.040	0.002	0.040
+2	0.020	0.040	0.220	0.040	0.278	0.040	0.226	0.040	0.158	0.040	0.100	0.040	0.039	0.040	0.011	0.040	0.005	0.040
+3	0.000	0.040	0.096	0.040	0.215	0.040	0.242	0.040	0.238	0.040	0.197	0.040	0.079	0.040	0.020	0.040	0.010	0.040
+4	0.000	0.040	0.026	0.040	0.062	0.040	0.148	0.040	0.188	0.040	0.140	0.040	0.051	0.040	0.032	0.040	0.010	0.040
+5	0.000	0.040	0.007	0.040	0.036	0.040	0.098	0.040	0.158	0.040	0.254	0.040	0.244	0.040	0.103	0.040	0.040	0.040
+6	0.000	0.040	0.006	0.040	0.016	0.040	0.031	0.040	0.061	0.040	0.124	0.040	0.156	0.040	0.111	0.040	0.096	0.040
+7	0.000	0.040	0.003	0.040	0.006	0.040	0.018	0.040	0.044	0.040	0.113	0.040	0.349	0.040	0.690	0.040	0.820	0.040
SUC	**0**		**0.5**		**1**		**1.5**		**2**		**3**		**5**		**10**		**20**	
+0	0.948	0.030	0.937	0.030	0.937	0.030	0.923	0.030	0.935	0.030	0.929	0.030	0.938	0.030	0.867	0.030	0.719	0.030
+1	0.046	0.030	0.057	0.030	0.056	0.030	0.068	0.030	0.058	0.030	0.057	0.030	0.048	0.030	0.060	0.030	0.064	0.030
+2	0.006	0.030	0.006	0.030	0.006	0.030	0.008	0.030	0.006	0.030	0.011	0.030	0.010	0.030	0.033	0.030	0.055	0.030
+3	0.000	0.030	0.000	0.030	0.000	0.030	0.001	0.030	0.000	0.030	0.001	0.030	0.002	0.030	0.009	0.030	0.020	0.030
+4	0.000	0.030	0.000	0.030	0.000	0.030	0.000	0.030	0.000	0.030	0.001	0.030	0.002	0.030	0.031	0.030	0.142	0.030
RUBP[a]	**0**		**0.5**		**1**		**1.5**		**2**		**3**		**5**		**10**		**20**	
+0	0.922	0.020	0.547	0.020	0.386	0.020	0.264	0.020	0.183	0.020	0.108	0.020	0.138	0.020	0.067	0.020	0.031	0.020
+1	0.060	0.020	0.328	0.020	0.355	0.020	0.304	0.020	0.257	0.020	0.153	0.020	0.079	0.020	0.025	0.020	0.007	0.020
+2	0.018	0.020	0.093	0.020	0.167	0.020	0.184	0.020	0.198	0.020	0.173	0.020	0.112	0.020	0.057	0.020	0.017	0.020
+3	0.000	0.020	0.025	0.020	0.072	0.020	0.176	0.020	0.217	0.020	0.278	0.020	0.186	0.020	0.089	0.020	0.031	0.020
+4	0.000	0.020	0.006	0.020	0.013	0.020	0.043	0.020	0.079	0.020	0.128	0.020	0.133	0.020	0.080	0.020	0.071	0.020
+5	0.000	0.020	0.001	0.020	0.007	0.020	0.028	0.020	0.066	0.020	0.161	0.020	0.351	0.020	0.682	0.020	0.843	0.020
GA[a]	**0**		**0.5**		**1**		**1.5**		**2**		**3**		**5**		**10**		**20**	
+0	1.000	0.010	1.000	0.010	1.000	0.010	1.000	0.010	1.000	0.010	1.000	0.010	1.000	0.010	1.000	0.010	1.000	0.010
+1	0.000	0.010	0.000	0.010	0.000	0.010	0.000	0.010	0.000	0.010	0.000	0.010	0.000	0.010	0.000	0.010	0.000	0.010

+2	0.000	0.010	0.000	0.010	0.000	0.010	0.000	0.010	0.000	0.010	0.000	0.010	0.000	0.010	0.000	0.010	0.000	0.010
+3	0.000	0.010	0.000	0.010	0.000	0.010	0.000	0.010	0.000	0.010	0.000	0.010	0.000	0.010	0.000	0.010	0.000	0.010

[a] Not included in INCA fitting due to one or more possible interfering peaks or low signals

Table A.6 Measured MDVs and Standard Error for *Synechocystis* sp. PCC 6803 Km

	Time (min)																	
2PG	**0**		**1**		**1.5**		**2**		**2.5**		**3**		**5**		**10**		**20**	
+0	0.975	0.024	0.967	0.024	0.959	0.024	0.947	0.024	0.946	0.024	0.929	0.024	0.869	0.024	0.677	0.024	0.577	0.024
+1	0.025	0.024	0.033	0.024	0.041	0.024	0.053	0.024	0.054	0.024	0.071	0.024	0.131	0.024	0.199	0.024	0.183	0.024
+2	0.000	0.024	0.000	0.024	0.000	0.024	0.000	0.024	0.000	0.024	0.000	0.024	0.000	0.024	0.125	0.024	0.241	0.024
3PG	**0**		**1**		**1.5**		**2**		**2.5**		**3**		**5**		**10**		**20**	
+0	0.953	0.030	0.865	0.030	0.730	0.030	0.670	0.030	0.582	0.030	0.439	0.030	0.291	0.030	0.139	0.030	0.111	0.030
+1	0.037	0.030	0.121	0.030	0.242	0.030	0.288	0.030	0.352	0.030	0.445	0.030	0.501	0.030	0.430	0.030	0.307	0.030
+2	0.009	0.030	0.013	0.030	0.024	0.030	0.035	0.030	0.053	0.030	0.088	0.030	0.141	0.030	0.237	0.030	0.272	0.030
+3	0.000	0.030	0.002	0.030	0.004	0.030	0.007	0.030	0.012	0.030	0.028	0.030	0.067	0.030	0.194	0.030	0.310	0.030
F6P	**0**		**1**		**1.5**		**2**		**2.5**		**3**		**5**		**10**		**20**	
+0	0.906	0.050	0.842	0.050	0.815	0.050	0.721	0.050	0.676	0.050	0.638	0.050	0.371	0.050	0.453	0.050	0.550	0.050
+1	0.072	0.050	0.092	0.050	0.135	0.050	0.181	0.050	0.210	0.050	0.184	0.050	0.252	0.050	0.142	0.050	0.081	0.050
+2	0.022	0.050	0.066	0.050	0.046	0.050	0.079	0.050	0.080	0.050	0.132	0.050	0.180	0.050	0.152	0.050	0.158	0.050
+3	0.000	0.050	0.000	0.050	0.004	0.050	0.013	0.050	0.024	0.050	0.030	0.050	0.114	0.050	0.105	0.050	0.073	0.050
+4	0.000	0.050	0.000	0.050	0.000	0.050	0.006	0.050	0.009	0.050	0.014	0.050	0.066	0.050	0.101	0.050	0.066	0.050
+5	0.000	0.050	0.000	0.050	0.000	0.050	0.000	0.050	0.001	0.050	0.002	0.050	0.009	0.050	0.028	0.050	0.033	0.050
+6	0.000	0.050	0.000	0.050	0.000	0.050	0.000	0.050	0.000	0.050	0.000	0.050	0.008	0.050	0.018	0.050	0.039	0.050
FUM	**0**		**1**		**1.5**		**2**		**2.5**		**3**		**5**		**10**		**20**	
+0	0.989	0.020	0.986	0.020	0.988	0.020	0.987	0.020	0.987	0.020	0.986	0.020	0.988	0.020	0.989	0.020	0.988	0.020
+1	0.011	0.020	0.014	0.020	0.012	0.020	0.013	0.020	0.013	0.020	0.014	0.020	0.012	0.020	0.011	0.020	0.012	0.020
+2	0.000	0.020	0.000	0.020	0.000	0.020	0.000	0.020	0.000	0.020	0.000	0.020	0.000	0.020	0.000	0.020	0.000	0.020
+3	0.000	0.020	0.000	0.020	0.000	0.020	0.000	0.020	0.000	0.020	0.000	0.020	0.000	0.020	0.000	0.020	0.000	0.020
+4	0.000	0.020	0.000	0.020	0.000	0.020	0.000	0.020	0.000	0.020	0.000	0.020	0.000	0.020	0.000	0.020	0.000	0.020
G6P	**0**		**1**		**1.5**		**2**		**2.5**		**3**		**5**		**10**		**20**	
+0	0.895	0.052	0.758	0.052	0.737	0.052	0.656	0.052	0.588	0.052	0.612	0.052	0.265	0.052	0.493	0.052	0.495	0.052
+1	0.061	0.052	0.096	0.052	0.166	0.052	0.198	0.052	0.252	0.052	0.193	0.052	0.228	0.052	0.107	0.052	0.070	0.052
+2	0.042	0.052	0.133	0.052	0.086	0.052	0.125	0.052	0.124	0.052	0.144	0.052	0.343	0.052	0.194	0.052	0.225	0.052
+3	0.002	0.052	0.006	0.052	0.008	0.052	0.016	0.052	0.027	0.052	0.035	0.052	0.089	0.052	0.085	0.052	0.072	0.052

+4	0.000	0.052	0.007	0.052	0.003	0.052	0.006	0.052	0.009	0.052	0.014	0.052	0.052	0.052	0.071	0.052	0.072	0.052
+5	0.000	0.052	0.000	0.052	0.000	0.052	0.000	0.052	0.001	0.052	0.003	0.052	0.015	0.052	0.034	0.052	0.040	0.052
+6	0.000	0.052	0.000	0.052	0.000	0.052	0.000	0.052	0.000	0.052	0.000	0.052	0.008	0.052	0.016	0.052	0.026	0.052
GA	**0**		**1**		**1.5**		**2**		**2.5**		**3**		**5**		**10**		**20**	
+0	0.985	0.010	0.983	0.010	0.978	0.010	0.974	0.010	0.971	0.010	0.962	0.010	0.957	0.010	0.950	0.010	0.979	0.010
+1	0.013	0.010	0.014	0.010	0.019	0.010	0.023	0.010	0.022	0.010	0.028	0.010	0.022	0.010	0.028	0.010	0.014	0.010
+2	0.002	0.010	0.003	0.010	0.004	0.010	0.003	0.010	0.005	0.010	0.008	0.010	0.008	0.010	0.009	0.010	0.003	0.010
+3	0.000	0.010	0.000	0.010	0.000	0.010	0.000	0.010	0.002	0.010	0.003	0.010	0.013	0.010	0.013	0.010	0.004	0.010
MAL	**0**		**1**		**1.5**		**2**		**2.5**		**3**		**5**		**10**		**20**	
+0	0.948	0.031	0.943	0.031	0.936	0.031	0.937	0.031	0.930	0.031	0.928	0.031	0.929	0.031	0.936	0.031	0.932	0.031
+1	0.043	0.031	0.047	0.031	0.054	0.031	0.051	0.031	0.056	0.031	0.057	0.031	0.054	0.031	0.045	0.031	0.054	0.031
+2	0.008	0.031	0.010	0.031	0.010	0.031	0.012	0.031	0.013	0.031	0.013	0.031	0.016	0.031	0.015	0.031	0.012	0.031
+3	0.000	0.031	0.000	0.031	0.000	0.031	0.000	0.031	0.001	0.031	0.001	0.031	0.001	0.031	0.003	0.031	0.001	0.031
+4	0.000	0.031	0.000	0.031	0.000	0.031	0.000	0.031	0.000	0.031	0.000	0.031	0.000	0.031	0.001	0.031	0.001	0.031
PEP	**0**		**1**		**1.5**		**2**		**2.5**		**3**		**5**		**10**		**20**	
+0	0.960	0.024	0.900	0.024	0.793	0.024	0.695	0.024	0.597	0.024	0.475	0.024	0.311	0.024	0.229	0.024	0.215	0.024
+1	0.033	0.024	0.093	0.024	0.185	0.024	0.268	0.024	0.350	0.024	0.431	0.024	0.485	0.024	0.401	0.024	0.261	0.024
+2	0.006	0.024	0.007	0.024	0.019	0.024	0.031	0.024	0.043	0.024	0.070	0.024	0.140	0.024	0.195	0.024	0.240	0.024
+3	0.000	0.024	0.000	0.024	0.003	0.024	0.005	0.024	0.010	0.024	0.024	0.024	0.064	0.024	0.175	0.024	0.285	0.024
R5P	**0**		**1**		**1.5**		**2**		**2.5**		**3**		**5**		**10**		**20**	
+0	0.931	0.020	0.901	0.020	0.914	0.020	0.894	0.020	0.891	0.020	0.868	0.020	0.731	0.020	0.823	0.020	0.604	0.020
+1	0.050	0.020	0.059	0.020	0.059	0.020	0.065	0.020	0.078	0.020	0.074	0.020	0.143	0.020	0.085	0.020	0.118	0.020
+2	0.018	0.020	0.040	0.020	0.025	0.020	0.038	0.020	0.025	0.020	0.052	0.020	0.073	0.020	0.047	0.020	0.103	0.020
+3	0.000	0.020	0.000	0.020	0.001	0.020	0.003	0.020	0.004	0.020	0.006	0.020	0.031	0.020	0.028	0.020	0.086	0.020
+4	0.000	0.020	0.000	0.020	0.000	0.020	0.000	0.020	0.001	0.020	0.001	0.020	0.022	0.020	0.011	0.020	0.058	0.020
+5	0.000	0.020	0.000	0.020	0.000	0.020	0.000	0.020	0.000	0.020	0.000	0.020	0.000	0.020	0.006	0.020	0.032	0.020
RU5P	**0**		**1**		**1.5**		**2**		**2.5**		**3**		**5**		**10**		**20**	
+0	0.902	0.040	0.786	0.040	0.526	0.040	0.680	0.040	0.649	0.040	0.496	0.040	0.375	0.040	0.429	0.040	0.236	0.040
+1	0.053	0.040	0.127	0.040	0.233	0.040	0.169	0.040	0.183	0.040	0.263	0.040	0.199	0.040	0.142	0.040	0.094	0.040
+2	0.014	0.040	0.070	0.040	0.117	0.040	0.067	0.040	0.063	0.040	0.128	0.040	0.227	0.040	0.195	0.040	0.189	0.040
+3	0.031	0.040	0.017	0.040	0.062	0.040	0.034	0.040	0.060	0.040	0.076	0.040	0.068	0.040	0.106	0.040	0.128	0.040
+4	0.000	0.040	0.000	0.040	0.062	0.040	0.050	0.040	0.046	0.040	0.037	0.040	0.131	0.040	0.128	0.040	0.260	0.040

+5	0.000	0.040	0.000	0.040	0.000	0.040	0.000	0.040	0.000	0.040	0.000	0.040	0.000	0.040	0.000	0.040	0.093	0.040
S7P	**0**		**1**		**1.5**		**2**		**2.5**		**3**		**5**		**10**		**20**	
+0	0.903	0.021	0.801	0.021	0.717	0.021	0.618	0.021	0.519	0.021	0.385	0.021	0.172	0.021	0.086	0.021	0.116	0.021
+1	0.068	0.021	0.128	0.021	0.207	0.021	0.235	0.021	0.275	0.021	0.300	0.021	0.272	0.021	0.175	0.021	0.127	0.021
+2	0.023	0.021	0.056	0.021	0.062	0.021	0.103	0.021	0.136	0.021	0.189	0.021	0.264	0.021	0.223	0.021	0.169	0.021
+3	0.003	0.021	0.010	0.021	0.011	0.021	0.028	0.021	0.048	0.021	0.083	0.021	0.172	0.021	0.217	0.021	0.160	0.021
+4	0.002	0.021	0.005	0.021	0.004	0.021	0.007	0.021	0.012	0.021	0.024	0.021	0.065	0.021	0.139	0.021	0.128	0.021
+5	0.000	0.021	0.000	0.021	0.000	0.021	0.002	0.021	0.004	0.021	0.009	0.021	0.033	0.021	0.090	0.021	0.145	0.021
+6	0.000	0.021	0.000	0.021	0.000	0.021	0.007	0.021	0.006	0.021	0.008	0.021	0.018	0.021	0.044	0.021	0.095	0.021
+7	0.000	0.021	0.000	0.021	0.000	0.021	0.000	0.021	0.000	0.021	0.002	0.021	0.004	0.021	0.025	0.021	0.059	0.021
SUC	**0**		**1**		**1.5**		**2**		**2.5**		**3**		**5**		**10**		**20**	
+0	0.950	0.010	0.963	0.010	0.931	0.010	0.953	0.010	0.932	0.010	0.944	0.010	0.955	0.010	0.950	0.010	0.951	0.010
+1	0.049	0.010	0.037	0.010	0.068	0.010	0.046	0.010	0.067	0.010	0.056	0.010	0.044	0.010	0.049	0.010	0.049	0.010
+2	0.000	0.010	0.000	0.010	0.001	0.010	0.000	0.010	0.001	0.010	0.001	0.010	0.000	0.010	0.001	0.010	0.001	0.010
+3	0.000	0.010	0.000	0.010	0.000	0.010	0.000	0.010	0.000	0.010	0.000	0.010	0.000	0.010	0.000	0.010	0.000	0.010
+4	0.000	0.010	0.000	0.010	0.000	0.010	0.000	0.010	0.000	0.010	0.000	0.010	0.000	0.010	0.000	0.010	0.000	0.010
ACO[a]	**0**		**1**		**1.5**		**2**		**2.5**		**3**		**5**		**10**		**20**	
+0	0.932	0.010	0.933	0.010	0.930	0.010	0.930	0.010	0.929	0.010	0.921	0.010	0.931	0.010	0.931	0.010	0.942	0.010
+1	0.067	0.010	0.066	0.010	0.069	0.010	0.069	0.010	0.070	0.010	0.077	0.010	0.068	0.010	0.067	0.010	0.056	0.010
+2	0.001	0.010	0.001	0.010	0.001	0.010	0.001	0.010	0.001	0.010	0.001	0.010	0.001	0.010	0.002	0.010	0.001	0.010
+3	0.000	0.010	0.000	0.010	0.000	0.010	0.000	0.010	0.000	0.010	0.000	0.010	0.000	0.010	0.000	0.010	0.000	0.010
+4	0.000	0.010	0.000	0.010	0.000	0.010	0.000	0.010	0.000	0.010	0.000	0.010	0.000	0.010	0.000	0.010	0.000	0.010
+5	0.000	0.010	0.000	0.010	0.000	0.010	0.000	0.010	0.000	0.010	0.000	0.010	0.000	0.010	0.000	0.010	0.000	0.010
+6	0.000	0.010	0.000	0.010	0.000	0.010	0.000	0.010	0.000	0.010	0.000	0.010	0.000	0.010	0.000	0.010	0.000	0.010
AKG[a]	**0**		**1**		**1.5**		**2**		**2.5**		**3**		**5**		**10**		**20**	
+0	0.992	0.010	0.991	0.010	0.992	0.010	0.993	0.010	0.989	0.010	0.990	0.010	0.993	0.010	0.992	0.010	0.989	0.010
+1	0.008	0.010	0.009	0.010	0.008	0.010	0.007	0.010	0.011	0.010	0.010	0.010	0.007	0.010	0.008	0.010	0.011	0.010
+2	0.000	0.010	0.000	0.010	0.000	0.010	0.000	0.010	0.000	0.010	0.000	0.010	0.000	0.010	0.000	0.010	0.000	0.010
+3	0.000	0.010	0.000	0.010	0.000	0.010	0.000	0.010	0.000	0.010	0.000	0.010	0.000	0.010	0.000	0.010	0.000	0.010
+4	0.000	0.010	0.000	0.010	0.000	0.010	0.000	0.010	0.000	0.010	0.000	0.010	0.000	0.010	0.000	0.010	0.000	0.010
+5	0.000	0.010	0.000	0.010	0.000	0.010	0.000	0.010	0.000	0.010	0.000	0.010	0.000	0.010	0.000	0.010	0.000	0.010
AP[a]	**0**		**1**		**1.5**		**2**		**2.5**		**3**		**5**		**10**		**20**	

+0	0.794	N/A	0.886	N/A	0.872	N/A	0.851	N/A	0.821	N/A	0.776	N/A	0.738	N/A	0.726	N/A	0.490	N/A
+1	0.019	N/A	0.021	N/A	0.026	N/A	0.025	N/A	0.037	N/A	0.046	N/A	0.074	N/A	0.055	N/A	0.094	N/A
+2	0.187	N/A	0.093	N/A	0.102	N/A	0.124	N/A	0.142	N/A	0.178	N/A	0.188	N/A	0.219	N/A	0.416	N/A
E4P[a]	**0**		**1**		**1.5**		**2**		**2.5**		**3**		**5**		**10**		**20**	
+0	0.643	N/A	0.502	N/A	0.631	N/A	0.613	N/A	0.498	N/A	0.521	N/A	0.383	N/A	0.361	N/A	0.282	N/A
+1	0.022	N/A	0.075	N/A	0.107	N/A	0.141	N/A	0.177	N/A	0.142	N/A	0.229	N/A	0.153	N/A	0.066	N/A
+2	0.308	N/A	0.365	N/A	0.232	N/A	0.208	N/A	0.288	N/A	0.296	N/A	0.313	N/A	0.408	N/A	0.570	N/A
+3	0.027	N/A	0.058	N/A	0.030	N/A	0.038	N/A	0.037	N/A	0.041	N/A	0.076	N/A	0.078	N/A	0.083	N/A
+4	0.000	N/A	0.000	N/A	0.000	N/A	0.000	N/A	0.000	N/A	0.000	N/A	0.000	N/A	0.000	N/A	0.000	N/A
FBP[a]	**0**		**1**		**1.5**		**2**		**2.5**		**3**		**5**		**10**		**20**	
+0	0.892	0.100	0.830	0.100	0.699	0.100	0.573	0.100	0.579	0.100	0.437	0.100	0.288	0.100	0.121	0.100	0.159	0.100
+1	0.072	0.100	0.142	0.100	0.195	0.100	0.274	0.100	0.267	0.100	0.306	0.100	0.204	0.100	0.202	0.100	0.162	0.100
+2	0.035	0.100	0.029	0.100	0.073	0.100	0.064	0.100	0.111	0.100	0.162	0.100	0.143	0.100	0.216	0.100	0.175	0.100
+3	0.000	0.100	0.000	0.100	0.032	0.100	0.089	0.100	0.033	0.100	0.075	0.100	0.250	0.100	0.265	0.100	0.140	0.100
+4	0.000	0.100	0.000	0.100	0.000	0.100	0.000	0.100	0.010	0.100	0.020	0.100	0.035	0.100	0.103	0.100	0.152	0.100
+5	0.000	0.100	0.000	0.100	0.000	0.100	0.000	0.100	0.000	0.100	0.000	0.100	0.079	0.100	0.094	0.100	0.212	0.100
+6	0.000	0.100	0.000	0.100	0.000	0.100	0.000	0.100	0.000	0.100	0.000	0.100	0.000	0.100	0.000	0.100	0.000	0.100
RUBP[a]	**0**		**1**		**1.5**		**2**		**2.5**		**3**		**5**		**10**		**20**	
+0	0.902	N/A	0.521	N/A	0.612	N/A	0.587	N/A	0.553	N/A	0.482	N/A	0.303	N/A	0.440	N/A	0.185	N/A
+1	0.053	N/A	0.100	N/A	0.136	N/A	0.202	N/A	0.235	N/A	0.273	N/A	0.240	N/A	0.127	N/A	0.122	N/A
+2	0.045	N/A	0.379	N/A	0.252	N/A	0.210	N/A	0.213	N/A	0.245	N/A	0.458	N/A	0.364	N/A	0.374	N/A
+3	0.000	N/A	0.000	N/A	0.000	N/A	0.000	N/A	0.000	N/A	0.000	N/A	0.000	N/A	0.068	N/A	0.127	N/A
+4	0.000	N/A	0.000	N/A	0.000	N/A	0.000	N/A	0.000	N/A	0.000	N/A	0.000	N/A	0.000	N/A	0.114	N/A
+5	0.000	N/A	0.000	N/A	0.000	N/A	0.000	N/A	0.000	N/A	0.000	N/A	0.000	N/A	0.000	N/A	0.077	N/A

[a] Not included in INCA fitting due to one or more possible interfering peaks or low signals

Table A.7 Measured MDVs and Standard Error for *Synechocystis* sp. PCC 6803 tktA

	Time (min)																	
3PG	**0**		**1**		**1.5**		**2**		**2.5**		**3**		**5**		**10**		**20**	
+0	0.940	0.022	0.801	0.022	0.654	0.022	0.538	0.022	0.433	0.022	0.319	0.022	0.256	0.022	0.186	0.022	0.185	0.022
+1	0.047	0.022	0.178	0.022	0.305	0.022	0.381	0.022	0.452	0.022	0.486	0.022	0.438	0.022	0.312	0.022	0.213	0.022
+2	0.012	0.022	0.017	0.022	0.033	0.022	0.059	0.022	0.084	0.022	0.129	0.022	0.174	0.022	0.213	0.022	0.215	0.022
+3	0.001	0.022	0.004	0.022	0.008	0.022	0.023	0.022	0.030	0.022	0.066	0.022	0.132	0.022	0.289	0.022	0.387	0.022
F6P	**0**		**1**		**1.5**		**2**		**2.5**		**3**		**5**		**10**		**20**	
+0	0.908	0.035	0.879	0.035	0.775	0.035	0.676	0.035	0.529	0.035	0.441	0.035	0.330	0.035	0.272	0.035	0.337	0.035
+1	0.068	0.035	0.112	0.035	0.194	0.035	0.243	0.035	0.297	0.035	0.262	0.035	0.189	0.035	0.086	0.035	0.088	0.035
+2	0.025	0.035	0.007	0.035	0.023	0.035	0.050	0.035	0.067	0.035	0.102	0.035	0.097	0.035	0.062	0.035	0.049	0.035
+3	0.000	0.035	0.002	0.035	0.005	0.035	0.022	0.035	0.059	0.035	0.108	0.035	0.177	0.035	0.168	0.035	0.112	0.035
+4	0.000	0.035	0.000	0.035	0.004	0.035	0.009	0.035	0.032	0.035	0.056	0.035	0.140	0.035	0.209	0.035	0.153	0.035
+5	0.000	0.035	0.000	0.035	0.000	0.035	0.000	0.035	0.008	0.035	0.014	0.035	0.047	0.035	0.120	0.035	0.142	0.035
+6	0.000	0.035	0.000	0.035	0.000	0.035	0.000	0.035	0.009	0.035	0.017	0.035	0.020	0.035	0.084	0.035	0.120	0.035
FUM	**0**		**1**		**1.5**		**2**		**2.5**		**3**		**5**		**10**		**20**	
+0	0.957	0.010	0.955	0.010	0.954	0.010	0.954	0.010	0.956	0.010	0.951	0.010	0.955	0.010	0.953	0.010	0.954	0.010
+1	0.043	0.010	0.045	0.010	0.045	0.010	0.045	0.010	0.043	0.010	0.047	0.010	0.043	0.010	0.046	0.010	0.041	0.010
+2	0.000	0.010	0.000	0.010	0.001	0.010	0.000	0.010	0.001	0.010	0.002	0.010	0.002	0.010	0.001	0.010	0.003	0.010
+3	0.000	0.010	0.000	0.010	0.000	0.010	0.000	0.010	0.000	0.010	0.000	0.010	0.000	0.010	0.000	0.010	0.000	0.010
+4	0.000	0.010	0.000	0.010	0.000	0.010	0.000	0.010	0.000	0.010	0.000	0.010	0.000	0.010	0.000	0.010	0.001	0.010
G6P	**0**		**1**		**1.5**		**2**		**2.5**		**3**		**5**		**10**		**20**	
+0	0.873	0.035	0.843	0.035	0.719	0.035	0.615	0.035	0.513	0.035	0.377	0.035	0.326	0.035	0.298	0.035	0.336	0.035
+1	0.066	0.035	0.101	0.035	0.185	0.035	0.236	0.035	0.239	0.035	0.235	0.035	0.162	0.035	0.090	0.035	0.076	0.035
+2	0.060	0.035	0.056	0.035	0.084	0.035	0.116	0.035	0.170	0.035	0.221	0.035	0.226	0.035	0.166	0.035	0.150	0.035
+3	0.000	0.035	0.000	0.035	0.010	0.035	0.026	0.035	0.049	0.035	0.091	0.035	0.144	0.035	0.131	0.035	0.089	0.035
+4	0.000	0.035	0.000	0.035	0.002	0.035	0.008	0.035	0.021	0.035	0.049	0.035	0.096	0.035	0.165	0.035	0.136	0.035
+5	0.000	0.035	0.000	0.035	0.000	0.035	0.000	0.035	0.006	0.035	0.016	0.035	0.033	0.035	0.093	0.035	0.124	0.035
+6	0.000	0.035	0.000	0.035	0.000	0.035	0.000	0.035	0.003	0.035	0.011	0.035	0.014	0.035	0.057	0.035	0.088	0.035
GA	**0**		**1**		**1.5**		**2**		**2.5**		**3**		**5**		**10**		**20**	
+0	0.986	0.010	0.987	0.010	0.985	0.010	0.984	0.010	0.985	0.010	0.984	0.010	0.985	0.010	0.983	0.010	0.982	0.010
+1	0.012	0.010	0.011	0.010	0.013	0.010	0.014	0.010	0.012	0.010	0.013	0.010	0.012	0.010	0.014	0.010	0.014	0.010

+2	0.002	0.010	0.002	0.010	0.002	0.010	0.002	0.010	0.002	0.010	0.003	0.010	0.002	0.010	0.002	0.010	0.002	0.010
+3	0.000	0.010	0.000	0.010	0.000	0.010	0.000	0.010	0.000	0.010	0.000	0.010	0.000	0.010	0.001	0.010	0.002	0.010
MAL	**0**		**1**		**1.5**		**2**		**2.5**		**3**		**5**		**10**		**20**	
+0	0.920	0.037	0.890	0.037	0.918	0.037	0.870	0.037	0.911	0.037	0.905	0.037	0.917	0.037	0.870	0.037	0.900	0.037
+1	0.066	0.037	0.092	0.037	0.067	0.037	0.108	0.037	0.072	0.037	0.074	0.037	0.065	0.037	0.102	0.037	0.067	0.037
+2	0.014	0.037	0.018	0.037	0.014	0.037	0.021	0.037	0.016	0.037	0.018	0.037	0.017	0.037	0.024	0.037	0.020	0.037
+3	0.001	0.037	0.001	0.037	0.001	0.037	0.001	0.037	0.001	0.037	0.001	0.037	0.002	0.037	0.003	0.037	0.006	0.037
+4	0.000	0.037	0.000	0.037	0.000	0.037	0.000	0.037	0.000	0.037	0.001	0.037	0.001	0.037	0.002	0.037	0.006	0.037
PEP	**0**		**1**		**1.5**		**2**		**2.5**		**3**		**5**		**10**		**20**	
+0	0.955	0.010	0.834	0.010	0.693	0.010	0.587	0.010	0.441	0.010	0.322	0.010	0.229	0.010	0.164	0.010	0.134	0.010
+1	0.038	0.010	0.151	0.010	0.279	0.010	0.347	0.010	0.452	0.010	0.485	0.010	0.460	0.010	0.314	0.010	0.200	0.010
+2	0.007	0.010	0.012	0.010	0.023	0.010	0.054	0.010	0.078	0.010	0.126	0.010	0.182	0.010	0.228	0.010	0.242	0.010
+3	0.001	0.010	0.002	0.010	0.004	0.010	0.013	0.010	0.029	0.010	0.067	0.010	0.130	0.010	0.295	0.010	0.424	0.010
R5P	**0**		**1**		**1.5**		**2**		**2.5**		**3**		**5**		**10**		**20**	
+0	0.911	0.024	0.897	0.024	0.831	0.024	0.836	0.024	0.791	0.024	0.697	0.024	0.692	0.024	0.635	0.024	0.454	0.024
+1	0.052	0.024	0.065	0.024	0.108	0.024	0.096	0.024	0.118	0.024	0.140	0.024	0.135	0.024	0.111	0.024	0.101	0.024
+2	0.036	0.024	0.038	0.024	0.056	0.024	0.044	0.024	0.063	0.024	0.099	0.024	0.079	0.024	0.097	0.024	0.119	0.024
+3	0.000	0.024	0.000	0.024	0.004	0.024	0.011	0.024	0.016	0.024	0.038	0.024	0.056	0.024	0.087	0.024	0.128	0.024
+4	0.000	0.024	0.000	0.024	0.000	0.024	0.012	0.024	0.009	0.024	0.018	0.024	0.027	0.024	0.035	0.024	0.094	0.024
+5	0.000	0.024	0.000	0.024	0.000	0.024	0.002	0.024	0.004	0.024	0.008	0.024	0.010	0.024	0.035	0.024	0.104	0.024
RU5P	**0**		**1**		**1.5**		**2**		**2.5**		**3**		**5**		**10**		**20**	
+0	0.906	0.024	0.784	0.024	0.670	0.024	0.748	0.024	0.546	0.024	0.472	0.024	0.367	0.024	0.427	0.024	0.336	0.024
+1	0.062	0.024	0.091	0.024	0.219	0.024	0.141	0.024	0.185	0.024	0.247	0.024	0.137	0.024	0.079	0.024	0.093	0.024
+2	0.031	0.024	0.125	0.024	0.111	0.024	0.112	0.024	0.130	0.024	0.133	0.024	0.225	0.024	0.223	0.024	0.200	0.024
+3	0.000	0.024	0.000	0.024	0.000	0.024	0.000	0.024	0.047	0.024	0.092	0.024	0.102	0.024	0.141	0.024	0.145	0.024
+4	0.000	0.024	0.000	0.024	0.000	0.024	0.000	0.024	0.091	0.024	0.037	0.024	0.136	0.024	0.086	0.024	0.142	0.024
+5	0.000	0.024	0.000	0.024	0.000	0.024	0.000	0.024	0.000	0.024	0.019	0.024	0.032	0.024	0.044	0.024	0.084	0.024
S7P	**0**		**1**		**1.5**		**2**		**2.5**		**3**		**5**		**10**		**20**	
+0	0.898	0.032	0.779	0.032	0.607	0.032	0.442	0.032	0.318	0.032	0.185	0.032	0.116	0.032	0.057	0.032	0.095	0.032
+1	0.076	0.032	0.156	0.032	0.265	0.032	0.317	0.032	0.306	0.032	0.274	0.032	0.154	0.032	0.088	0.032	0.080	0.032
+2	0.022	0.032	0.041	0.032	0.089	0.032	0.156	0.032	0.202	0.032	0.243	0.032	0.221	0.032	0.138	0.032	0.110	0.032
+3	0.002	0.032	0.008	0.032	0.025	0.032	0.057	0.032	0.103	0.032	0.173	0.032	0.221	0.032	0.183	0.032	0.125	0.032

+4	0.002	0.032	0.003	0.032	0.006	0.032	0.012	0.032	0.034	0.032	0.063	0.032	0.142	0.032	0.178	0.032	0.111	0.032
+5	0.000	0.032	0.001	0.032	0.002	0.032	0.004	0.032	0.018	0.032	0.026	0.032	0.093	0.032	0.154	0.032	0.149	0.032
+6	0.000	0.032	0.012	0.032	0.006	0.032	0.010	0.032	0.011	0.032	0.018	0.032	0.037	0.032	0.115	0.032	0.170	0.032
+7	0.000	0.032	0.000	0.032	0.000	0.032	0.003	0.032	0.009	0.032	0.017	0.032	0.017	0.032	0.086	0.032	0.160	0.032
SUC	**0**		**1**		**1.5**		**2**		**2.5**		**3**		**5**		**10**		**20**	
+0	0.922	0.043	0.949	0.043	0.941	0.043	0.947	0.043	0.942	0.043	0.939	0.043	0.943	0.043	0.944	0.043	0.933	0.043
+1	0.070	0.043	0.051	0.043	0.054	0.043	0.048	0.043	0.053	0.043	0.054	0.043	0.050	0.043	0.048	0.043	0.054	0.043
+2	0.008	0.043	0.001	0.043	0.005	0.043	0.005	0.043	0.005	0.043	0.007	0.043	0.006	0.043	0.007	0.043	0.010	0.043
+3	0.000	0.043	0.000	0.043	0.000	0.043	0.000	0.043	0.000	0.043	0.000	0.043	0.000	0.043	0.000	0.043	0.002	0.043
+4	0.000	0.043	0.000	0.043	0.000	0.043	0.000	0.043	0.000	0.043	0.000	0.043	0.000	0.043	0.000	0.043	0.002	0.043
2PG[a]	**0**		**1**		**1.5**		**2**		**2.5**		**3**		**5**		**10**		**20**	
+0	0.974	0.010	0.973	0.010	0.961	0.010	0.938	0.010	0.945	0.010	0.922	0.010	0.914	0.010	0.869	0.010	0.770	0.010
+1	0.026	0.010	0.027	0.010	0.039	0.010	0.062	0.010	0.055	0.010	0.078	0.010	0.086	0.010	0.066	0.010	0.096	0.010
+2	0.000	0.010	0.000	0.010	0.000	0.010	0.000	0.010	0.000	0.010	0.000	0.010	0.000	0.010	0.065	0.010	0.133	0.010
ACO[a]	**0**		**1**		**1.5**		**2**		**2.5**		**3**		**5**		**10**		**20**	
+0	0.928	0.010	0.931	0.010	0.931	0.010	0.930	0.010	0.930	0.010	0.931	0.010	0.931	0.010	0.930	0.010	0.928	0.010
+1	0.071	0.010	0.067	0.010	0.067	0.010	0.068	0.010	0.068	0.010	0.068	0.010	0.068	0.010	0.068	0.010	0.070	0.010
+2	0.001	0.010	0.001	0.010	0.001	0.010	0.002	0.010	0.002	0.010	0.001	0.010	0.002	0.010	0.002	0.010	0.002	0.010
+3	0.000	0.010	0.000	0.010	0.000	0.010	0.000	0.010	0.000	0.010	0.000	0.010	0.000	0.010	0.000	0.010	0.000	0.010
+4	0.000	0.010	0.000	0.010	0.000	0.010	0.000	0.010	0.000	0.010	0.000	0.010	0.000	0.010	0.000	0.010	0.000	0.010
+5	0.000	0.010	0.000	0.010	0.000	0.010	0.000	0.010	0.000	0.010	0.000	0.010	0.000	0.010	0.000	0.010	0.000	0.010
+6	0.000	0.010	0.000	0.010	0.000	0.010	0.000	0.010	0.000	0.010	0.000	0.010	0.000	0.010	0.000	0.010	0.000	0.010
AKG[a]	**0**		**1**		**1.5**		**2**		**2.5**		**3**		**5**		**10**		**20**	
+0	0.989	0.010	0.985	0.010	0.989	0.010	0.989	0.010	0.991	0.010	0.988	0.010	0.988	0.010	0.988	0.010	0.988	0.010
+1	0.011	0.010	0.015	0.010	0.011	0.010	0.011	0.010	0.009	0.010	0.012	0.010	0.012	0.010	0.012	0.010	0.012	0.010
+2	0.000	0.010	0.000	0.010	0.000	0.010	0.000	0.010	0.000	0.010	0.000	0.010	0.000	0.010	0.000	0.010	0.000	0.010
+3	0.000	0.010	0.000	0.010	0.000	0.010	0.000	0.010	0.000	0.010	0.000	0.010	0.000	0.010	0.000	0.010	0.000	0.010
+4	0.000	0.010	0.000	0.010	0.000	0.010	0.000	0.010	0.000	0.010	0.000	0.010	0.000	0.010	0.000	0.010	0.000	0.010
+5	0.000	0.010	0.000	0.010	0.000	0.010	0.000	0.010	0.000	0.010	0.000	0.010	0.000	0.010	0.000	0.010	0.000	0.010
AP[a]	**0**		**1**		**1.5**		**2**		**2.5**		**3**		**5**		**10**		**20**	
+0	0.821	N/A	0.655	N/A	0.690	N/A	0.585	N/A	0.658	N/A	0.631	N/A	0.580	N/A	0.471	N/A	0.538	N/A
+1	0.024	N/A	0.017	N/A	0.030	N/A	0.026	N/A	0.040	N/A	0.061	N/A	0.068	N/A	0.048	N/A	0.058	N/A

+2	0.155	N/A	0.328	N/A	0.280	N/A	0.389	N/A	0.302	N/A	0.308	N/A	0.352	N/A	0.481	N/A	0.404	N/A
E4P[a]	**0**		**1**		**1.5**		**2**		**2.5**		**3**		**5**		**10**		**20**	
+0	0.754	N/A	0.713	N/A	0.670	N/A	0.580	N/A	0.521	N/A	0.475	N/A	0.370	N/A	0.345	N/A	0.255	N/A
+1	0.065	N/A	0.092	N/A	0.155	N/A	0.229	N/A	0.239	N/A	0.266	N/A	0.289	N/A	0.180	N/A	0.149	N/A
+2	0.128	N/A	0.139	N/A	0.126	N/A	0.141	N/A	0.172	N/A	0.173	N/A	0.163	N/A	0.175	N/A	0.205	N/A
+3	0.052	N/A	0.056	N/A	0.050	N/A	0.050	N/A	0.069	N/A	0.085	N/A	0.148	N/A	0.204	N/A	0.239	N/A
+4	0.000	N/A	0.000	N/A	0.000	N/A	0.000	N/A	0.000	N/A	0.000	N/A	0.030	N/A	0.095	N/A	0.152	N/A
FBP[a]	**0**		**1**		**1.5**		**2**		**2.5**		**3**		**5**		**10**		**20**	
+0	0.746	N/A	0.459	N/A	0.388	N/A	0.298	N/A	0.212	N/A	0.133	N/A	0.162	N/A	0.109	N/A	0.108	N/A
+1	0.061	N/A	0.102	N/A	0.185	N/A	0.182	N/A	0.220	N/A	0.199	N/A	0.103	N/A	0.042	N/A	0.049	N/A
+2	0.053	N/A	0.072	N/A	0.089	N/A	0.106	N/A	0.128	N/A	0.175	N/A	0.120	N/A	0.218	N/A	0.186	N/A
+3	0.059	N/A	0.178	N/A	0.150	N/A	0.165	N/A	0.221	N/A	0.186	N/A	0.287	N/A	0.292	N/A	0.255	N/A
+4	0.036	N/A	0.085	N/A	0.077	N/A	0.083	N/A	0.128	N/A	0.195	N/A	0.178	N/A	0.128	N/A	0.141	N/A
+5	0.029	N/A	0.077	N/A	0.071	N/A	0.112	N/A	0.054	N/A	0.083	N/A	0.100	N/A	0.148	N/A	0.163	N/A
+6	0.016	N/A	0.026	N/A	0.041	N/A	0.054	N/A	0.037	N/A	0.029	N/A	0.050	N/A	0.063	N/A	0.099	N/A
RUBP[a]	**0**		**1**		**1.5**		**2**		**2.5**		**3**		**5**		**10**		**20**	
+0	0.918	0.010	0.745	0.010	0.573	0.010	0.497	0.010	0.375	0.010	0.257	0.010	0.338	0.010	0.299	0.010	0.237	0.010
+1	0.044	0.010	0.112	0.010	0.237	0.010	0.277	0.010	0.337	0.010	0.358	0.010	0.167	0.010	0.103	0.010	0.078	0.010
+2	0.038	0.010	0.143	0.010	0.190	0.010	0.226	0.010	0.221	0.010	0.263	0.010	0.320	0.010	0.288	0.010	0.195	0.010
+3	0.000	0.010	0.000	0.010	0.000	0.010	0.000	0.010	0.067	0.010	0.094	0.010	0.123	0.010	0.115	0.010	0.140	0.010
+4	0.000	0.010	0.000	0.010	0.000	0.010	0.000	0.010	0.000	0.010	0.028	0.010	0.030	0.010	0.095	0.010	0.172	0.010
+5	0.000	0.010	0.000	0.010	0.000	0.010	0.000	0.010	0.000	0.010	0.000	0.010	0.023	0.010	0.100	0.010	0.179	0.010

[a] Not included in INCA fitting due to one or more possible interfering peaks or low signal

Table A.8 Measured MDVs and Standard Error for *Synechocystis* sp. PCC 6803 70glpX

	Time (min)																	
3PG	**0**		**0.5**		**1**		**1.5**		**2**		**3**		**5**		**10**		**20**	
+0	0.960	0.030	0.895	0.030	0.836	0.030	0.770	0.030	0.758	0.030	0.734	0.030	0.646	0.030	0.533	0.030	0.489	0.030
+1	0.032	0.030	0.093	0.030	0.149	0.030	0.210	0.030	0.212	0.030	0.216	0.030	0.271	0.030	0.342	0.030	0.319	0.030
+2	0.008	0.030	0.011	0.030	0.014	0.030	0.017	0.030	0.027	0.030	0.043	0.030	0.072	0.030	0.103	0.030	0.163	0.030
+3	0.000	0.030	0.001	0.030	0.001	0.030	0.003	0.030	0.003	0.030	0.007	0.030	0.011	0.030	0.023	0.030	0.029	0.030
AKG	**0**		**0.5**		**1**		**1.5**		**2**		**3**		**5**		**10**		**20**	
+0	0.950	0.020	0.944	0.020	0.950	0.020	0.945	0.020	0.951	0.020	0.948	0.020	0.945	0.020	0.954	0.020	0.929	0.020
+1	0.043	0.020	0.056	0.020	0.050	0.020	0.055	0.020	0.049	0.020	0.052	0.020	0.055	0.020	0.046	0.020	0.058	0.020
+2	0.007	0.020	0.000	0.020	0.000	0.020	0.000	0.020	0.000	0.020	0.000	0.020	0.000	0.020	0.000	0.020	0.013	0.020
+3	0.000	0.020	0.000	0.020	0.000	0.020	0.000	0.020	0.000	0.020	0.000	0.020	0.000	0.020	0.000	0.020	0.001	0.020
+4	0.000	0.020	0.000	0.020	0.000	0.020	0.000	0.020	0.000	0.020	0.000	0.020	0.000	0.020	0.000	0.020	0.000	0.020
+5	0.000	0.020	0.000	0.020	0.000	0.020	0.000	0.020	0.000	0.020	0.000	0.020	0.000	0.020	0.000	0.020	0.000	0.020
F6P	**0**		**0.5**		**1**		**1.5**		**2**		**3**		**5**		**10**		**20**	
+0	0.944	0.016	0.882	0.016	0.766	0.016	0.670	0.016	0.666	0.016	0.584	0.016	0.549	0.016	0.509	0.016	0.488	0.016
+1	0.056	0.016	0.118	0.016	0.198	0.016	0.238	0.016	0.243	0.016	0.291	0.016	0.276	0.016	0.258	0.016	0.309	0.016
+2	0.000	0.016	0.000	0.016	0.031	0.016	0.086	0.016	0.079	0.016	0.105	0.016	0.117	0.016	0.148	0.016	0.016	0.016
+3	0.000	0.016	0.000	0.016	0.005	0.016	0.007	0.016	0.012	0.016	0.020	0.016	0.043	0.016	0.062	0.016	0.120	0.016
+4	0.000	0.016	0.000	0.016	0.000	0.016	0.000	0.016	0.000	0.016	0.000	0.016	0.014	0.016	0.023	0.016	0.055	0.016
+5	0.000	0.016	0.000	0.016	0.000	0.016	0.000	0.016	0.000	0.016	0.000	0.016	0.000	0.016	0.000	0.016	0.009	0.016
+6	0.000	0.016	0.000	0.016	0.000	0.016	0.000	0.016	0.000	0.016	0.000	0.016	0.000	0.016	0.000	0.016	0.003	0.016
G6P	**0**		**0.5**		**1**		**1.5**		**2**		**3**		**5**		**10**		**20**	
+0	0.897	0.016	0.816	0.016	0.746	0.016	0.682	0.016	0.618	0.016	0.543	0.016	0.434	0.016	0.438	0.016	0.380	0.016
+1	0.056	0.016	0.120	0.016	0.182	0.016	0.224	0.016	0.242	0.016	0.278	0.016	0.275	0.016	0.243	0.016	0.252	0.016
+2	0.041	0.016	0.058	0.016	0.065	0.016	0.082	0.016	0.122	0.016	0.151	0.016	0.238	0.016	0.223	0.016	0.202	0.016
+3	0.003	0.016	0.004	0.016	0.005	0.016	0.010	0.016	0.013	0.016	0.022	0.016	0.043	0.016	0.074	0.016	0.113	0.016
+4	0.003	0.016	0.003	0.016	0.002	0.016	0.003	0.016	0.006	0.016	0.007	0.016	0.010	0.016	0.017	0.016	0.039	0.016
+5	0.000	0.016	0.000	0.016	0.000	0.016	0.000	0.016	0.000	0.016	0.000	0.016	0.000	0.016	0.005	0.016	0.010	0.016
+6	0.000	0.016	0.000	0.016	0.000	0.016	0.000	0.016	0.000	0.016	0.000	0.016	0.000	0.016	0.000	0.016	0.003	0.016
PEP	**0**		**0.5**		**1**		**1.5**		**2**		**3**		**5**		**10**		**20**	
+0	0.955	0.020	0.900	0.020	0.825	0.020	0.753	0.020	0.723	0.020	0.664	0.020	0.591	0.020	0.497	0.020	0.459	0.020

+1	0.038	0.020	0.091	0.020	0.163	0.020	0.229	0.020	0.252	0.020	0.297	0.020	0.342	0.020	0.381	0.020	0.362	0.020
+2	0.007	0.020	0.008	0.020	0.011	0.020	0.016	0.020	0.022	0.020	0.034	0.020	0.059	0.020	0.104	0.020	0.147	0.020
+3	0.000	0.020	0.001	0.020	0.001	0.020	0.002	0.020	0.003	0.020	0.004	0.020	0.008	0.020	0.019	0.020	0.033	0.020
R5P	**0**		**0.5**		**1**		**1.5**		**2**		**3**		**5**		**10**		**20**	
+0	0.953	0.030	0.902	0.030	0.856	0.030	0.797	0.030	0.729	0.030	0.700	0.030	0.698	0.030	0.600	0.030	0.469	0.030
+1	0.047	0.030	0.098	0.030	0.144	0.030	0.203	0.030	0.228	0.030	0.231	0.030	0.193	0.030	0.239	0.030	0.271	0.030
+2	0.000	0.030	0.000	0.030	0.000	0.030	0.000	0.030	0.044	0.030	0.062	0.030	0.093	0.030	0.128	0.030	0.200	0.030
+3	0.000	0.030	0.000	0.030	0.000	0.030	0.000	0.030	0.000	0.030	0.007	0.030	0.017	0.030	0.033	0.030	0.060	0.030
+4	0.000	0.030	0.000	0.030	0.000	0.030	0.000	0.030	0.000	0.030	0.000	0.030	0.000	0.030	0.000	0.030	0.000	0.030
+5	0.000	0.030	0.000	0.030	0.000	0.030	0.000	0.030	0.000	0.030	0.000	0.030	0.000	0.030	0.000	0.030	0.000	0.030
S7P	**0**		**0.5**		**1**		**1.5**		**2**		**3**		**5**		**10**		**20**	
+0	0.928	0.020	0.823	0.020	0.679	0.020	0.608	0.020	0.547	0.020	0.454	0.020	0.384	0.020	0.384	0.020	0.238	0.020
+1	0.072	0.020	0.152	0.020	0.253	0.020	0.292	0.020	0.319	0.020	0.348	0.020	0.320	0.020	0.272	0.020	0.270	0.020
+2	0.000	0.020	0.022	0.020	0.060	0.020	0.084	0.020	0.108	0.020	0.154	0.020	0.209	0.020	0.191	0.020	0.247	0.020
+3	0.000	0.020	0.004	0.020	0.009	0.020	0.016	0.020	0.026	0.020	0.044	0.020	0.083	0.020	0.109	0.020	0.174	0.020
+4	0.000	0.020	0.000	0.020	0.000	0.020	0.000	0.020	0.000	0.020	0.000	0.020	0.000	0.020	0.032	0.020	0.037	0.020
+5	0.000	0.020	0.000	0.020	0.000	0.020	0.000	0.020	0.000	0.020	0.000	0.020	0.005	0.020	0.012	0.020	0.034	0.020
+6	0.000	0.020	0.000	0.020	0.000	0.020	0.000	0.020	0.000	0.020	0.000	0.020	0.000	0.020	0.000	0.020	0.000	0.020
+7	0.000	0.020	0.000	0.020	0.000	0.020	0.000	0.020	0.000	0.020	0.000	0.020	0.000	0.020	0.000	0.020	0.000	0.020
RU5P	**0**		**0.5**		**1**		**1.5**		**2**		**3**		**5**		**10**		**20**	
+0	0.953	0.030	0.863	0.030	0.793	0.030	0.706	0.030	0.673	0.030	0.585	0.030	0.522	0.030	0.545	0.030	0.485	0.030
+1	0.047	0.030	0.104	0.030	0.173	0.030	0.250	0.030	0.265	0.030	0.326	0.030	0.331	0.030	0.263	0.030	0.276	0.030
+2	0.000	0.030	0.034	0.030	0.034	0.030	0.044	0.030	0.062	0.030	0.077	0.030	0.122	0.030	0.147	0.030	0.174	0.030
+3	0.000	0.030	0.000	0.030	0.000	0.030	0.000	0.030	0.000	0.030	0.012	0.030	0.026	0.030	0.045	0.030	0.065	0.030
+4	0.000	0.030	0.000	0.030	0.000	0.030	0.000	0.030	0.000	0.030	0.000	0.030	0.000	0.030	0.000	0.030	0.000	0.030
+5	0.000	0.030	0.000	0.030	0.000	0.030	0.000	0.030	0.000	0.030	0.000	0.030	0.000	0.030	0.000	0.030	0.000	0.030
MAL	**0**		**0.5**		**1**		**1.5**		**2**		**3**		**5**		**10**		**20**	
+0	0.952	0.020	0.941	0.020	0.921	0.020	0.908	0.020	0.912	0.020	0.899	0.020	0.854	0.020	0.809	0.020	0.931	0.020
+1	0.038	0.020	0.047	0.020	0.066	0.020	0.078	0.020	0.070	0.020	0.078	0.020	0.106	0.020	0.122	0.020	0.051	0.020
+2	0.010	0.020	0.012	0.020	0.013	0.020	0.014	0.020	0.018	0.020	0.022	0.020	0.035	0.020	0.056	0.020	0.015	0.020
+3	0.000	0.020	0.000	0.020	0.000	0.020	0.000	0.020	0.000	0.020	0.000	0.020	0.004	0.020	0.013	0.020	0.003	0.020
+4	0.000	0.020	0.000	0.020	0.000	0.020	0.000	0.020	0.000	0.020	0.000	0.020	0.000	0.020	0.000	0.020	0.000	0.020

SUC	**0**		**0.5**		**1**		**1.5**		**2**		**3**		**5**		**10**		**20**	
+0	0.953	0.020	0.952	0.020	0.953	0.020	0.953	0.020	0.955	0.020	0.955	0.020	0.956	0.020	0.952	0.020	0.954	0.020
+1	0.042	0.020	0.044	0.020	0.043	0.020	0.042	0.020	0.041	0.020	0.042	0.020	0.041	0.020	0.044	0.020	0.043	0.020
+2	0.004	0.020	0.004	0.020	0.004	0.020	0.004	0.020	0.004	0.020	0.003	0.020	0.004	0.020	0.004	0.020	0.002	0.020
+3	0.000	0.020	0.000	0.020	0.000	0.020	0.000	0.020	0.000	0.020	0.000	0.020	0.000	0.020	0.000	0.020	0.000	0.020
+4	0.000	0.020	0.000	0.020	0.000	0.020	0.000	0.020	0.000	0.020	0.000	0.020	0.000	0.020	0.000	0.020	0.000	0.020
FBP[a]	**0**		**0.5**		**1**		**1.5**		**2**		**3**		**5**		**10**		**20**	
+0	0.871	0.040	0.688	0.040	0.439	0.040	0.332	0.040	0.363	0.040	0.298	0.040	0.308	0.040	0.329	0.040	0.238	0.040
+1	0.060	0.040	0.084	0.040	0.128	0.040	0.116	0.040	0.128	0.040	0.139	0.040	0.187	0.040	0.230	0.040	0.135	0.040
+2	0.036	0.040	0.088	0.040	0.155	0.040	0.163	0.040	0.165	0.040	0.187	0.040	0.180	0.040	0.184	0.040	0.207	0.040
+3	0.007	0.040	0.029	0.040	0.052	0.040	0.088	0.040	0.072	0.040	0.090	0.040	0.093	0.040	0.076	0.040	0.116	0.040
+4	0.018	0.040	0.075	0.040	0.141	0.040	0.196	0.040	0.179	0.040	0.209	0.040	0.153	0.040	0.124	0.040	0.208	0.040
+5	0.005	0.040	0.018	0.040	0.035	0.040	0.041	0.040	0.047	0.040	0.047	0.040	0.045	0.040	0.036	0.040	0.055	0.040
+6	0.004	0.040	0.019	0.040	0.050	0.040	0.064	0.040	0.047	0.040	0.030	0.040	0.035	0.040	0.022	0.040	0.041	0.040
GAP[a]	**0**		**0.5**		**1**		**1.5**		**2**		**3**		**5**		**10**		**20**	
+0	1.000	0.030	1.000	0.030	1.000	0.030	0.804	0.030	0.869	0.030	0.735	0.030	0.742	0.030	0.686	0.030	0.668	0.030
+1	0.000	0.030	0.000	0.030	0.000	0.030	0.196	0.030	0.131	0.030	0.265	0.030	0.178	0.030	0.252	0.030	0.234	0.030
+2	0.000	0.030	0.000	0.030	0.000	0.030	0.000	0.030	0.000	0.030	0.000	0.030	0.000	0.030	0.000	0.030	0.000	0.030
+3	0.000	0.030	0.000	0.030	0.000	0.030	0.000	0.030	0.000	0.030	0.000	0.030	0.079	0.030	0.061	0.030	0.098	0.030
RUBP[a]	**0**		**0.5**		**1**		**1.5**		**2**		**3**		**5**		**10**		**20**	
+0	0.827	N/A	0.738	N/A	0.696	N/A	0.451	N/A	0.549	N/A	0.507	N/A	0.370	N/A	0.276	N/A	0.212	N/A
+1	0.055	N/A	0.129	N/A	0.192	N/A	0.208	N/A	0.224	N/A	0.247	N/A	0.242	N/A	0.287	N/A	0.202	N/A
+2	0.059	N/A	0.085	N/A	0.058	N/A	0.134	N/A	0.110	N/A	0.141	N/A	0.211	N/A	0.251	N/A	0.239	N/A
+3	0.012	N/A	0.019	N/A	0.013	N/A	0.031	N/A	0.029	N/A	0.027	N/A	0.061	N/A	0.074	N/A	0.082	N/A
+4	0.022	N/A	0.010	N/A	0.023	N/A	0.124	N/A	0.044	N/A	0.037	N/A	0.066	N/A	0.067	N/A	0.172	N/A
+5	0.025	N/A	0.020	N/A	0.017	N/A	0.052	N/A	0.044	N/A	0.041	N/A	0.050	N/A	0.046	N/A	0.094	N/A

[a] Not included in INCA fitting due to one or more possible interfering peaks or low signal

Table A.9 INST-MFA Estimated Fluxes for *Synechocystis* sp. PCC 6803 Km

	SSR = 386.2 [321.4 428.4] [a]	**Value**	**LB** [b]	**UB** [b]
R1	dummy -> Sink	100.0	100.0	100.0
R2	G6P -> Sink	100.0	100.0	100.0
R3	F6P -> Sink	100.0	100.0	100.0
R4	R5P -> Sink	100.0	100.0	100.0
R6	0*G6P.c -> G6P	49.2	38.4	58.8
R7	0*G6P.x -> G6P	50.8	41.2	61.6
R8	0*F6P.c -> F6P	47.3	35.2	57.6
R9	0*F6P.x -> F6P	52.7	42.4	64.8
R10	0*R5P.c -> R5P	100.0	45.1	100.0
R11	0*R5P.x -> R5P	0.0	0.0	54.9
CO2 net	CO2.x <-> CO2	100.4	100.4	100.4
RBC	RUBP + CO2 -> 3PGA + 3PGA + dummy	234.7	194.3	23762.0
GAPDH net	3PGA <-> GAP.c	459.5	380.8	74984.0
TPI net	GAP.c <-> DHAP.c	218.2	178.6	48913.0
FBP net	DHAP.c + GAP.c <-> FBP	179.9	132.6	23710.0
ALD	DHAP.c + E4P -> SBP	38.4	0.0	2270.1
PFK net	FBP <-> F6P.c	179.9	132.6	23710.0
SBP	SBP -> S7P	38.4	0.0	2270.1
PGI net	F6P.c <-> G6P.c	140.7	101.3	23597.0
G6PDH	G6P.c + dummy -> RU5P + CO2	136.9	97.4	23593.0
TK1 net	X5P <-> GAP.c + EC2	-60.6	-4689.8	-60.6
TK2 net	F6P.c <-> E4P + EC2	22.3	22.3	5243.9
TK3 net	S7P <-> R5P.c + EC2	38.4	38.4	2466.3
TA1 net	F6P.c <-> GAP.c + EC3	0.0	-241.1	2493.9
TA2 net	S7P <-> E4P + EC3	0.0	-2493.9	241.1
PKT1	X5P -> GAP.c + AP	0.0	0.0	17.2
PKT2	F6P.c -> E4P + AP	16.9	0.0	17.2
PTA net	AP <-> ACA	16.9	16.9	17.2
PPE net	RU5P <-> X5P	-60.6	-4847.6	-60.6
PPI net	RU5P <-> R5P.c	-37.2	-2465.2	-37.2
PRK	RU5P -> RUBP	234.7	195.2	49466.0
PGM net	3PGA <-> 2PGA	7.0	7.0	2418.5
ENO	2PGA -> PEP	7.0	7.0	2418.5
PK	PEP -> PYR	0.0	0.0	13.1
PDH	PYR + dummy -> ACA + CO2	0.0	0.0	2411.5
CS	OAA + ACA -> CIT	2.0	2.0	2300.4
ACO net	CIT <-> ICI	2.0	2.0	2300.4
IDH	ICI + dummy -> AKG + CO2	2.0	2.0	2300.4
OGDA	AKG + dummy -> SSA + CO2	0.0	0.0	2298.5
SSAD	SSA -> SUC	0.0	0.0	2298.5

SDH net	SUC <-> FUM	0.0	0.0	2298.5
FUM net	FUM <-> MAL	0.9	0.9	2299.4
MDH net	MAL <-> OAA	-0.3	NaN	-0.3
ME	MAL + dummy -> PYR + CO2	1.2	1.2	3335.1
PPC	PEP + CO2 -> OAA + dummy	5.5	5.5	3339.3
RBOX	RUBP -> 3PGA + 2PG	0.0	0.0	165.7
PGP	2PG -> GLC	0.0	0.0	165.7
GDH	GLC -> GLY	0.0	0.0	165.7
GDC net	GLY + GLY + dummy <-> SER + CO2	-0.3	-0.3	82.5
SGA	SER -> GA	0.0	0.0	84.7
GK	GA -> 3PGA	0.0	0.0	84.7
GLUDH	AKG -> GLU	0.9	0.0	77.5
3PGDH	GLU + 3PGA -> AKG + SER	0.9	0.0	77.5
Growth Km	0.509*R5P.c + 6.39*ACA + 1.64*G6P.c + 0.328*E4P + 0.868*3PGA + 0.656*PEP + 0.523*PYR + 1.38*OAA + 0.836*AKG + 0.326*GAP.c + 0.25*SER + 0.275*GLY + 0.17*dummy -> Biomass + 0.396*FUM	2.3	2.3	2.3

[a] Sum of squared residuals (SSR), and the expected range in square brackets [$\chi^2_{a/2}(n-p)$, $\chi^2_{1-a/2}(n-p)$]

[b] Lower bounds (LB) and upper bounds (UB) represent the 95% CI as determined via the parameter continuation method

Table A.10 INST-MFA Estimated Fluxes for *Synechocystis* sp. PCC 6803 70glpX

	SSR = 363.2 [315.8 422.0] [a]	**Value**	**LB** [b]	**UB** [b]
R1	dummy -> Sink	100.0	100.0	100.0
R2	G6P -> Sink	100.0	100.0	100.0
R3	F6P -> Sink	100.0	100.0	100.0
R4	R5P -> Sink	100.0	100.0	100.0
R6	0*G6P.c -> G6P	75.0	72.4	78.9
R7	0*G6P.x -> G6P	25.0	21.1	27.6
R8	0*F6P.c -> F6P	63.3	60.6	66.7
R9	0*F6P.x -> F6P	36.7	33.3	39.4
R10	0*R5P.c -> R5P	89.9	79.2	98.7
R11	0*R5P.x -> R5P	10.1	1.3	20.8
CO2 net	CO2.x <-> CO2	100.1	100.1	100.1
RBC	RUBP + CO2 -> 3PGA + 3PGA + dummy	96.6	NaN	120.5
GAPDH net	3PGA <-> GAP.c	181.3	NaN	224.1
TPI net	GAP.c <-> DHAP.c	77.7	NaN	94.9
FBP net	DHAP.c + GAP.c <-> FBP	40.9	25.0	89.5
ALD	DHAP.c + E4P -> SBP	36.8	0.0	52.6
PFK net	FBP <-> F6P.c	40.9	25.0	89.5
SBP	SBP -> S7P	36.8	0.0	52.6
PGI net	F6P.c <-> G6P.c	3.2	3.2	3.2
G6PDH	G6P.c + dummy -> RU5P + CO2	0.0	0.0	0.0
TK1 net	X5P <-> GAP.c + EC2	-74.6	-91.7	NaN
TK2 net	F6P.c <-> E4P + EC2	37.7	NaN	46.3
TK3 net	S7P <-> R5P.c + EC2	36.8	NaN	45.4
TA1 net	F6P.c <-> GAP.c + EC3	0.0	-15.8	42.8
TA2 net	S7P <-> E4P + EC3	0.0	-42.8	15.8
PKT1	X5P -> GAP.c + AP	12.4	0.0	12.4
PKT2	F6P.c -> E4P + AP	0.0	0.0	NaN
PTA net	AP <-> ACA	12.4	10.4	12.4
PPE net	RU5P <-> X5P	-62.2	-79.6	-62.2
PPI net	RU5P <-> R5P.c	-34.4	-42.9	NaN
PRK	RU5P -> RUBP	96.6	96.6	121.9
PGM net	3PGA <-> 2PGA	9.2	NaN	17.2
ENO	2PGA -> PEP	9.2	NaN	17.2
PK	PEP -> PYR	0.0	0.0	2.0
PDH	PYR + dummy -> ACA + CO2	0.3	NaN	8.3
CS	OAA + ACA -> CIT	2.3	2.3	10.3
ACO net	CIT <-> ICI	2.3	2.3	10.3
IDH	ICI + dummy -> AKG + CO2	2.3	2.3	10.3
OGDA	AKG + dummy -> SSA + CO2	0.0	0.0	8.0
SSAD	SSA -> SUC	0.0	0.0	8.0
SDH net	SUC <-> FUM	0.0	0.0	8.0

FUM net	FUM <-> MAL	1.7	1.7	9.7
MDH net	MAL <-> OAA	0.0	-2.0	0.0
ME	MAL + dummy -> PYR + CO2	1.7	1.7	9.6
PPC	PEP + CO2 -> OAA + dummy	7.4	7.4	15.3
RBOX	RUBP -> 3PGA + 2PG	0.0	0.0	2.1
PGP	2PG -> GLC	0.0	0.0	2.1
GDH	GLC -> GLY	0.0	0.0	2.1
GDC net	GLY + GLY + dummy <-> SER + CO2	-0.4	-0.4	0.7
SGA	SER -> GA	0.0	0.0	0.0
GK	GA -> 3PGA	0.0	0.0	0.0
GLUDH	AKG -> GLU	1.1	0.0	1.1
3PGDH	GLU + 3PGA -> AKG + SER	1.1	0.0	1.1
Growth 70glpX	0.928*R5P.c + 3.892*ACA + 1.183*G6P.c + 0.336*E4P + 0.584*3PGA + 0.672*PEP + 0.536*PYR + 1.931*OAA + 0.857*AKG + 0.186*GAP.c + 0.256*SER + 0.282*GLY + 0.047*dummy -> Biomass + 0.638*FUM	2.7	2.7	2.7

[a] Sum of squared residuals (SSR), and the expected range in square brackets [$\chi^2_{a/2}(n-p)$, $\chi^2_{1-a/2}(n-p)$]

[b] Lower bounds (LB) and upper bounds (UB) represent the 95% CI as determined via the parameter continuation method

Table A.11 INST-MFA Estimated Fluxes for *Synechocystis* sp. PCC 6803 tktA

	SSR = 396.7 [327.0 434.8] [a]	**Value**	**LB** [b]	**UB** [b]
R1	dummy -> Sink	100.0	100.0	100.0
R2	G6P -> Sink	100.0	100.0	100.0
R3	F6P -> Sink	100.0	100.0	100.0
R4	R5P -> Sink	100.0	100.0	100.0
R5	RU5P -> Sink	100.0	100.0	100.0
R6	0*G6P.c -> G6P	67.3	62.9	71.5
R7	0*G6P.x -> G6P	32.7	28.5	37.1
R8	0*F6P.c -> F6P	67.1	62.4	71.7
R9	0*F6P.x -> F6P	32.9	28.3	37.6
R10	0*R5P.c -> R5P	43.8	36.2	55.2
R11	0*R5P.x -> R5P	56.2	44.8	63.8
R12	0*RU5P.c -> RU5P	61.3	57.8	65.6
R13	0*RU5P.x -> RU5P	38.7	34.4	42.2
CO2 net	CO2.x <-> CO2	100.5	100.5	100.5
RBC	RUBP + CO2 -> 3PGA + 3PGA + dummy	110.4	99.9	173.2
GAPDH net	3PGA <-> GAP.c	210.8	191.2	317.8
TPI net	GAP.c <-> DHAP.c	93.2	85.1	138.0
FBP net	DHAP.c + GAP.c <-> FBP	86.7	73.5	129.3
ALD	DHAP.c + E4P -> SBP	6.5	2.0	16.3
PFK net	FBP <-> F6P.c	86.7	73.5	129.3
SBP	SBP -> S7P	6.5	2.0	16.3
PGI net	F6P.c <-> G6P.c	16.8	6.5	30.0
G6PDH	G6P.c + dummy -> RU5P.c + CO2	12.4	2.2	25.6
TK1 net	X5P <-> GAP.c + EC2	-76.4	-111.4	NaN
TK2 net	F6P.c <-> E4P + EC2	38.7	NaN	56.1
TK3 net	S7P <-> R5P.c + EC2	37.8	NaN	55.3
TA1 net	F6P.c <-> GAP.c + EC3	31.3	22.8	47.5
TA2 net	S7P <-> E4P + EC3	-31.3	-47.5	-22.8
PKT1	X5P -> GAP.c + AP	14.9	0.0	14.9
PKT2	F6P.c -> E4P + AP	0.0	0.0	14.9
PTA net	AP <-> ACA	14.9	9.8	14.9
PPE net	RU5P.c <-> X5P	-61.6	-97.4	NaN
PPI net	RU5P.c <-> R5P.c	-36.4	-53.9	NaN
PRK	RU5P.c -> RUBP	110.4	100.4	173.2
PGM net	3PGA <-> 2PGA	8.0	8.0	26.4
ENO	2PGA -> PEP	8.0	8.0	26.4
PK	PEP -> PYR	0.0	0.0	5.1
PDH	PYR + dummy -> ACA + CO2	0.0	0.0	18.4
CS	OAA + ACA -> CIT	2.5	2.2	19.9
ACO net	CIT <-> ICI	2.5	2.2	19.9
IDH	ICI + dummy -> AKG + CO2	2.5	2.2	19.9

OGDA	AKG + dummy -> SSA + CO2	0.3	0.0	17.7
SSAD	SSA -> SUC	0.3	0.0	17.7
SDH net	SUC <-> FUM	0.3	0.0	17.7
FUM net	FUM <-> MAL	1.3	1.0	18.7
MDH net	MAL <-> OAA	-0.1	-5.1	0.0
ME	MAL + dummy -> PYR + CO2	1.4	1.1	19.8
PPC	PEP + CO2 -> OAA + dummy	6.3	5.9	24.7
RBOX	RUBP -> 3PGA + 2PG	0.0	0.0	15.1
PGP	2PG -> GLC	0.0	0.0	15.1
GDH	GLC -> GLY	0.0	0.0	15.1
GDC net	GLY + GLY + dummy <-> SER + CO2	-0.4	-0.4	7.2
SGA	SER -> GA	16.9	14.7	27.3
GK	GA -> 3PGA	16.9	14.7	27.3
GLUDH	AKG -> GLU	17.9	11.8	28.3
3PGDH	GLU + 3PGA -> AKG + SER	17.9	11.8	28.3
Growth tktA2	0.533*R5P.c + 4.89*ACA + 1.74*G6P.c + 0.348*E4P + 0.361*3PGA + 0.697*PEP + 0.556*PYR + 1.46*OAA + 0.888*AKG + 0.24*GAP.c + 0.265*SER + 0.292*GLY + 0.182*dummy -> Biomass + 0.416*FUM	2.5	2.5	2.5

[a] Sum of squared residuals (SSR), and the expected range in square brackets [$\chi^2_{a/2}(n-p)$, $\chi^2_{1-a/2}(n-p)$]

[b] Lower bounds (LB) and upper bounds (UB) represent the 95% CI as determined via the parameter continuation method

Table A.12 BG-11 Media Composition

Component	Stock solution	Amount of stock solution added	Final Concentration (mM)
$NaNO_3$	30 g/200 mL	10 mL/L	17.6
K_2HPO_4	0.8 g/200 mL	10 mL/L	0.23
$MgSO_4 \cdot 7H_2O$	1.5 g/200 mL	10 mL/L	0.3
$CaCl_2 \cdot 2H_2O$	0.72 g/200 mL	10 mL/L	0.24
Citric Acid$\cdot H_2O$	0.12 g/200 mL	10 mL/L	0.031
Ferric Ammonium Citrate	0.12 g/200 mL	10 mL/L	0.021
$Na_2EDTA \cdot 2H_2O$	0.02 g/200 mL	10 mL/L	0.0027
Na_2CO_3	0.4 g/200 mL	10 mL/L	0.19
Trace Metals Solution	N/A	1 mL	N/A

Table A.13 BG-11 Trace Metals Solution

Component	Amount added	Final Concentration (mM)
H_3BO_3	2.86 g/L	46
$MnCl_2 \cdot 4H_2O$	1.81 g/L	9
$ZnSO_4 \cdot 7H_2O$	0.22 g/L	0.77
$Na_2MoO_4 \cdot 2H_2O$	0.39 g/L	1.6
$CuSO_4 \cdot 5H_2O$	0.079 g/L	0.3
$Co(NO_3)_2 \cdot 6H_2O$	49.4 mg/L	0.17

Table A.14 BG-11 PC Media Composition [27]

Component	Stock solution	Amount of stock solution added	Final Concentration (mM)
$NaNO_3$	15 g/50 mL	5 mL/L	17.6
K_2HPO_4	0.4 g/50 mL	5 mL/L	0.23
$MgSO_4 \cdot 7H_2O$	0.75 g/50 mL	5 mL/L	0.3
$CaCl_2 \cdot 2H_2O$	0.36 g/50 mL	5 mL/L	0.24
EDTA	0.15 g/50 mL	5 mL/L	0.05
Na_2CO_3	0.2 g/50 mL	5 mL/L	0.19
$FeCl_3 \cdot 6H_2O$	0.041 g/50 mL	5 mL/L	0.0015
HEPES	24 g/50 mL	5 mL/L	10
Trace Metals Solution	N/A	1 mL	N/A

BG-11 PC is used to avoid addition of citric acid, an organic carbon source.

REFERENCES

[1] A. L. Carroll, A. E. Case, A. Zhang, and S. Atsumi, "Metabolic engineering tools in model cyanobacteria," *Metab. Eng.*, Mar. 2018, doi: 10.1016/J.YMBEN.2018.03.014.

[2] J. Diao, X. Song, L. Zhang, J. Cui, L. Chen, and W. Zhang, "Tailoring cyanobacteria as a new platform for highly efficient synthesis of astaxanthin," *Metab. Eng.*, vol. 61, pp. 275–287, Sep. 2020, doi: 10.1016/j.ymben.2020.07.003.

[3] J. Ungerer, L. Tao, M. Davis, M. Ghirardi, P. C. Maness, and J. Yu, "Sustained photosynthetic conversion of CO2 to ethylene in recombinant cyanobacterium Synechocystis 6803," *Energy Environ. Sci.*, vol. 5, no. 10, pp. 8998–9006, Oct. 2012, doi: 10.1039/c2ee22555g.

[4] J. Dexter and P. Fu, "Metabolic engineering of cyanobacteria for ethanol production," *Energy Environ. Sci.*, vol. 2, no. 8, pp. 857–864, Jul. 2009, doi: 10.1039/b811937f.

[5] M. Santos-Merino, M. P. Garcillán-Barcia, and F. De La Cruz, "Engineering the fatty acid synthesis pathway in Synechococcus elongatus PCC 7942 improves omega-3 fatty acid production," *Biotechnol. Biofuels*, vol. 11, no. 1, pp. 1–13, Sep. 2018, doi: 10.1186/s13068-018-1243-4.

[6] U. Sauer, "Metabolic networks in motion: 13C-based flux analysis," *Molecular Systems Biology*, vol. 2. Mol Syst Biol, May 16, 2006, doi: 10.1038/msb4100109.

[7] J. A. Bassham, A. A. Benson, L. D. Kay, A. Z. Harris, A. T. Wilson, and M. Calvin, "The Path of Carbon in Photosynthesis. XXI. The Cyclic Regeneration of Carbon Dioxide Acceptor [1]," *J. Am. Chem. Soc.*, vol. 76, no. 7, pp. 1760–1770, Apr. 1954, doi: 10.1021/ja01636a012.

[8] K. Ueda, T. Nakajima, K. Yoshikawa, Y. Toya, F. Matsuda, and H. Shimizu, "Metabolic flux of the oxidative pentose phosphate pathway under low light conditions in Synechocystis sp. PCC 6803," *J. Biosci. Bioeng.*, vol. 126, no. 1, pp. 38–43, Jul. 2018, doi: 10.1016/j.jbiosc.2018.01.020.

[9] W. Xiong *et al.*, "Phosphoketolase pathway contributes to carbon metabolism in cyanobacteria," *Nat. Plants*, vol. 2, no. 1, p. 15187, Dec. 2015, doi: 10.1038/nplants.2015.187.

[10] C. Peterhansel *et al.*, “Engineering photorespiration: current state and future possibilities,” *Plant Biol.*, vol. 15, no. 4, pp. 754–758, Jul. 2013, doi: 10.1111/j.1438-8677.2012.00681.x.

[11] B. L. Montgomery, S. Lechno-Yossef, and C. A. Kerfeld, “Interrelated modules in cyanobacterial photosynthesis: the carbon-concentrating mechanism, photorespiration, and light perception.,” *J. Exp. Bot.*, vol. 67, no. 10, pp. 2931–40, May 2016, doi: 10.1093/jxb/erw162.

[12] B. Sunil, D. Saini, R. B. Bapatla, V. Aswani, and A. S. Raghavendra, “Photorespiration is complemented by cyclic electron flow and the alternative oxidase pathway to optimize photosynthesis and protect against abiotic stress,” *Photosynthesis Research*, vol. 139, no. 1–3. Springer Netherlands, pp. 67–79, Sep. 05, 2019, doi: 10.1007/s11120-018-0577-x.

[13] D. C. Ducat, J. C. Way, and P. A. Silver, “Engineering cyanobacteria to generate high-value products,” *Trends Biotechnol.*, vol. 29, no. 2, pp. 95–103, Feb. 2011, doi: 10.1016/j.tibtech.2010.12.003.

[14] X.-G. Zhu, Y. Wang, D. R. Ort, and S. P. Long, “e-Photosynthesis: a comprehensive dynamic mechanistic model of C3 photosynthesis: from light capture to sucrose synthesis.,” *Plant. Cell Environ.*, vol. 36, no. 9, pp. 1711–27, Sep. 2013, doi: 10.1111/pce.12025.

[15] G. Petterson and U. Ryde-Petterson, “Dependence of the Calvin cycle activity on kinetic parameters for the interaction of non-equilibrium cycle enzymes with their substrates.,” *Eur. J. Biochem.*, vol. 186, pp. 683–687, 1989.

[16] M. Janasch, J. Asplund-Samuelsson, R. Steuer, and E. P. Hudson, “Kinetic modeling of the Calvin cycle identifies flux control and stable metabolomes in Synechocystis carbon fixation,” *J. Exp. Bot.*, vol. 70, no. 3, pp. 1017–1031, Oct. 2019, doi: 10.1093/jxb/ery382.

[17] J. Jablonsky, H. Bauwe, and O. Wolkenhauer, “Modeling the Calvin-Benson cycle.,” *BMC Syst. Biol.*, vol. 5, no. 1, p. 185, Jan. 2011, doi: 10.1186/1752-0509-5-185.

[18] L. Michelet *et al.*, “Redox regulation of the Calvin-Benson cycle: something old, something new.,” *Front. Plant Sci.*, vol. 4, p. 470, Jan. 2013, doi: 10.3389/fpls.2013.00470.

[19] N. Battchikova, J. P. Vainonen, N. Vorontsova, M. Keränen, D. Carmel, and E.-M. Aro, “Dynamic Changes in the Proteome of *Synechocystis* 6803 in Response to CO_2 Limitation Revealed by Quantitative Proteomics,” *J. Proteome Res.*, vol. 9, no. 11, pp. 5896–5912, Nov. 2010, doi: 10.1021/pr100651w.

[20] M. Jahn *et al.*, “Growth of Cyanobacteria Is Constrained by the Abundance of Light and Carbon Assimilation Proteins,” *Cell Rep.*, vol. 25, no. 2, pp. 478-486.e8, Oct. 2018, doi: 10.1016/j.celrep.2018.09.040.

[21] M. H. Abernathy, L. He, and Y. J. Tang, “Channeling in native microbial pathways: Implications and challenges for metabolic engineering,” *Biotechnology Advances*, vol. 35, no. 6. Elsevier, pp. 805–814, Nov. 01, 2017, doi: 10.1016/j.biotechadv.2017.06.004.

[22] M. H. Abernathy, J. J. Czajka, D. K. Allen, N. C. Hill, J. C. Cameron, and Y. J. Tang, “Cyanobacterial carboxysome mutant analysis reveals the influence of enzyme compartmentalization on cellular metabolism and metabolic network rigidity,” *Metab. Eng.*, vol. 54, pp. 222–231, Jul. 2019, doi: 10.1016/j.ymben.2019.04.010.

[23] N. Mangan and M. Brenner, “Systems analysis of the CO2 concentrating mechanism in cyanobacteria.,” *Elife*, vol. 3, p. e02043, Apr. 2014, doi: 10.7554/eLife.02043.

[24] L. L. Baers *et al.*, “Proteome Mapping of a Cyanobacterium Reveals Distinct Compartment Organization and Cell-Dispersed Metabolism.,” *Plant Physiol.*, vol. 181, no. 4, pp. 1721–1738, 2019, doi: 10.1104/pp.19.00897.

[25] A. O. Adebiyi, L. J. Jazmin, and J. D. Young, “13C flux analysis of cyanobacterial metabolism,” *Photosynthesis Research*, vol. 126, no. 1. Springer Netherlands, pp. 19–32, Oct. 04, 2015, doi: 10.1007/s11120-014-0045-1.

[26] J. D. Young, A. A. Shastri, G. Stephanopoulos, and J. A. Morgan, “Mapping photoautotrophic metabolism with isotopically nonstationary 13C flux analysis,” *Metab. Eng.*, vol. 13, no. 6, pp. 656–665, Nov. 2011, doi: 10.1016/j.ymben.2011.08.002.

[27] P. van Alphen, H. Abedini Najafabadi, F. Branco dos Santos, and K. J. Hellingwerf, “Increasing the Photoautotrophic Growth Rate of Synechocystis sp. PCC 6803 by Identifying the Limitations of Its Cultivation,” *Biotechnol. J.*, vol. 13, no. 8, p. 1700764, Mar. 2018, doi: 10.1002/biot.201700764.

[28] J. D. Young, “INCA: A computational platform for isotopically non-stationary metabolic flux analysis,” *Bioinformatics*, vol. 30, no. 9, pp. 1333–1335, May 2014, doi: 10.1093/bioinformatics/btu015.

[29] C. B. Prasannan, D. Jaiswal, R. Davis, and P. P. Wangikar, “An improved method for extraction of polar and charged metabolites from cyanobacteria,” *PLoS One*, vol. 13, no. 10, p. e0204273, Oct. 2018, doi: 10.1371/journal.pone.0204273.

[30] B. Luo, K. Groenke, R. Takors, C. Wandrey, and M. Oldiges, “Simultaneous determination of multiple intracellular metabolites in glycolysis, pentose phosphate pathway and tricarboxylic acid cycle by liquid chromatography–mass spectrometry,” *J. Chromatogr. A*, vol. 1147, no. 2, pp. 153–164, 2007, doi: 10.1016/j.chroma.2007.02.034.

[31] F. Ma, L. J. Jazmin, J. D. Young, and D. K. Allen, “Isotopically nonstationary metabolic flux analysis (INST-MFA) of photosynthesis and photorespiration in plants,” in *Methods in Molecular Biology*, vol. 1653, Humana Press, New York, NY, 2017, pp. 167–194.

[32] U. K. Aryal, Z. Ding, V. Hedrick, T. J. P. Sobreira, D. Kihara, and L. A. Sherman, “Analysis of Protein Complexes in the Unicellular Cyanobacterium Cyanothece ATCC 51142,” *J. Proteome Res.*, vol. 17, no. 11, pp. 3628–3643, Nov. 2018, doi: 10.1021/acs.jproteome.8b00170.

[33] A. D. Polpitiya *et al.*, “DAnTE: A statistical tool for quantitative analysis of -omics data,” *Bioinformatics*, vol. 24, no. 13, pp. 1556–1558, Jul. 2008, doi: 10.1093/bioinformatics/btn217.

[34] T. Zavřel *et al.*, “Quantitative insights into the cyanobacterial cell economy,” *Elife*, vol. 8, Feb. 2019, doi: 10.7554/elife.42508.

[35] P. Hsieh, J. Z. Pedersen, and L. Bruno, “Photoinhibition of cyanobacteria and its application in cultural heritage conservation,” *Photochem. Photobiol.*, vol. 90, no. 3, pp. 533–543, May 2014, doi: 10.1111/php.12208.

[36] B. C. Tripathy and R. Oelmüller, “Reactive oxygen species generation and signaling in plants.,” *Plant Signal. Behav.*, vol. 7, no. 12, pp. 1621–33, Dec. 2012, doi: 10.4161/psb.22455.

[37] X. Zheng and E. K. O’Shea, “Cyanobacteria Maintain Constant Protein Concentration despite Genome Copy-Number Variation,” *Cell Rep.*, vol. 19, no. 3, pp. 497–504, Apr. 2017, doi: 10.1016/J.CELREP.2017.03.067.

[38] K. Nakahara, “Purification and Characterization of Class-I and Class-II Fructose-1,6-bisphosphate Aldolases from the Cyanobacterium Synechocystis sp. PCC 6803,” *Plant Cell Physiol.*, vol. 44, no. 3, pp. 326–333, Mar. 2003, doi: 10.1093/pcp/pcg044.

[39] J. Jablonsky, D. Schwarz, and M. Hagemann, “Multi-level kinetic model explaining diverse roles of isozymes in prokaryotes,” *PLoS One*, vol. 9, no. 8, p. e105292, Aug. 2014, doi: 10.1371/journal.pone.0105292.

[40] D. Shih-Wei Chuang and J. C. Liao, “Role of cyanobacterial phosphoketolase in energy regulation and glucose secretion under dark anaerobic and osmotic stress conditions,” *Metab. Eng.*, Dec. 2020, doi: 10.1016/j.ymben.2020.12.004.

[41] T. ap Rees and S. A. Hill, “Metabolic control analysis of plant metabolism,” *Plant, Cell & Environment*, vol. 17, no. 5. John Wiley & Sons, Ltd, pp. 587–599, May 01, 1994, doi: 10.1111/j.1365-3040.1994.tb00151.x.

[42] L. Wu, W. Wang, W. A. Van Winden, W. M. Van Gulik, and J. J. Heijnen, “A new framework for the estimation of control parameters in metabolic pathways using lin-log kinetics,” *Eur. J. Biochem.*, vol. 271, no. 16, pp. 3348–3359, Jul. 2004, doi: 10.1111/j.0014-2956.2004.04269.x.

[43] H. Link and D. Weuster-Botz, “Steady-state analysis of metabolic pathways: Comparing the double modulation method and the lin-log approach,” *Metab. Eng.*, vol. 9, no. 5–6, pp. 433–441, Sep. 2007, doi: 10.1016/j.ymben.2007.07.002.

[44] G. Pettersson, “Error associated with experimental flux control coefficient determinations in the Calvin cycle,” *Biochim. Biophys. Acta - Gen. Subj.*, vol. 1289, no. 2, Mar. 1996, doi: 10.1016/0304-4165(95)00078-X.

[45] J. R. Small, “Flux control coefficients determined by inhibitor titration: the design and analysis of experiments to minimize errors,” *Biochem. J.*, vol. 296, no. 2, Dec. 1993, doi: 10.1042/bj2960423.

[46] D. A. Fell, “Increasing the flux in metabolic pathways: A metabolic control analysis perspective,” *Biotechnol. Bioeng.*, vol. 58, no. 2–3, Apr. 1998, doi: 10.1002/(SICI)1097-0290(19980420)58:2/3<121::AID-BIT2>3.0.CO;2-N.

[47] F. Liang and P. Lindblad, “Effects of overexpressing photosynthetic carbon flux control enzymes in the cyanobacterium Synechocystis PCC 6803,” *Metab. Eng.*, vol. 38, pp. 56–64, 2016, doi: 10.1016/j.ymben.2016.06.005.

[48] X.-G. Zhu, E. de Sturler, and S. P. Long, “Optimizing the distribution of resources between enzymes of carbon metabolism can dramatically increase photosynthetic rate: a numerical simulation using an evolutionary algorithm.,” *Plant Physiol.*, vol. 145, no. 2, pp. 513–26, Oct. 2007, doi: 10.1104/pp.107.103713.

[49] C. Bro, B. Regenberg, G. Lagniel, J. Labarre, M. Montero-Lomelí, and J. Nielsen, "Transcriptional, proteomic, and metabolic responses to lithium in galactose-grown yeast cells," *J. Biol. Chem.*, vol. 278, no. 34, pp. 32141–32149, Aug. 2003, doi: 10.1074/jbc.M304478200.

[50] C. Wu *et al.*, "A generalized computational framework to streamline thermodynamics and kinetics analysis of metabolic pathways," *Metab. Eng.*, vol. 57, pp. 140–150, Jan. 2020, doi: 10.1016/j.ymben.2019.08.006.

[51] N. Wan *et al.*, "Cyanobacterial carbon metabolism: Fluxome plasticity and oxygen dependence," *Biotechnol. Bioeng.*, vol. 114, no. 7, pp. 1593–1602, Jul. 2017, doi: 10.1002/bit.26287.

[52] S. Zhang, X. Qian, S. Chang, G. C. Dismukes, and D. A. Bryant, "Natural and Synthetic Variants of the Tricarboxylic Acid Cycle in Cyanobacteria: Introduction of the GABA Shunt into Synechococcus sp. PCC 7002.," *Front. Microbiol.*, vol. 7, p. 1972, 2016, doi: 10.3389/fmicb.2016.01972.

[53] A. A. Shastri and J. A. Morgan, "Flux balance analysis of photoautotrophic metabolism.," *Biotechnol. Prog.*, vol. 21, no. 6, pp. 1617–26, Jan. 2005, doi: 10.1021/bp050246d.

[54] J. Huege, J. Goetze, D. Schwarz, H. Bauwe, M. Hagemann, and J. Kopka, "Modulation of the Major Paths of Carbon in Photorespiratory Mutants of Synechocystis," *PLoS One*, vol. 6, no. 1, p. e16278, Jan. 2011, doi: 10.1371/journal.pone.0016278.

[55] F. Ma, L. J. Jazmin, J. D. Young, and D. K. Allen, "Isotopically nonstationary 13C flux analysis of changes in Arabidopsis thaliana leaf metabolism due to high light acclimation.," *Proc. Natl. Acad. Sci. U. S. A.*, vol. 111, no. 47, pp. 16967–72, Nov. 2014, doi: 10.1073/pnas.1319485111.

[56] R. Agarwal, S. Ortleb, J. K. Sainis, and M. Melzer, "Immunoelectron microscopy for locating Calvin cycle enzymes in the thylakoids of synechocystis 6803," *Mol. Plant*, vol. 2, no. 1, pp. 32–42, Jan. 2009, doi: 10.1093/mp/ssn075.

[57] D. N. Dani and J. K. Sainis, "Isolation and characterization of a thylakoid membrane module showing partial light and dark reactions," *Biochim. Biophys. Acta - Biomembr.*, vol. 1669, no. 1, pp. 43–52, May 2005, doi: 10.1016/j.bbamem.2005.01.001.

[58] K. H. Süss, C. Arkona, R. Manteuffel, and K. Adler, “Calvin cycle multienzyme complexes are bound to chloroplast thylakoid membranes of higher plants in situ,” *Proc. Natl. Acad. Sci. U. S. A.*, vol. 90, no. 12, pp. 5514–5518, Jun. 1993, doi: 10.1073/pnas.90.12.5514.

[59] R. Alscher-Herman, “Chloroplast Alkaline Fructose 1,6-Bisphosphatase Exists in a Membrane-Bound Form,” *Plant Physiol.*, vol. 70, no. 3, pp. 728–734, Sep. 1982, doi: 10.1104/PP.70.3.728.

[60] L. E. Anderson, N. Gatla, and A. A. Carol, “Enzyme co-localization in pea leaf chloroplasts: glyceraldehyde-3-P dehydrogenase, triose-P isomerase, aldolase and sedoheptulose bisphosphatase,” *Photosynth. Res.*, vol. 83, no. 3, pp. 317–328, Mar. 2005, doi: 10.1007/s11120-005-0790-2.

[61] A. R. Andres, J. J. Lazaro, A. Chueca, R. Hermoso, and J. L. Gorge, “Effect of alcohols on the association of photosynthetic fructose-1,6-bisphosphatase to thylakoid membranes,” *Physiol. Plant.*, vol. 78, no. 3, pp. 409–413, Mar. 1990, doi: 10.1111/j.1399-3054.1990.tb09056.x.

[62] R. Hermoso, M. R. de Felipe, A. Vivó, A. Chueca, J. J. Lázaro, and J. L. Gorge, “Immunogold localization of photosynthetic fructose-1,6-bisphosphatase in pea leaf tissue.,” *Plant Physiol.*, vol. 89, no. 1, pp. 381–5, Jan. 1989, doi: 10.1104/pp.89.1.381.

[63] P. E. López-Calcagno, T. P. Howard, and C. A. Raines, “The CP12 protein family: A thioredoxin-mediated metabolic switch?,” *Frontiers in Plant Science*, vol. 5, no. JAN. Frontiers, p. 9, Jan. 30, 2014, doi: 10.3389/fpls.2014.00009.

[64] L. Marri *et al.*, “In vitro characterization of Arabidopsis CP12 isoforms reveals common biochemical and molecular properties,” *J. Plant Physiol.*, vol. 167, no. 12, pp. 939–950, Aug. 2010, doi: 10.1016/j.jplph.2010.02.008.

[65] P. Trost *et al.*, “Thioredoxin-dependent regulation of photosynthetic glyceraldehyde-3-phosphate dehydrogenase: Autonomous vs. CP12-dependent mechanisms,” *Photosynthesis Research*, vol. 89, no. 3. Springer, pp. 263–275, Dec. 01, 2006, doi: 10.1007/s11120-006-9099-z.

[66] O. Koksharova, M. Schubert, S. Shestakov, and R. Cerff, “Genetic and biochemical evidence for distinct key functions of two highly divergent GAPDH genes in catabolic and anabolic carbon flow of the cyanobacterium Synechocystis sp. PCC 6803,” *Plant Mol. Biol.*, vol. 36, no. 1, pp. 183–194, Jan. 1998, doi: 10.1023/A:1005925732743.

[67] T. P. Howard, M. Metodiev, J. C. Lloyd, and C. A. Raines, “Thioredoxin-mediated reversible dissociation of a stromal multiprotein complex in response to changes in light availability,” *Proc. Natl. Acad. Sci. U. S. A.*, vol. 105, no. 10, pp. 4056–4061, Mar. 2008, doi: 10.1073/pnas.0710518105.

[68] N. Yu King Hing, F. Liang, P. Lindblad, and J. A. Morgan, “Combining isotopically non-stationary metabolic flux analysis with proteomics to unravel the regulation of the Calvin-Benson-Bassham cycle in Synechocystis sp. PCC 6803,” *Metab. Eng.*, vol. 56, pp. 77–84, Dec. 2019, doi: 10.1016/j.ymben.2019.08.014.

[69] L. J. Jazmin, Y. Xu, Y. E. Cheah, A. O. Adebiyi, C. H. Johnson, and J. D. Young, “Isotopically nonstationary13C flux analysis of cyanobacterial isobutyraldehyde production,” *Metab. Eng.*, vol. 42, pp. 9–18, Jul. 2017, doi: 10.1016/j.ymben.2017.05.001.

[70] R. L. Burnap, M. Hagemann, and A. Kaplan, “Regulation of CO2 Concentrating Mechanism in Cyanobacteria.,” *Life (Basel, Switzerland)*, vol. 5, no. 1, pp. 348–71, Jan. 2015, doi: 10.3390/life5010348.

[71] F. Klemke *et al.*, “Identification of the light-independent phosphoserine pathway as an additional source of serine in the cyanobacterium Synechocystis sp. PCC 6803,” *Microbiology*, vol. 161, no. 5, pp. 1050–1060, May 2015, doi: 10.1099/mic.0.000055.

[72] M. H. Abernathy *et al.*, “Deciphering cyanobacterial phenotypes for fast photoautotrophic growth via isotopically nonstationary metabolic flux analysis,” *Biotechnol. Biofuels*, vol. 10, no. 1, p. 273, Dec. 2017, doi: 10.1186/s13068-017-0958-y.

[73] J. Nogales, S. Gudmundsson, E. M. Knight, B. O. Palsson, and I. Thiele, “Detailing the optimality of photosynthesis in cyanobacteria through systems biology analysis.,” *Proc. Natl. Acad. Sci. U. S. A.*, vol. 109, no. 7, pp. 2678–83, Feb. 2012, doi: 10.1073/pnas.1117907109.

[74] A. Werner, C. D. Broeckling, A. Prasad, and C. A. M. Peebles, “A comprehensive time-course metabolite profiling of the model cyanobacterium Synechocystis sp. PCC 6803 under diurnal light:dark cycles,” *Plant J.*, vol. 99, no. 2, p. tpj.14320, Apr. 2019, doi: 10.1111/tpj.14320.

[75] D. Jaiswal and P. P. Wangikar, “Dynamic Inventory of Intermediate Metabolites of Cyanobacteria in a Diurnal Cycle,” *iScience*, vol. 23, no. 11, p. 101704, Nov. 2020, doi: 10.1016/j.isci.2020.101704.

[76] X. Lv *et al.*, "Synthetic metabolic channel by functional membrane microdomains for compartmentalized flux control," *Metab. Eng.*, vol. 59, pp. 106–118, May 2020, doi: 10.1016/j.ymben.2020.02.003.

[77] T. Zavřel, M. A. Sinetova, D. Búzová, P. Literáková, and J. Červený, "Characterization of a model cyanobacterium Synechocystis sp: PCC 6803 autotrophic growth in a flat-panel photobioreactor," *Eng. Life Sci.*, vol. 15, no. 1, pp. 122–132, Jan. 2015, doi: 10.1002/elsc.201300165.

[78] N. B. Ivleva and S. S. Golden, "Protein Extraction, Fractionation, and Purification From Cyanobacteria," Humana Press, 2007, pp. 365–373.

[79] M. Dubois, K. A. Gilles, J. K. Hamilton, P. A. Rebers, and F. Smith, "Colorimetric Method for Determination of Sugars and Related Substances," *Anal. Chem.*, 1956, doi: 10.1021/ac60111a017.

[80] T. Masuko, A. Minami, N. Iwasaki, T. Majima, S.-I. Nishimura, and Y. C. Lee, "Carbohydrate analysis by a phenol–sulfuric acid method in microplate format," *Anal. Biochem.*, vol. 339, no. 1, pp. 69–72, Apr. 2005, doi: 10.1016/J.AB.2004.12.001.

[81] M. Axelsson and F. Gentili, "A Single-Step Method for Rapid Extraction of Total Lipids from Green Microalgae," *PLoS One*, vol. 9, no. 2, p. e89643, Feb. 2014, doi: 10.1371/journal.pone.0089643.

[82] B. H. Kim *et al.*, "Simple method for RNA preparation from cyanobacteria," *J. Phycol.*, vol. 42, no. 5, pp. 1137–1141, 2006, doi: 10.1111/j.1529-8817.2006.00263.x.

[83] J. Cox, M. Y. Hein, C. A. Luber, I. Paron, N. Nagaraj, and M. Mann, "Accurate proteome-wide label-free quantification by delayed normalization and maximal peptide ratio extraction, termed MaxLFQ.," vol. 13, no. 9, Sep. 2014, doi: 10.1074/mcp.M113.031591.

[84] J. Cox and M. Mann, "MaxQuant enables high peptide identification rates, individualized p.p.b.-range mass accuracies and proteome-wide protein quantification," *Nat. Biotechnol.*, vol. 26, no. 12, pp. 1367–1372, Dec. 2008, doi: 10.1038/nbt.1511.

[85] J. Cox, N. Neuhauser, A. Michalski, R. A. Scheltema, J. V. Olsen, and M. Mann, "Andromeda: A peptide search engine integrated into the MaxQuant environment," *J. Proteome Res.*, vol. 10, no. 4, pp. 1794–1805, Apr. 2011, doi: 10.1021/pr101065j.

[86] L. Feng *et al.*, “Structural and biochemical characterization of fructose-1,6/sedoheptulose-1,7-bisphosphatase from the cyanobacterium Synechocystis strain 6803,” *FEBS J.*, vol. 281, no. 3, pp. 916–926, Feb. 2014, doi: 10.1111/febs.12657.

[87] M. Khozaei *et al.*, “Overexpression of plastid transketolase in tobacco results in a thiamine auxotrophic phenotype.,” *Plant Cell*, vol. 27, no. 2, pp. 432–47, Feb. 2015, doi: 10.1105/tpc.114.131011.

[88] P. I. Lukienko, N. G. Mel’nichenko, I. V. Zverinskii, and S. V. Zabrodskaya, “Antioxidant properties of thiamine,” *Bull. Exp. Biol. Med.*, vol. 130, no. 3, pp. 874–876, Sep. 2000, doi: 10.1007/BF02682257.

[89] O. Björnberg, P. Rowland, S. Larsen, and K. F. Jensen, “Active site of dihydroorotate dehydrogenase A from Lactococcus lactis investigated by chemical modification and mutagenesis,” *Biochemistry*, vol. 36, no. 51, pp. 16197–16205, 1997, doi: 10.1021/bi971628y.

[90] M. Havaux, G. Guedeney, M. Hagemann, N. Yeremenko, H. C. P. Matthijs, and R. Jeanjean, “The chlorophyll-binding protein IsiA is inducible by high light and protects the cyanobacterium Synechocystis PCC6803 from photooxidative stress,” *FEBS Lett.*, vol. 579, no. 11, pp. 2289–2293, Apr. 2005, doi: 10.1016/j.febslet.2005.03.021.

[91] M. D. Zurbriggen, V. B. Tognetti, and N. Carrillo, “Stress-inducible flavodoxin from photosynthetic microorganisms. The mystery of flavodoxin loss from the plant genome,” in *IUBMB Life*, Jan. 2007, vol. 59, no. 4–5, pp. 355–360, doi: 10.1080/15216540701258744.

[92] V. B. Tognetti *et al.*, “Functional Replacement of Ferredoxin by a Cyanobacterial Flavodoxin in Tobacco Confers Broad-Range Stress Tolerance,” *PLANT CELL ONLINE*, vol. 18, no. 8, pp. 2035–2050, 2006, doi: 10.1105/tpc.106.042424.

[93] M. Kriek, F. Martins, M. R. Challand, A. Croft, and P. L. Roach, “Thiamine biosynthesis in Escherichia coli: Identification of the intermediate and by-product derived from tyrosine,” *Angew. Chemie - Int. Ed.*, vol. 46, no. 48, pp. 9223–9226, Dec. 2007, doi: 10.1002/anie.200702554.

[94] Y. Miyagawa, M. Tamoi, and S. Shigeoka, “Overexpression of a cyanobacterial fructose-1,6-/sedoheptulose-1,7-bisphosphatase in tobacco enhances photosynthesis and growth,” *Nat. Biotechnol.*, vol. 19, no. 10, pp. 965–969, Oct. 2001, doi: 10.1038/nbt1001-965.

[95] A. J. De Porcellinis *et al.*, "Overexpression of bifunctional fructose-1,6-bisphosphatase/sedoheptulose-1,7-bisphosphatase leads to enhanced photosynthesis and global reprogramming of carbon metabolism in Synechococcus sp. PCC 7002," *Metab. Eng.*, vol. 47, pp. 170–183, May 2018, doi: 10.1016/j.ymben.2018.03.001.

[96] M. Tamoi, M. Nagaoka, Y. Miyagawa, and S. Shigeoka, "Contribution of Fructose-1,6-bisphosphatase and Sedoheptulose-1,7-bisphosphatase to the Photosynthetic Rate and Carbon Flow in the Calvin Cycle in Transgenic Plants," *Plant Cell Physiol.*, vol. 47, no. 3, pp. 380–390, Mar. 2006, doi: 10.1093/pcp/pcj004.

[97] R. Schwarz and K. Forchhammer, "Acclimation of unicellular cyanobacteria to macronutrient deficiency: emergence of a complex network of cellular responses," *Microbiology*, vol. 151, no. 8, pp. 2503–2514, Aug. 2005, doi: 10.1099/mic.0.27883-0.

[98] S. Arrivault *et al.*, "Dissecting the subcellular compartmentation of proteins and metabolites in arabidopsis leaves using non-aqueous fractionation," *Mol. Cell. Proteomics*, vol. 13, no. 9, 2014, doi: 10.1074/mcp.M114.038190.